Coastal erosion and climate description of Nørlev Strand area

Master Thesis

Ofelia Yocasta Rivero
Civil engineering
Aalborg University

June 15, 2017

AALBORG UNIVERSITY
STUDENT REPORT

The School of Engineering and Science
Study Board of Civil Engineering
Thomas Manns Vej 23, 9220 Aalborg
Phone +45 9940 8484
E-mail civil@civil.aau.dk
http://www.civil.aau.dk/

Title:

Coastal erosion and climate description of Nørlev Strand area

Project:

9th-10th Semester

Project period:

September 2016 - June 2017

Project author:

Ofelia Yocasta Rivero

Supervisors:

Peter Bak Frigaard
Lucia Margheritini

Editions: 1
Report pages: 70
Appendix pages: 13
Completed June 15, 2017

Synopsis:

Most of the sandy beaches in the world are suffering from erosion. This is true also in the case of Nørlev Strand, located in the West coast of Denmark. The focus of this thesis is to develop a model that can be used in the description of Nørlev Strand's climate and that can serve to assess past, present and future climatic conditions in the area.
During the study, it has been found out the existence of important climatic and morphological changes in the system, which are pointed as main cause in the acceleration of beach erosion. In particular, an increase in the storm intensity from 1999 until 2012. The climatic model can be easily adapted to represent the climate of Nørlev Strand, and offers very good results when estimating the net sediment transport.

Preface

This report is the master thesis of a 10th semester student at Aalborg University in the programme of Structural and Civil Engineering.

Prerequisites for reading the report is knowledge in statistics, basic coastal dynamics and numerical modelling.

The author would like to extends her grattitudes to her supervisors Peter Frigaard and Lucia Margheritini.

Reading guide

Through the report source references in the form of the Harvard method will appear and these are all listed at the back of the report. References from books, homepages or the like will appear with the last name of the author and the year of publication in the form of [Author, Year]. They can furthermore appear with specific reference to a chapter, page, figure or table.

Figures and tables in the report are numbered according to the respective chapter. In this way the first figure in chapter 3 has number 3.1, the second number 3.2 and so on. Explanatory text is found under the given figures and over the tables. Figures without references are composed by the author.

Ofelia Yocasta Rivero

Table of contents

0.1 Introduction . . . 1
0.1.1 Project area and objectives . . . 1
0.1.2 Document's content structure . . . 1

Chapter 1 Problem description **3**
1.1 Area of study . . . 3
1.1.1 Location . . . 3
1.1.2 Population . . . 4
1.1.3 Social and political context . . . 4
1.2 Characterization of the maritime climate and sea features . . . 5
1.2.1 General North Sea features . . . 5
1.2.2 General features of Nørlev Strand . . . 7
1.3 Geological description . . . 8
1.3.1 Geology of Denmark . . . 8
1.3.2 Geology of Nørlev Strand . . . 9

Chapter 2 Preliminary studies **11**
2.1 Analysis of available weather data . . . 11
2.1.1 Available whether data . . . 11
2.1.2 Data treatment . . . 12
2.1.3 Seasonal and directional variability of wave data . . . 13
2.1.4 Wave climate evolution . . . 14
2.2 Analysis of the bathymetric surveys . . . 16
2.2.1 Estimation of the sediment budget . . . 16
2.2.2 Evolution of beach profiles . . . 18
2.3 Quantification of shoreline change using aerial photography . . . 22

Chapter 3 Numerical modelling and definition of inputs **25**
3.1 Description of the numerical model and application to the project . . . 25
3.1.1 Important assumptions and preconditions to use Littoral Processes FM . . . 25
3.1.2 Littoral drift . . . 26
3.2 Definition of morphological characteristics of the beach . . . 27
3.2.1 Cross-shore profiles . . . 27
3.3 Definition of sediment characteristics . . . 28
3.3.1 Constants used in the calculations . . . 28
3.3.2 Depth of closure . . . 29
3.3.3 Critical Shields Parameter . . . 29
3.3.4 Effective Shields parameter . . . 30
3.3.5 Nikuradse bed roughness . . . 31
3.3.6 Fall velocity . . . 31

3.3.7 Results of the calculations . . . 32
3.4 Definition of climatic characteristics . . . 32
3.4.1 General aspects . . . 32
3.4.2 Significant wave events . . . 33
3.4.3 Wave height . . . 35
3.4.4 Mean wave direction . . . 36
3.4.5 Event duration . . . 37
3.4.6 Wave period . . . 40
3.4.7 Currents . . . 42
3.4.8 Water level variation . . . 42
3.4.9 Analysis of correlation in between climate variables . . . 44

Chapter 4 Implementation and results **49**
4.1 Generation of climate realizations: climate model . . . 49
4.1.1 Inputs for the generation model and calibration . . . 49
4.1.2 Selection of copula model and use in the generation model . . . 52
4.1.3 Adaptability of the climate model . . . 53
4.2 Model sensitivity . . . 54
4.2.1 Mean grain size and fall velocity . . . 54
4.2.2 Water level variation . . . 56
4.2.3 Wave height . . . 57
4.2.4 Wave period . . . 58
4.2.5 Event duration . . . 59
4.2.6 Bed roughness . . . 60
4.2.7 Coastline alignment . . . 60
4.2.8 Quatification of difference in between Rayleigh and Battjes and Janssen formulation . . . 62
4.2.9 Confidence interval of the transport results . . . 62

Chapter 5 Conclusion **65**

Bibliography **67**

Appendix A Appendix to preliminary studies

Appendix B Appendix to description of numerical model and inputs

0.1 Introduction

Most sandy coasts in the world are suffering a process of chronic erosion, particularly due to the reduction of the sediments supply rate and the changes in the mean sea level [Bird, 1985]. These two phenomena, among others, suppose a rupture in the beach dynamics, and thus, a rupture of its natural equilibrium. This is also the case of the West coast of Jutland (Denmark), mainly composed by sandy beaches and soft cliffs. Last 20 years, the erosion rates in the north west coast of Jutland have been around 2 to 4 meters per year [Pranzini and Williams, 2013].

First attempts of controlling land erosion in Denmark date back to 1550, when dikes where built by farmers in the Wadden Sea to protect their properties. Formal coastal protection schemes started in 1874 with the Dike Protection Law. Since the building of the first groin in 1875, coastal protection has evolve from application of hard solutions (dikes, seawalls...) to implementation of soft solutions (beach nourishment) [Pranzini and Williams, 2013]. However, due to the complex nature of the physical phenomena that interact in the coastal environment, each case has distinctive features that need to be studied in order to establish an appropriate measure.

0.1.1 Project area and objectives

The focus of this thesis is placed on Nørlev Strand, a locality of Hjørring Kommune in the Northwest coast of Denmark. Nørlev Strand is a small residential area of summer houses, and therefore it doesn't represent a key point of the national plan of coastal protection. Apart from national actuations, in Denmark the responsibility of coastal protection in these situations of local interest, lies on the proprietaries of the houses. Even though, the area has experienced for decades the harassment of the sea and the coastline has showed a clear setback, which has lead to the loss of some of the houses.

The core of this thesis is then, the development of a model that describes properly the climate and that can be adapted to different design conditions. This model is intended to be used as a tool to assess the main agents participating in the erosion of Nørlev Strand coast and eventually the simulation of past, present and future climate conditions, and their relation with the progression of the coastal damage. All of these must be understood within the context of the thesis and the assumptions and limitations that are outline in this paper.

0.1.2 Document's content structure

Chapter One: Problem description. It contains the generalities of the problem. The thesis starts with a global description of socio-economical, climatic and geological features of the area.

Chapter Two: Preliminary studies. It contains a study of the given data, particularly wave data, and two studies to quantify the extension of the erosion and coastline retraction. These last two studies are used later in the project to calibrate the numerical model.

Chapter Three: Numerical model and definition of inputs. It discusses the numerical model employed, the assumptions regarding its utilization and the application

given to it. It also explains the characteristics of the inputs used in the model, and how are they calculated.

Chapter Four: Implementation and results. It exposes the application of the climate model which basis is explained in Chapter three. It also assesses the importance of each parameter in the determination of the sediment transport and the level of accuracy of the model.

Chapter Five: Conclusion. It presents the conclusion of the paper.

Problem description 1

1.1 Area of study

Even though the whole Danish west coast is under the harassment of the maritime climate, the focus of the thesis is more local, and will be limited to the study of Nørlev Strand.

1.1.1 Location

Nørlev Strand is a locality of Hjørring kommune located in the North West coast of Denmark, and thus, limiting to the West with the North Sea. Figure 1.1 shows the location of Nørlev Strand in Denmark, while Figure 1.2 shows a detailed map of Nørlev Strand.

Figure 1.1. Location of Nørlev Strand in Denmark. Ellaboration with QGIS and Kortforsyningen tool [Styrelsen for Dataforsyning og Effektivisering].

Figure 1.2. Detailed Map of Nørlev Strand. Ellaboration with QGIS and Kortforsyningen tool [Styrelsen for Dataforsyning og Effektivisering].

1.1.2 Population

Nørlev Strand is a residential area with a population that varies strongly seasonally as most of these houses are only habited during the summer months. According to Gammelgaard [2016], there are 288 landowners in Nørlev Strand. Speaking about Hjørring kommune, it counted with 65,307 inhabitants by January 2017, 104 inhabitants less than in January 2016 and 3,172 inhabitants less than in 2000, which implies that the population is decreasing year by year [Hjørring kommune. Økonomisk Forvaltning, 2016][Hjørring kommune. Økonomisk Forvaltning, 2017]. Extrapolating this situation to Nørlev Strand, it could be expected a decrease in the population in the future.

1.1.3 Social and political context

Every year the sea gains terrain to the land. As a result, the coastline approaches the houses until the point in which several of them are being damaged or are in risk of being damaged [Thorngaard, 2015]. Due to this situation, several landowners' associations, such as Grundejerforeningen Nørlev Strand af 1986, Grundejerforeningen Nørlev Strand, Grundejerforeningen Strandgården and Fællesgrunden, have arisen [Kystdirektoratet, 2015] [Grundejerforeningen Nørlev Strand, 2016]. These associations stand for the protection of the landowners' interests. According to Denmark's legislation for coastal protection, the safeguard of the landowners' properties is their own responsibility, but any action requires permission from the Danish Coastal Authority and the municipality to preserve general interests [Kystdirektoratet, 2017].

In this context, the landowners have proposed a way of defending their properties through the construction of a slope protection with granite that posteriorly will be covered by sand feeding Kystdirektoratet [2015]. This revetment spans 70 m in front of the houses

with larger risk of collapsing, which are those located in Morgenvej. In successive years, maintenance of this revetment must be carried out. The funding of the revetment must be distributed among the landowners, specially those ones with properties in Morgenvej. The cost of the protection, according to the Coastal Authority, will suppose more than kr. 120 million over the next 25 years. A little more than half of this cost will be covered by Hjørring and the Skallerup Seaside Resort [Gammelgaard, 2016] [Bøje and Nørgaard, 2016].

Another part of the negotiations implies the groins built by the Skallerup Seaside Resort in 1981, as the landowners associations are convinced of the negative effects of these protections on the coastal dynamics [Kystdirektoratet, 2015]. They proposed the withdrawal of the groins should be financed and lead by the Skallerup Seaside Resort [Grundejerforeningen Nørlev Strand, 2016]

Finally, according to Gammelgaard [2016] and Bøje and Nørgaard [2016] around 70 houses could disappear in the next 25 to 30 years if nothing is done. However, the Coastal Authority has approve the construction of the revetment and they should be finished by winter 2017 [Bøje and Nørgaard, 2016] [Grundejerforeningen Nørlev Strand, 2016].

1.2 Characterization of the maritime climate and sea features

This section includes a characterization of the whether of the area and the main factors affecting it. It starts with the general premises of the North Sea system until it reaches the particularities of Nørlev Strand. It is also described the available data as well as the treatment it has been subdued to.

1.2.1 General North Sea features

The North Sea is a basin inside the Atlantic Ocean, limited to the east with Norway, Sweden and Denmark, to the south with Germany, the Netherlands, Belgium and France, and to the west with the Great Britain. It is opened to the north towards the Atlantic Ocean, but it is considered to has its northernmost point in the Shetland Isles [Van de Noort, 2011]. The North Sea laps the whole West coast of Denmark, and thus Nørlev Strand, becoming relevant to this study.

There are two predominant currents in the North Atlantic Ocean: the Gulf stream, which is a subtropical gyre system and the Labrador current, which is a subpolar gyre system. The Gulf stream is the one affecting the North Sea through a subsystem called North Atlantic Current. The Gulf stream is generated in the Gulf of Mexico and therefore is a warm current [Robinson and Kenneth H. Brink, 1998]. Due to this reason, the North Sea, and the continental mass surrounding it, are warmer than their analogues at the same latitude [Korevaar, 2012]. However, only a small part of the North Atlantic current descends to the east of Great Britain, and circulates along North Europe and the West coast of Denmark, as the current is divided in several subsystems as it moves through the North Sea. The larger volume of water being moved passes through the strait of Skagerrak, in between North Denmark and South Norway (Thick blue arrows at the top of Figure 1.3) [Robinson

and Kenneth H. Brink, 1998]. Here in Skagerrak, is where Nørlev Strand is located.

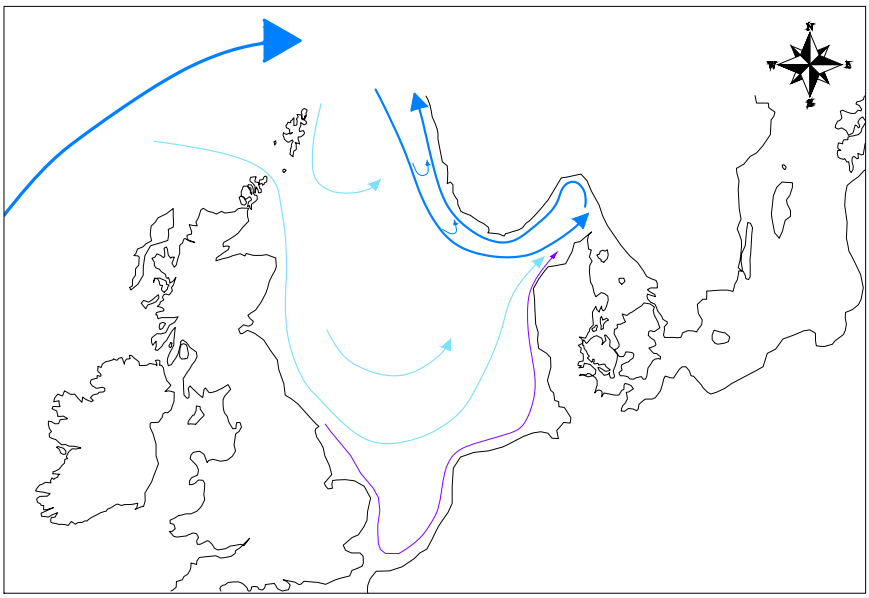

Figure 1.3. Simplified scheme of North Sea currents. The thicker blue arrow to the north, represents the contribution from the North Atlantic Current. The light blue and thiner arrows represent the circulation towards the south part of the basin. This is a part of the North Atlantic current, and the purple and thinest arrow is a even smaller percentage of the main current, that flows along the North coast of Europe. Self ellaboration based on a map from Robinson and Kenneth H. Brink [1998]

Skagerrak is characterized by the large depths of the Norwegian trench, which in its lowest point reaches around 700 m depth. It is along this trench, below 270 m depth that the largest mass transport of the North Atlantic Current is produced. In contrast, the rest of the North Sea is quite shallow, specially the southern section of the basin, from Dogger Bank until the continental shell, which includes the North and West coasts of Denmark [Robinson and Kenneth H. Brink, 1998].

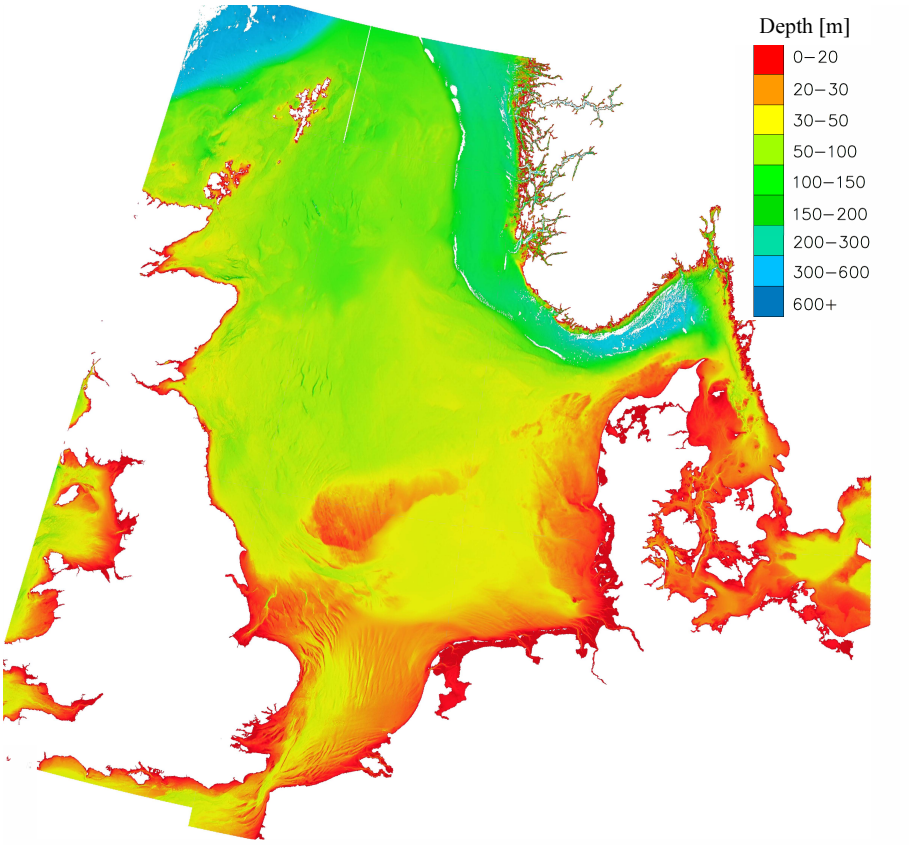

Figure 1.4. North Sea bathymetry. Self ellaboration with QGIS and data from European Marine Observation and Data Network

All of this means that, despite of being in Skagerrak, Nørlev Strand is not affected by the large volumes of water being moved due to its location within the shallow part of the North Sea.

1.2.2 General features of Nørlev Strand

Generally, waves come from the NNW, direction in which the longest fetches are found. Therefore, only this direction is duration limited, while the rest are fetch limited [Korevaar, 2012].

At the entrance of the Skagerrak strait, astronomical tides are of the order of 0.2 m. According to Saye and Pye [2006], the total water level variation along the West coast of Denmark is approximately 0.8 m. This number is smaller to the north, where it will approximate to the Skagerrak value, while to the south is even larger. The area is also characterized by a strong stratification in the water and a salinity of around 3%, due to the fresh water inflow from the Baltic Sea [Robinson and Kenneth H. Brink, 1998].

The North Sea is located in between the Azores High and the Icelandic Low, with a prevailing eastward propagation of the wind. The predominant directions from 1961 until 1980 where: NNW and SW. The stronger winds are produced during November, December and January, which is also coincident with the largest wave heights in the area of Nørlev Strand. The softest winds take place in June [Korevaar, 2012].

Nørlev Strand coast is, in general, very uniform in the longshore direction, and spans approximately 5 km. From the available information, the largest water depths are approximately −20 m, and are located at around 4 km from the coastline. A detail of the bathymetry is shown in Figure 1.5, which is elaborated with data from 2012 using the mesh generator of MIKE 21, by DHI.

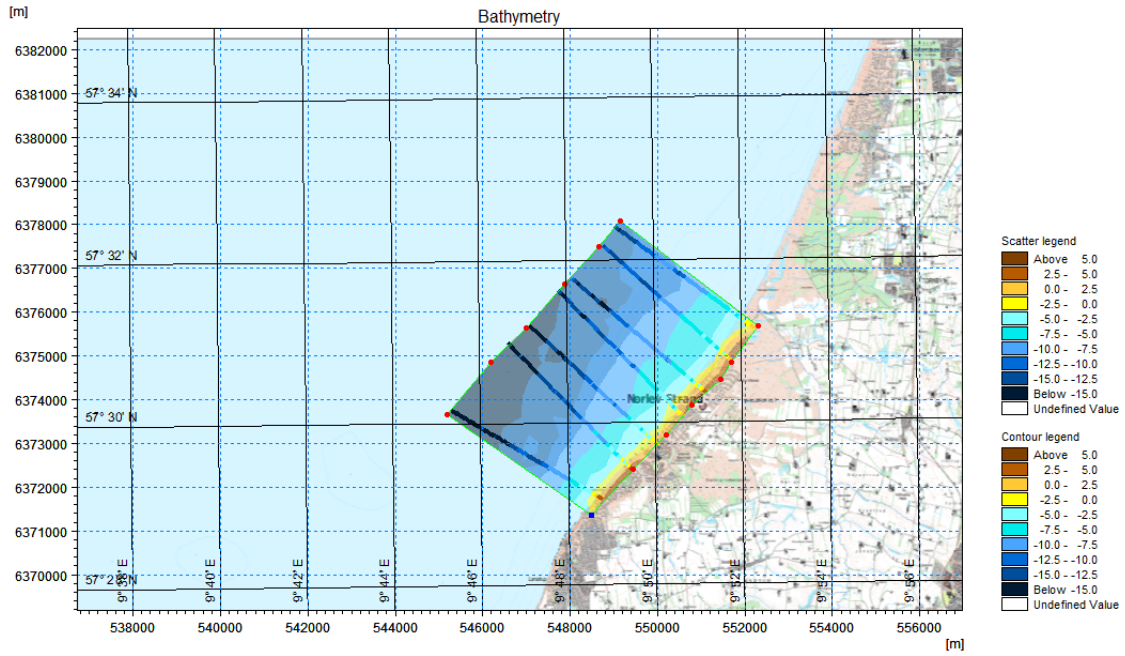

Figure 1.5. Detail of Nørlev Strand bathymetry (2012). The background image is a map 1:25,000 of 2016 from Kortforsyningen tool [Styrelsen for Dataforsyning og Effektivisering] for QGIS, its purpose is illustrative.

1.3 Geological description

In this section it is given an insight into the general geologic characteristics of Denmark. Then it is particularized to Nørlev Strand and its sediment characteristics

1.3.1 Geology of Denmark

Subsequent subsection based on Lorenz [1980].

Landforms in Denmark are mainly consequence of glaciers action over the land during the Pleistocene (around 2.6 million B.P.). Glaciers movement, retraction or advance, produces erosion. Erosion produced by glaciers results in the production of sediments called moraine. The moraine is transported and deposited due to the action of glaciers and meltwater. This sediments are in general poorly sorted, as the transport does not spans great lengths [Williams]. Most of the Danish soil is constituted in its majority of moraine, specially till and meltwater sand and gravels. Prior to the Pleistocene, almost no outcrops are found in Danish territories.

The long exposition of the land to ice action caused also deformation of underlaying soil layers due to ice weight. During the last glaciation, the Weichselian, ice covered mostly the north and the east of Denmark. After the ice melted, this north east part started to suffer

a slow process of isostatic uplift due to the decompression of the layers, while the south west part of Denmark slowly began to sink. The current implications of this phenomena is that the south west of Denmark experiences flooding and it is more exposed to the action of the climate. In the future, this will mean that the north coast will experience with less intensity the effects of the sea level rise.

The effect of the transgression of the sea in between glaciations is also of great importance. Particularly, several outcrops are elevated marine deposits, which initially lied under the transgressive sea and were lately uplifted. The deposits correspondent to the transgressions are gravel, sands and clays, and they have a large erosive tendency.

1.3.2 Geology of Nørlev Strand

Subsequent subsection based on Lorenz [1980] and information obtained from the Geological Survey of Denmark and Greenland, GEUS.

In between the Weichselian glaciation and the Flandrian inter glaciation, the Yoldia Sea took place. With this name is known a phase of the Baltic Sea in which the Atlantic Ocean and the Baltic Sea where connected through Närke's strait. Yoldia Sea deposits date back from around 10,300 to 9,500 years B.P.

Nørlev Strand and surroundings present a large amount of deposits from the Yoldia Sea. These deposits are largely consolidated respect to the rest of the soils in the area. As a consequence, they are not affected by the erosion as much as the rest. Even though Yoldia Sea deposits constitute the older type of soil, outcrops of in between 25 and 30 meters can be found in the area.

The beach front is composed of saltwater gravel and sand. These two materials are not consolidated and thus they are the main material being eroded by sea actions. Finally, most of the area is covered by a layer of aeolian sand, which is also easily transported by the wind.

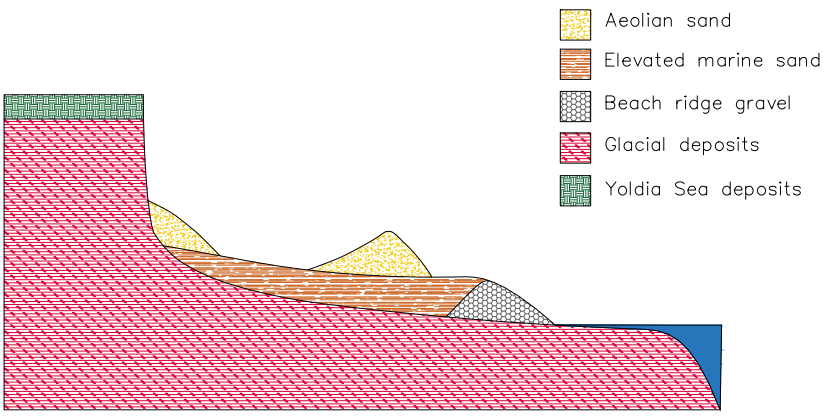

Figure 1.6. General sediment profile from Nørlev Strand. Based on information acquired from GEUS. Not to scale.

Mainly, the soil in Nørlev Strand is sand. Different types of sand and sediment characteristics can be found, but predominantly it is meltwater postglacial sand. Meltwater is the flow formed under glaciers due to the ice being melted. Under glaciers, the flow is limited to tunnels of small section, but when it reaches the outer part of the glacier, the section increases. Applying the continuity equation, an increase of section produces a decrease in flow velocity. This leads to deposition of sediments such as gravel and sand.

As explained in Subsection 1.3.1, the influence of the glacial era in the Danish landforms and geology is of great importance, as the majority of the deposits that constitute the Danish soil are a consequence of this.

According to Saye and Pye [2006], the sediment size of the sand in the area is 0.233 mm.

Preliminary studies 2

2.1 Analysis of available weather data

This section deals more in deep with the particularities of the climate in Nørlev Strand. The available data is checked, corrected and analysed, and the results are presented on this section.

2.1.1 Available whether data

Initial data available for this project is wave data and tides data. Wave data is found from buoy 1041, located at approximately 26 km to the west from Nørlev Strand coast. The UTM coordinates of the buoy are 524,559E, 6,381,744N, and it is over a depth of 17 m. The first record available from this buoy is from the 11th of August 1999, at 12:00 p.m., while the last one is the 29th of August 2012, at 5:30 p.m.

Wave data is not directly available. The records contain statistical results derived from the wave time series, each 3 h, in the form of water elevation. There are given several definitions of wave height and period, from which significant wave height, peak period and mean wave direction are used in this project.

Tides data is obtained from the Sea Level Station Monitoring Facility web page [UNESCO/IOC and the Flanders Marine Institute , VLIZ]. The actual provider of this information is the Danish Meteorological Institute (DMI). The UTM coordinates of the gauge are 557,614.52E, 6,384,092.78N, which corresponds to Hirtshals port. The data represents a month of measurements of water level variation respect to mean water level every ten minutes. Two years of predictions from the DMI are also available from the Tidal Tables at their homepage [Nielsen, 2015]. This data is referenced respect to the lowest astronomical tide.

Figure 2.1. Location of buoy 1041 and Hirtshals port.

Only 13 years of wave data are available, while only 1 month of tidal data and 2 years of predictions are available. None of them represent large samples, and thus, the usage of this data cannot be only based on annual significant events. On the other hand, using all data is not possible either. Around a 9% of the total data is missing and the quality and independence of the data cannot be guaranteed.

2.1.2 Data treatment

A priori, the data cannot be used without analysing and cleaning it. Basic corrections applied to the data are enlisted below:

- Removal of negative values
- Removal of empty values
- Removal of outliers. Values that had been assessed to be too small or too large to correspond to a real record.
- Interpolation of missing values of mean wave direction.
- Calculation of missing wave and period values when possible, through wave relations and period relations.

On the other hand, wave data has to reflect a plausible phenomena and, therefore, it is filtered according to these criteria:

- The project is dealing with *gravity waves*, defined as those which period lies within $1\,\mathrm{s} < T < 30\,\mathrm{s}$ [Andersen, 2016]. Waves which period falls outside, are eliminated.
- Wave stability: during a storm, it can hardly ever be found a wave which steepness fulfils $\frac{H}{L} > \frac{1}{10}$. Equally, the wave becomes also unstable and breaks by water depth, if the relation $\frac{H_S}{h} \leq 0.5$ is fulfilled, [Thomas Lykke Andersen and Burcharth, 2014]. According to these criteria, waves that are theoretically breaking, are also eliminated.
- Empirical wave relations: the wave height used is the significant wave height, H_{m0}. However, due to the lack of H_{m0} data, H_s and H_m data is used to complete Hm_0 by means of relation in Equation (2.1) [Liu and Frigaard, 1999]. These same relations are also used to identify possible outliers.

$$H_s = 1.2 \cdot H_m$$
$$H_{m0} \simeq 1.07 \cdot H_s \tag{2.1}$$

2.1.3 Seasonal and directional variability of wave data

To describe properly the seasonal variations of the climate, the wave data is separated using the oceanographic definition of winter and summer. The first is defined as the year period that spans from October until March, while the latter, as the period that spans from April until September. Same separation was adopted also by Li et al. [2014]. Moreover, the wave data is divided in 8 main directions: N, NE, E, SE, S, SW, W and NW. In Figure 2.2, wave roses of summer and winter are shown.

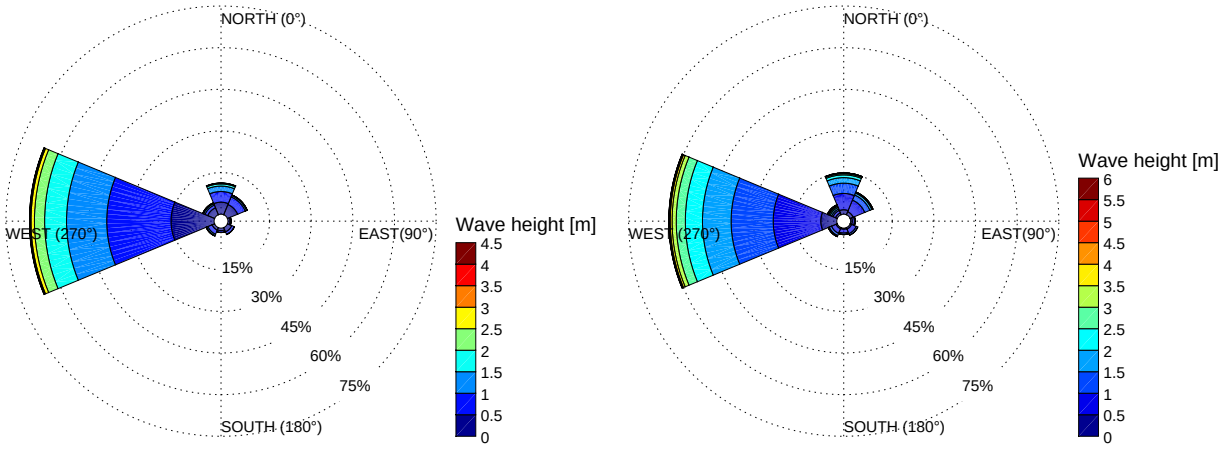

Figure 2.2. Wave roses representative of the period August, 1999 - August, 2012. Left: H_{m0}, summer. Right: H_{m0}, winter.

At first sight, there is no significant variation in the directional distribution from summer to winter. In winter the waves drift slightly towards north. The main difference reside in the magnitude of the waves, which are clearly larger in winter. Around a 50% of the summer waves are larger than 1.5 m height, while in winter 50% are above 2.5 m height.

From Figure 2.2, it becomes clear as well that two circular sectors are predominant. In first place the sector comprised in between 250° and 295°, and in second place the sector comprised in between 340° and 25°. These two sectors count for approximately a 75% of the waves in summer and winter. There is a third circular sector that might catch the reader's attention which is the one that spans from 25° until 70°. Because of its relative position respect to Hirtshals, Nørlev Strand is sheltered from waves comming from the NE.

As a result, the wave data is divided in four groups depending on its direction and its season:

Table 2.1. Data division in groups

Group	Season	Direction	
G1	Summer	North	$[340° - 25°]$
G2	Summer	West	$[250° - 295°]$
G3	Winter	North	$[340° - 25°]$
G4	Winter	West	$[250° - 295°]$

The validity of this division is proved in Subsection 3.4.2.

2.1.4 Wave climate evolution

Two characteristics of the wave data are analysed here: in first place, the evolution of the wave height with the years. It is selected to plot the annual mean of the significant wave height, H_{m0}. Figure 2.3 shows both the evolution with the years and the trend followed by the wave heights. Summer and winter data are analysed individually.

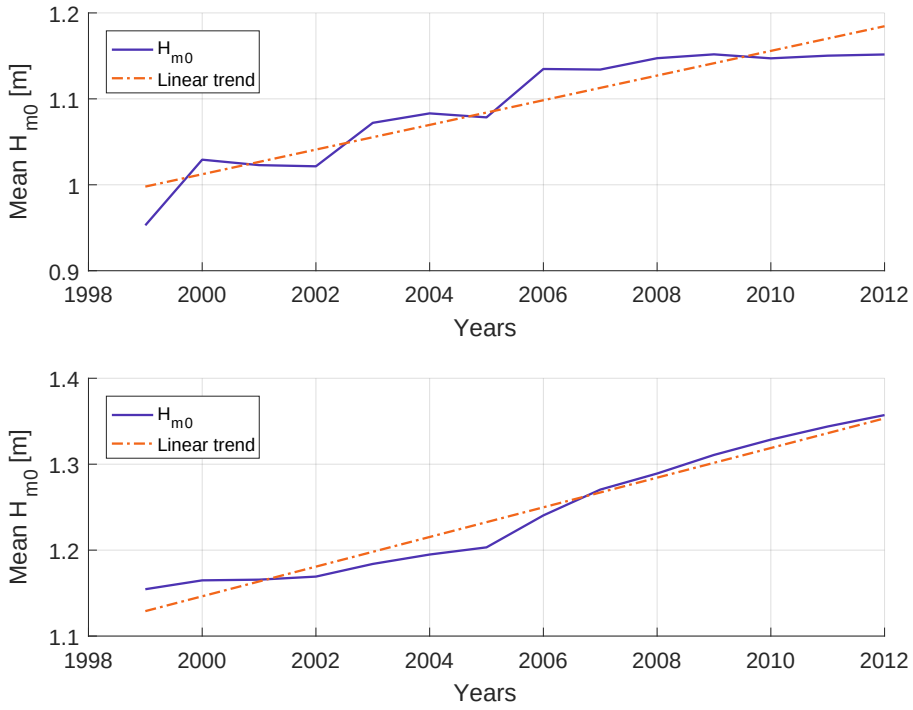

Figure 2.3. Evolution of significant wave height, H_{m0}. Top: summer. Bottom: winter.

Both waves in summer and waves in winter have a clear tendency to increase in height. The growth rate of summer waves is 0.0144 m/year and the winter rate is 0.0173 m/year. This means that every year waves approaching the coast are larger than in the previous year.

In second place, it is analysed the evolution of the mean wave directions, A. A is weighted respect to the significant wave height as follows:

$$A_{weight} = \frac{\sum_{n=1}^{N} A_{mean,n} \cdot H_{m0,n}}{\sum_{n=1}^{N} H_{m0,n}} \tag{2.2}$$

The directions are weighted in order to account for the greater importance of larger wave heights in the sediment transport respect to smaller waves. Again, directions and waves are separated in winter and summer events. The results are shown in Figure 2.4.

In summer, A varies after 2006. The sediment transport is very sensitive to the angle formed in between waves and coastline alignment. A larger angle, as it is from 2000 to 2006, means that the northerly component of the waves is more relevant during these years, and thus the net sediment transport becomes potentially smaller. The net sediment transport, as forwarded in Subsection 1.2.2 goes towards the north. This is due to the predominant westerly component of the waves. As the northerly component produces transport in the opposite direction (towards the south), the net balance of the transport is reduced when both components are acting together.

In winter, A has the opposite evolution, with steeper angles after 2006, which means that the net sediment transport produced during winter events should be smaller in recent years, than before 2006.

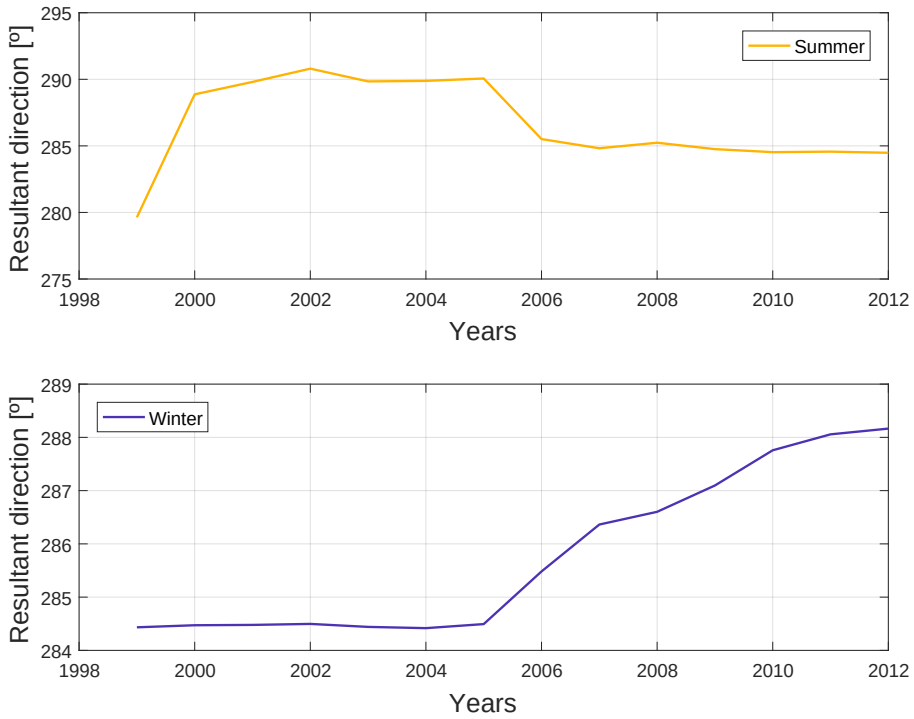

Figure 2.4. Evolution of mean wave direction, A. Top: summer. Bottom: winter.

All wave roses of every year can be found in Appendix A.1. They illustrate further the distribution of the waves by direction. In this section, only four representative wave roses from summer and winter are presented

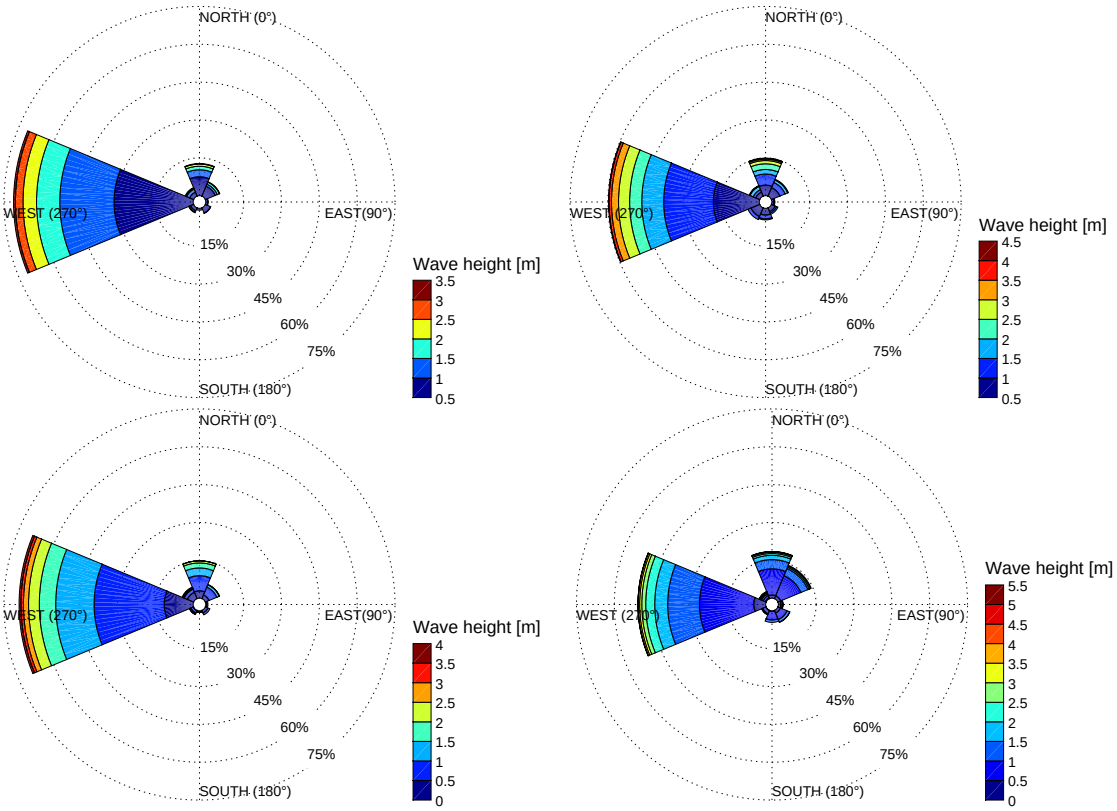

Figure 2.5. Annual wave roses. Top left: summer 2002. Top right: winter 2002. Bottom left: summer 2010. Bottom right: winter 2010.

2.2 Analysis of the bathymetric surveys

In this section, the available bathymetry is used in to quantify volumetric variations of the beach shoreface. The bathymetry used corresponds to surveys made by the Danish Coastal Authority, from 1970 to 2012. In recent years these surveys are made each four years.

2.2.1 Estimation of the sediment budget

The bathymetry of Nørlev Strand is described by 8 profiles, which can be seen in display in Figure 2.6. Available bathymetry covers 19 years, from 1970 until 2012.

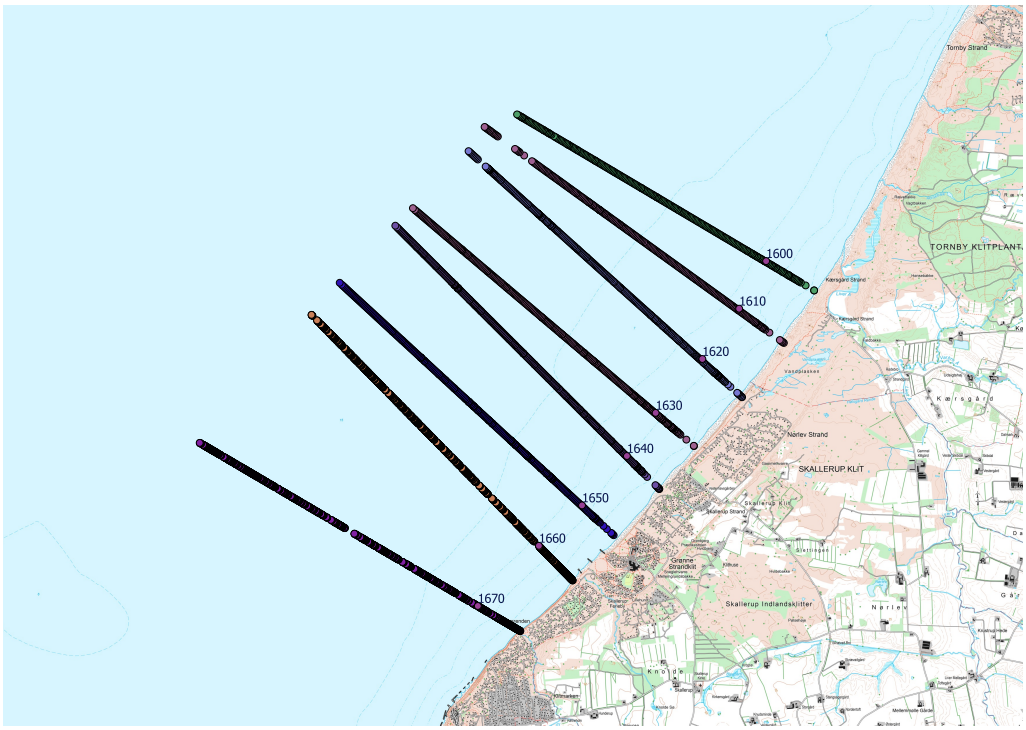

Figure 2.6. Location of the profiles in Nørlev Strand

For each year, the profiles are imported to AutoCad Civil 3D, which allows to create surfaces from groups of points. Each point imported must contain its position in space (in X, Y and Z). From the surfaces created, the program is able to calculate the volume contained in between each two of them. This volume represents the amount of sand that is loss or gained in between the two years that are considered. If all the resultant volumes are added, the net annual volume change can be obtained [Aouiche et al., 2016].

From Figure 2.7 it can be observed the evolution of the erosion/accretion of Nørlev Strand. In the figure, positive values represent accretion while negative values represent erosion. In average, the net annual volume mobilized in the beach is negative, which means that there is erosion. This erosion is 271.269 m^3/year. This annual lost volume corresponds to local net sediment transport in the beach.

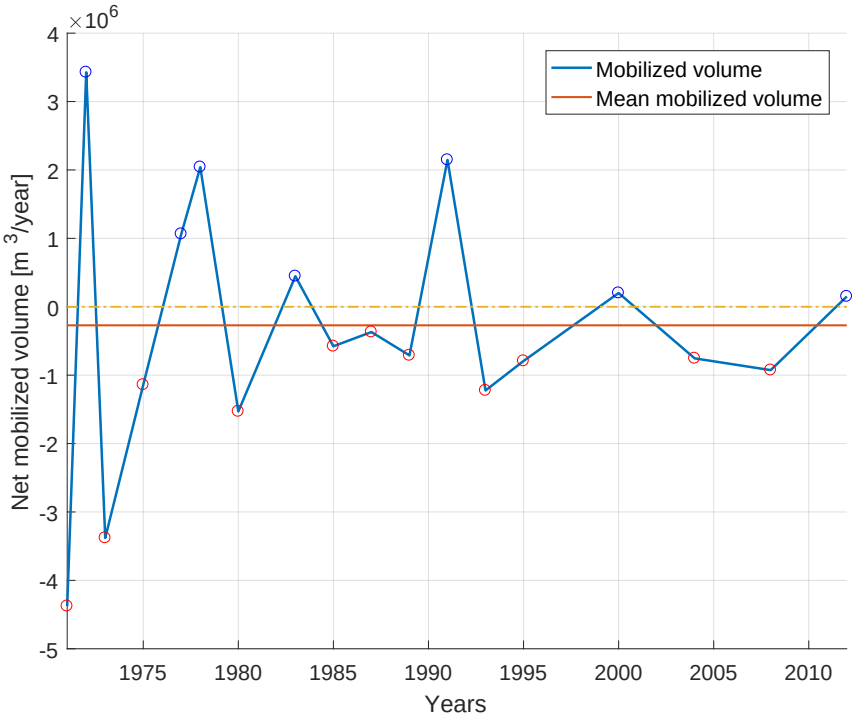

Figure 2.7. Evolution of the net sediment transport with the years. Peaks of accretion most probably correspond to nourishment campaigns.

The results from this study are used as a calibration parameter for the numerical model. Littoral Processes FM calculates local sediment transport, which means that does not take into consideration the transport upstream. Therefore, the result gives only the sediment that is added or subtracted from the main transport.

2.2.2 Evolution of beach profiles

Each profile is studied individually. It is made an integration in between the profiles of two successive years to obtain how it varies the amount of material lost or gained in different years. This operation serves to the purpose of evaluating the expected behaviour of each profile.

Each profile is plotted each 20 years to asses, not only volumetric changes, but also how some of its individual features change, such as slope and bars.

In this subsection, only four profiles are going to be shown in detailed: profile 1670, which is upstream of the groins, profile 1650, which is immediately downstream of the groins, profile 1630 which is around of the beach midpoint and profile 1600 which is at the very end of the beach, downstream. It is expected that this last profile is not affected directly by the groins action. Figures 2.8, 2.9, 2.10 and 2.11 show, on the left side, the morphological evolution of the profiles. The right side shows the evolution of the profile's total volume per meter.

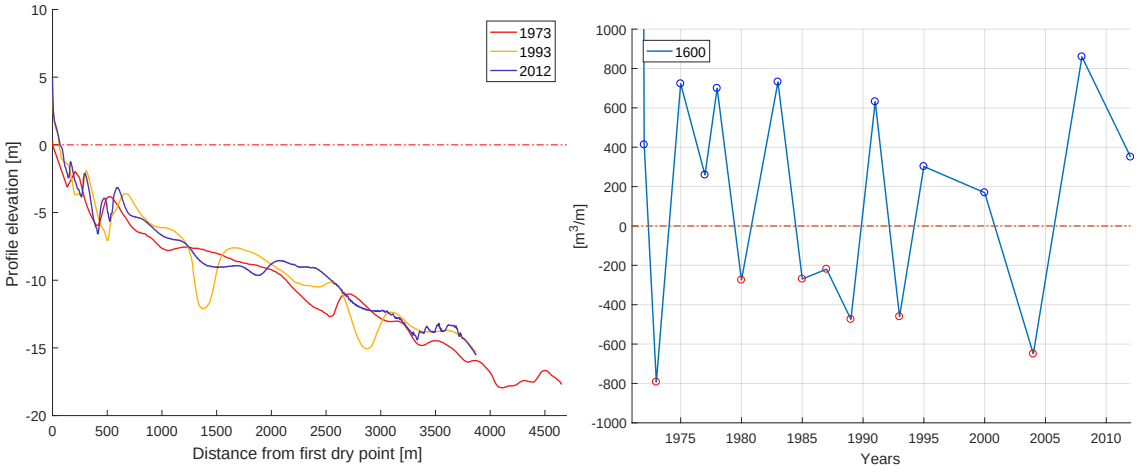

Figure 2.8. Profile 1600. Left: Morphological evolution. Right: Volumetric evolution $[m^3/m]$.

In general, most of the profiles have developed steeper slopes and larger bars. These bars have also moved towards onshore. This suggests that larger waves are breaking closer to the coast, intensifying the erosive process. The exception to this is profile 1600, which steepness was reduced and which bars have moved offshore. Finally, profile 1670 has remained stable in most of the profile cross shore length, only becoming deeper in the first 2000 m. This profile is located in front of beach revetments, and no dry beach. Profile 1670 increases its volume in the shoreface of the beach in recent years, probably as consequence of beach nourishment, however, the shallower bar had moved offshore. This might be a result from the reflection of waves introduced by the revetment.

Both profile 1600 and 1670 have a positive balance from 2008 to 2012, which could be due to beach nourishment.

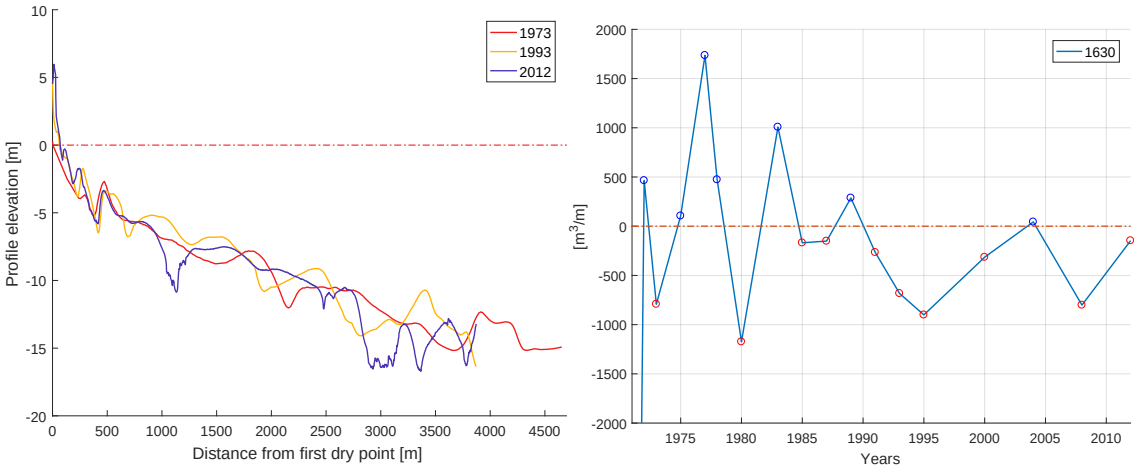

Figure 2.9. Profile 1630. Left: Morphological evolution. Right: Volumetric evolution $[m^3/m]$.

On the other hand, new bars have been formed and existent ones are shorter in the cross-shore direction. The increase in the number of bars leads to successive episodes of breaking and reformation of waves, which increases the stirring, and thus the amount of sediment

in suspension. This eventually provokes a potential rise in the transport.

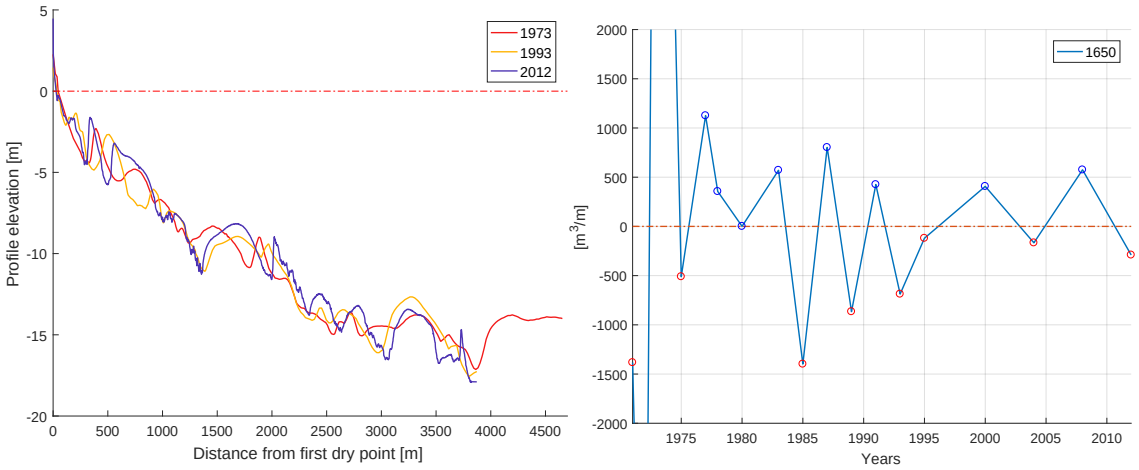

Figure 2.10. Profile 1650. Left: Morphological evolution. Right: Volumetric evolution $[m^3/m]$.

Profile 1650 is located upstream of Morgenvej houses. In the first 1500 m, the steepness of this profile is notoriously larger than in the rest of the profiles. In 1973, this section was already steep, but it can be observed that its steepness has been intensified until 2012. This may be one of the causes of the vulnerability of this part of the beach.

It is interesting to note that most of the drastic changes are produced within the first 1500 m of the profile cross-shore length, in all profiles. This section is within the active zone. The theoretical depth of closure is in between 6.25 m and 8.01 m (obtained in Subsection 3.3.2, and thus is largely affected by the waves action. At this respect, the most interesting is profile 1650, which has clearly undergone a lot of changes, product of the groins construction, one of which seem to be the increase in the profile steepness.

Even though, profile 1630 is the most affected by the erosion, and has loss the largest amount of volume per meter. This loss is localized outside the depth of closure and after 2500 m. The increase in volume from 2008 to 2012 seems to be also due to beach nourishment.

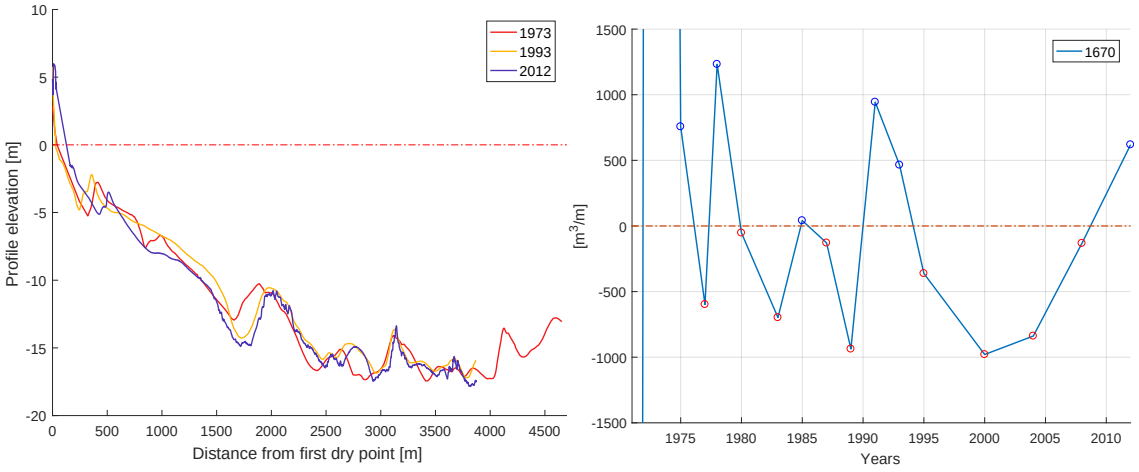

Figure 2.11. Profile 1670. Left: Morphological evolution. Right: Volumetric evolution $[m^3/m]$.

In Appendix A.2, all profiles are plotted. If compared successive profiles, it is also patent that there is no continuity of the morphological features. Most bars are not a continuous horizontally, which creates a different behaviour in the coastal dynamics alongshore. For instance, the beakers line would not be a parallel line to the coast, but waves will break at different distances from the shoreline depending on the characteristics of the profile. As a consequence, it appears a gradient in the alongshore sediment transport. Where the gradient are negative, there tends to be deposition, while where the gradient is positive, erosion is produced [Silva et al., 2016] [Davidson-Arnott and Pollard, 1980].

In Table 2.2 the numerical results of the accumulated erosion are presented. The table is divided in three columns. Each column presents the accumulated net sediment transport in $\frac{m^3}{m}$ for each profile. The first column represent the accumulated sediment transport in the period 1973-2012, the second column, the period 1973-1981 and the third column, the period 1981-2012. This division is made to find out whether there are significant differences before the groins are built and after the groins are build. The result however, does not seem useful, as before 1981, in only 8 years it is produced a disproportionate accumulation of sediments compare to what is produced in the 31 following years. The calculation of the accumulated transport is done adding when accretion is produced and subtracting when erosion is produced. It is possible that there exist a problem with the data pre 1981, resulting in this large difference.

Some profiles seem to be showing accretion, which is the case of profiles 1600 and 1610. As explained before, this is consequence of beach nourishment and possibly due to the influence of the river affluent located close to profile 1600. This last profile has a very stable tendency after 1981, however the most stable profile during the whole record, in terms of volume per meter, is profile 1650.

Table 2.2. Total net sediment transport per profile

Profile nr.	Acc.1973-2012 [m^3/m]	Acc.1973-1981 [m^3/m]	Acc.1981-2012 [m^3/m]
1600	20,055	19,816	239
1610	26,467	25,481	986
1620	-37,894	-35,324	-2,571
1630	-12,683	-9,581	-3,102
1640	-37,217	-35,054	-2,163
1650	2,548	3,867	-1,319
1660	-32,604	-32,429	-175
1670	-15,495	-14,185	-1,310

Overall, this study suggest that the beach nourishment is pursuing its objective of maintaining a fixed volume of sediment per profile. However, these nourishment campaigns do not cover the loss of material in deeper waters, as they are outside the active zone. The drastic increase in depth in the offshore contours allows larger waves to approach the coast, and thus increases the risk of erosive processes such as the ones that lead to the destruction of houses.

2.3 Quantification of shoreline change using aerial photography

Aerial photographies, or orthophotos, are a useful tool to evaluate the evolution of visible features of a certain area [Boak and Turner, 2005]. These pictures are normally taken from a plane with high resolution equipment. Orthohotos are usually taken in the same time of the year, at the same hour, to avoid distortions due to seasonal changes or different illumination.

The objective is to asses how the shoreline has changed in the recent years. For this project, there is data available since 1945 until 2016.

As it is explained by Boak and Turner [2005], the first problem that is encountered when analysing the evolution of the shoreline, is the capability to define the shoreline, as it is a dynamic entity. Normally, it is necessary to adopt a shoreline indicator, which is used to represent the shoreline in a systematic manner [Boak and Turner, 2005]. In this project, three shoreline indicators are used, to account as much as possible for the inaccuracies of the technique.

Among the uncertainties introduced in the use of orthophotos to determine shoreline advance or retraction, it can be found:

- Manual digitalization from a raster image.
- Subjectivity in the definition and detection of the shoreline due to its dynamic nature [Boak and Turner, 2005]
- Quality of the raster image
- Quality of the georeferenciation

- Difficulties in the differentiation in between seasonal variations of the coastline (short term response) and actual long term changes [Baptista et al., 2014]

In first place, it is used the instant water line [Morton and McKenna, 1999]. In second instance, it is used the wet-dry line [Zarillo et al., 2008] combined with the landward edge of the shore protection structure [Moore et al., 1999] where the revetment of Skallerup Klit is placed. An example of this is shown in Figure 2.12. In the image all three types of shoreline indicators are plotted. The background image is an ortophoto from 2016 obtained by using the tool of Kortforsyningen for QGIS [Styrelsen for Dataforsyning og Effektivisering]. The shorelines are digitalized manually from the orthophotos.

Figure 2.12. Example of shoreline indicators used. Elaborated with QGIS and Kortforsyningen tool [Styrelsen for Dataforsyning og Effektivisering].

It is measured the relative distance in between consecutive shorelines in time, in the place of the aforementioned 8 profiles. These profiles location was seen in Figure 2.6.

The results of the coastline relapse from the ortophotos can be used to have an order the magnitude when calibrating the coastline relapse in a numerical model [Boak and Turner, 2005], from which more exact results can be expected. On the other hand, it becomes an useful insight to assess which sections of the beach have a larger risk of being damaged. In Table 2.3, the rates of shoreline change obtained from the digitalizations are shown.

Table 2.3. Rate of shoreline change by using aerial photography. Rate 1 corresponds to a instant water line as indicator. Rate 2 corresponds to the wet-dry line used as indicator (first approach). Rate 3 corresponds to the wet-dry line used as indicator (second approach).

Year	P1600	P1610	P1620	P1630	P1640	P1650	P1660	P1670
Rate 1 [m/year]	-0.40	0.50	0.58	-0.79	-1.38	-2.27	-1.60	-1.63
Rate 2 [m/year]	0.23	-0.15	-0.85	-1.18	-1.90	-2.75	-1.22	-0.92
Rate 3 [m/year]	0.51	0.14	-0.86	-0.86	-1.67	-2.72	-1.37	-1.44

Appendix A.3 has all the operations and relative distances in between shorelines.

The main difference in between Rate 2 and Rate 3 consist in the addition on the landward edge of the shore protection structure as indicator or not. In second place the difference comes from the subjectivity of the detection in the shoreline, which is what is pretended to be shown by displaying both rates. On the other hand, these last two digitalizations are made with less years, as they are done by using the GIS server of Miljø- og Fødevareministeriet and COWI.

The further away from the groins, the more stable becomes the shoreline position, though the beach retraction does not disappear. This suggests that the effect of the groins over the transport reach up to profile 1640 (downstream of Morgenvej), having its maximum in the vicinity of the last groin, downstream of them (1650).

Finally, in relation to the previous study, it can be concluded that most of the profiles are eroding. Rate 3 is the one that agrees the most with the results of the bathymetry surveys, showing that profiles 1600 and 1610 advance instead of retreat. These two profiles are the furthest from the groins. They are located downstream of Nørlev Strand, close to an affluent. The accretion can be product both of the sediment nourishment from the affluent and the artificial nourishment.

The houses that are more affected by storms are located in between profiles 1640 and 1650, both which tend to show the greatest shoreline retraction. This is a common effect produced to the morphology of the coast, when hard solutions are applied in coastal protection and stabilization. However, and as seen in the analysis of the bathymetry surveys, the underlying problem is not limited to the groins and the revetment of Skallerup Klit. Other parts of the beach, that are not directly affected by the groins, show also retraction, though in smaller proportions. From here it can be guessed that the erosion of Nørlev Strand is structural, as in most of the Danish West coast, though exacerbated in specific points by anthropogenic actions.

Numerical modelling and definition of inputs 3

The following chapter is divided in two main parts:

First, it is introduced the numerical model that is used, the most important assumptions linked to its use and the utilization given to it in the project.

Secondly, there are three sections regarding modelling of the input parameters, and the calculations involved in their determination. The inputs are divided in three categories: morphological characteristics of the beach, sediment characteristics and climatic characteristics.

3.1 Description of the numerical model and application to the project

In this project it is decided to use the module Littoral Processes FM from DHI. The reason to choose this module lies in a good balance in between module capabilities and simplicity of the software. In addition, the module is very light and therefore the simulations times are short.

This section is based on the information provided in the User Guide of MIKE by DHI [2016]

Littoral Processes FM is a tool that integrates a set of different models in order to evaluate sediment transport in coastal areas. Littoral Processes FM is constituted by four different models:

- Transport in a point
- Littoral drift
- Table generation
- Coastal evolution

Littoral drift is the module used in this project.

3.1.1 Important assumptions and preconditions to use Littoral Processes FM

There are several assumptions and considerations that have to be made in order to be able to use the module:

Non-cohesive transport

The module works with non-cohesive transport. It is assumed that Nørlev Strand transport is purely of granular non-cohesive material. Most of the sediments in the area are sand or gravel from different precedence, but glacial deposits have also a certain content of clay and limes as it can be seen in Figure 1.6. However, it is assumed that the these cohesive materials do not affect the transport.

One-line theory

The module is based on one-line theory, which means that it does not consider changes in the cross-shore profiles. Due to this, no output representing the profile evolution can be expected from this module. On the other hand, it means that the bathymetry contours must be quasi-parallel to the coastline and the beach profiles perpendicular to those. The coastal morphology is, thus, described by the coastline position. As a result, the coastal dynamics are dominated by alongshore currents.

The coastline in Nørlev Strand is almost a straight line, and even though there are some visible features that make the coast heterogeneous (see Figure 1.5), it is also assumed that in overall the contours are quasi-parallel to the coast. Regarding the dominance of the alongshore current, this statement is true for the West Coast of Denmark, and in particular for Nørlev Strand.

Selected area to model

Even though the module does not need a mesh to be generated, it has one important condition in the definition of the area: it has to be large enough so the boundaries do not influence the area of interest. Figure 1.5 was elaborated using the same extensions as those used in the simulations.

The coordinate system used in this project is UTM ED50 Zone 32.

3.1.2 Littoral drift

Littoral drift is used to calculate the sediment budget. It consists of two main operations. First it solves the hydrodynamic equations of the problem, including wave propagation towards the coast, shoaling and breaking and calculation of driven forces. These forces come from the radiation stress gradient and the momentum balance equation in the cross- and longshore direction. Secondly, it calculates the sediment transport from the generated hydrodynamic conditions and the sediment characteristics.

Each simulation covers a year. Important outputs for this project are the annual net sediment transport for the selected cross-shore profiles and the Q-α curves, which give the net annual transport depending on the angle that forms the coastline alignment.

This model is calibrated by using the results from Section 2.2, in particular the results of the net sediment transport from Subsection 2.2.1. It is possible to calibrate the model using these results because the module only considers the local sediment transport, i.e., as long as there is not input from the outside conditions of the selected area, it only gives the results of what is calculates within.

3.2 Definition of morphological characteristics of the beach

The morphological characteristics of the beach are defined by the coastline position and the cross-shore profiles.

3.2.1 Cross-shore profiles

In order to input the cross-shore profiles, it is necessary to give the geographical coordinates of the first grid point, defined as the first offshore point of the cross-shore profile [MIKE by DHI, 2016]. The profile is given by the Z coordinate of the points which are equispaced, with a constant grid spacing. Furthermore, all profiles must have the same number of grid points [MIKE by DHI, 2016]. Finally, the orientation of the grid must be given. The following sign criteria apply:

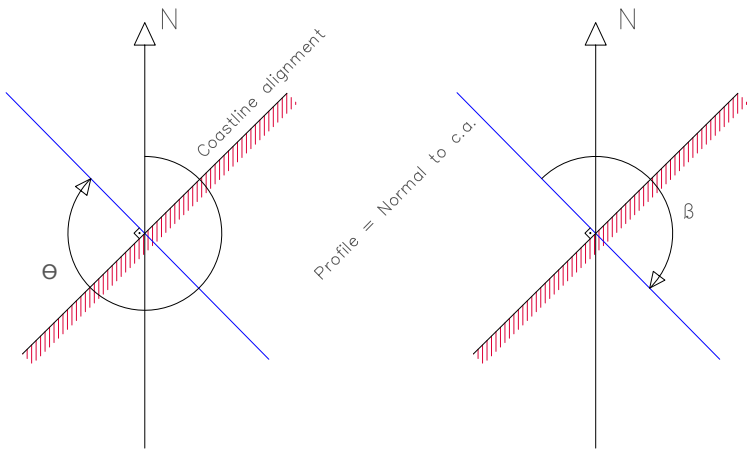

Figure 3.1. Sign criteria in Littoral Processes FM. Left: definition of coastline orientation. Right: definition of profile orientation.

The cross shore profiles given by the Danish Coastal Authority are given by their UTM coordinates. From the coordinates is easy to obtain the length in between grid points by applying Pythagoras' theorem. The distance is not equispaced, and therefore it is made a linear interpolation in between the grid points with a defined grid distance. The interpolation is also applied to the UTM coordinates in order to obtain those from the first grid point. In this case, it was selected to use 2 m in between points. Finally, from the 8 cross-shore profiles, it is selected the one with the smallest length, and the rest of the profiles are cut in consequence. The number of grid points depend on the year considered, as the most recent bathymetry has a larger resolution, however, all of the profiles contain more than 2000 grid points.

There are two checks that must be done to assess whether the quality of the bathymetry is sufficient for the model. The first one consist on testing the length of the profile, which must be sufficiently long so as the breaking does not generate sediment transport in the first meters of the profile [MIKE by DHI, 2016]. The second one consist on checking whether

the resolution of the bathymetry is enough. The resultant current velocity through the profile should be smooth [MIKE by DHI, 2016].

The first check is done by simulating the most extreme event of the register which corresponds to a wave height of 6.4 m, a peak period of 10.8 s and a mean wave direction of 285°. The event lasts 1 h. The results show that the bathymetry is long enough, but very tightly for all profiles, except for profile 1610. This is due to the low water depth at the beginning of the profiles, which suddenly reduces from −17 m to even −13 m. The profile that is further from fulfilling this requirement is profile 1670. Unfortunately, it is not a possibility to extend the profiles, as there is no more information available.

The second check is done by simulating a mean event with a wave height of 1.4 m, a peak period of 5.2 s and a mean wave direction of 276°. Again, the event last 1 h. The results are very smooth, and so the resolution is sufficient.

Figure 3.2 is an example of the results for profile 1610, which as said before, provides the best results. The rest of the plots can be seen in Appendix B.1.

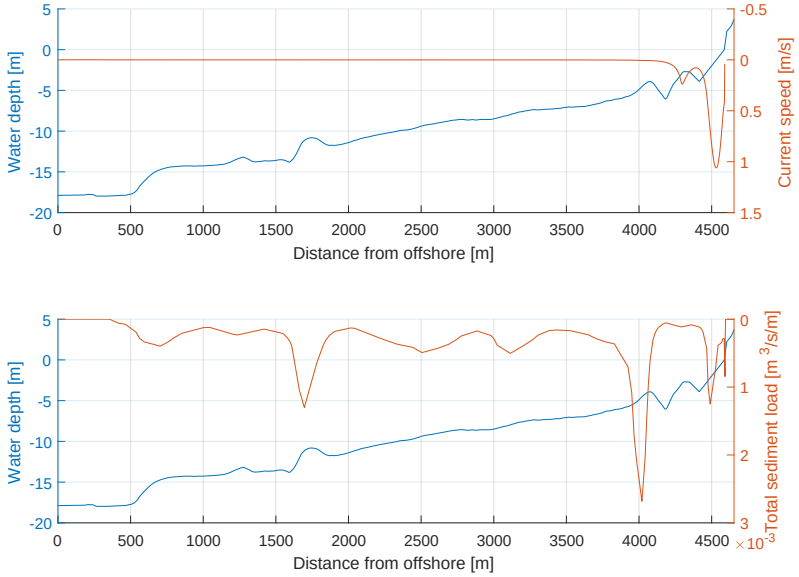

Figure 3.2. Top: mean event simulation. Resolution check. Bottom: extreme event simulation. Length check.

It is also required that the last point of the profile is dry during simulations, which means that the profile should finish in a higher point than 0 m over the mean water level. Profiles 1600 and 1630 do not fulfil this requirement, and thus, they cannot be used in the simulations.

3.3 Definition of sediment characteristics

3.3.1 Constants used in the calculations

Table 3.1 displays the constants used in the calculations performed in this section.

Table 3.1. Constants used to obtain the sediment characteristics

Parameter	Symbol	Value	Unit
Water depth	h	17	m
Gravity acceleration	g	9.81	m/s
Mean grain diameter	d_{50}	0.233	mm
Water density	ρ	1025	kg/m^3
Sand density	ρ_s	2650	kg/m^3
Relative density	s	2.59	-
Kinematic viscosity	ν	10^{-6}	m^2/s

In the rest of the subsections, only the symbol shown in the table is used. At the end of the section, the results of all calculations are presented.

3.3.2 Depth of closure

The depth of closure defines the limit of the active zone of the beach, or the limit of the seasonal variations of the beach profile [Dean, 2003]. The formulation purposed by Birkemeier [1985] is used to estimate the depth of closure:

$$h_c = 1.75H_e - 57.9\left(\frac{H_e^2}{gT_e^2}\right) \tag{3.1}$$

where H_e is the wave height exceeded 12 h a year, and T_e its associated period. H_e can be calculated by using Equation (3.2), which depends on the annual mean significant wave height and the standard deviation in the wave height [Dean, 2003]

$$H_e = \overline{H} + 5.6 \cdot \sigma_H \tag{3.2}$$

The depth of closure is not used directly as a model input, but is used to estimate the extension of the active zone.

3.3.3 Critical Shields Parameter

The depth at which we can define the threshold of movement fulfils that $\theta > \theta_c$, being θ the Shields parameter and θ_c the critical Shields parameter. This parameter helps to evaluate whether the profiles length is enough to describe the whole transport process. In fact, the depth of closure is defined as the depth where $\theta > 2 \cdot \theta_c$ [Liu, 1999].

θ_c depends on the sediment fluid parameter:

$$S_w = \frac{d_{50}\sqrt{(s-1)\cdot g \cdot d_{50}}}{4\nu} \tag{3.3}$$

and can be read from the Shields diagram.

The default value of the critical Shield's parameter is 0.0045. This values cannot be changed without introducing other changes such as the porosity of the soil and the ripple constants. These constants are not recommended to be changed and the porosity of the soil is unknown.

3.3.4 Effective Shields parameter

This procedure is obtained from Liu [1999]

The expression of the effective Shields' parameter is as follows:

$$\theta' = \frac{\tau_{w,max}}{\rho(s-1)gd} \tag{3.4}$$

It depends on the maximum shear stress in the bottom generated by the water particles, $\tau_{w,max}$, the gravity acceleration constant, g, the particle diameter, d, the water density, ρ and the relative density of the particle s, which in this case is sand.

The expression for the maximum shear stress in the bottom is:

$$\tau_{w,max} = \frac{1}{2}\rho f_m U_m^2 \tag{3.5}$$

which depends on the wave friction factor, f_w:

$$f_w = \exp\left(5.5 \cdot \left(\frac{\kappa_s}{A}\right)^{0.2} - 6.3\right) \tag{3.6}$$

and the horizontal particle velocity in the bottom, U_m:

$$U_m = A \cdot w = A \cdot \frac{2\pi}{T} \tag{3.7}$$

From these two expressions it is still necessary to define κ_s, which is the bed roughness. When calculating the effective Shields parameter it is imposed Equation (3.8)

$$\kappa_s = 2.5 \cdot d_{50}; \tag{3.8}$$

The value of d_{50} is specified in Table 3.1.

Another unknown parameter is A, which is defined as the amplitude of the oscillation of the water particle on the sea bed

$$A = \frac{H}{2} \cdot \frac{1}{\sinh\left(\frac{2\pi h}{L}\right)} \tag{3.9}$$

A is used in both expression (3.7) and (3.6).

Finally, L is the wave length, calculated by iteration and by applying linear wave theory:

$$L = \frac{gT^2}{2\pi} \cdot \tanh\left(\frac{2\pi h}{L}\right) \tag{3.10}$$

The value for the period is obtained by using the relations (3.23) and (3.24).

Finally, the wave height, periods and wave length used are summarized in Table 3.2. Mean wave heights of wave groups G2 and G4 are used.

Table 3.2. Wave heights, peak periods and wave lengths used in the determination of sediment characteristics.

	Wave height [m]	Peak period [s]	Wave length [m]
Summer	1.04	4.26	28.30
Winter	1.38	4.68	34.10

The effective Shields parameter is used to calculate Nikuradse's bed roughness, which is an important calibration parameter.

3.3.5 Nikuradse bed roughness

Based on [Liu, 1999]

Nikuradse's bed roughness is defined as an interval:

$$H_r \leq \kappa \leq 4 \cdot H_r \tag{3.11}$$

It depends on the ripple steepness H_r, which equation is:

$$\frac{H_r}{L_r} = 0.182 - 0.24 \cdot (\theta')^{\frac{3}{2}} \tag{3.12}$$

where θ' is the effective Shields parameter calculated in Equation (3.4), and L_r is the ripple length.

$$L_r = 2 \cdot A \tag{3.13}$$

Nikuradse's bed roughness is used as a parameter associated to each profile in the numerical model. Due to the fact that the result is not a single value but a range, several values of the bed roughness are tested.

3.3.6 Fall velocity

Due to lack of data to define the grading coefficient according to the specifications of the software

$$\sigma_g = \frac{\sqrt{d_{84}}}{\sqrt{d_{16}}} \tag{3.14}$$

the sand will be considered uniform and the fall velocity must be specified.

According to Ahrens [2000] the following formulations lead us to a determination of the fall velocity with a small error. First, the fall velocity is defined as:

$$\omega = \frac{C_1 \cdot \Delta g d^2}{\nu} + C_t \sqrt{\Delta g d} \tag{3.15}$$

where A is the Archimedes buoyancy index and d is the characteristic diameter, in this case taken as d_{50}. The Archimedes buoyancy is defined as:

$$A = \frac{\Delta g d^3}{\nu^2}; \tag{3.16}$$

Finally, the coefficients C_1 and C_t are:

$$\begin{aligned} C_1 &= 0.055 \tanh\left(12 A^{-0.59} \cdot e^{-0.0004A}\right) \\ C_t &= 1.06 \tanh\left(0.016 A^{0.5} \cdot e^{\frac{-120}{A}}\right) \end{aligned} \tag{3.17}$$

3.3.7 Results of the calculations

The results from the calculations in Subsections 3.3.2, 3.3.3, 3.3.4, 3.3.5 and 3.3.6 are displayed in Table 3.3.

Table 3.3. Numerical values of the sediment characteristics.

Constant	Summer	Winter
h_c [m]	6.25	8.01
θ_c	0.0048	0.0048
θ'	0.0043	0.0145
κ [m]	0.0087-0.0349	0.0217-0.0869
ω [m/s]	0.0289	0.0289

It can be observed that the value of the critical Shields parameter is very close to the default value (0.0045), which is recommended by the *User Guide* to maintain [MIKE by DHI, 2016]. On the other hand, the depth of closure is in well agreement with the plots in Subsection 2.2.2.

The numerical value for all the parameters used in the calculations are in display in Table B.1 in Appendix B.2.

3.4 Definition of climatic characteristics

The climatic characteristics that are defined in this section are: wave heights, wave periods, wave directions, event duration, current and water level variation

3.4.1 General aspects

As the beach erosion is not a phenomena dependent on one single climatic variable, it is necessary to define a model that can gather information from the different factors that influence the erosion, and the relations in between those.

In order to make use of the climate data and establish a proper relation with the beach erosion, it is defined a set of variables that represent the climate of Nørlev Strand. Each of the variables that compose the climate is described statistically. Several authors have proposed different combinations of variables. De Michele et al. [2007] proposed to use a combination of sea storm significant wave height, H, storm duration, D, storm direction, A and interval in between consecutive storms, I. Corbella and Stretch [2012], proposed a similar combination as De Michele et al. [2007] but adding as well the water level, W and wave period T. Finally, Li et al. [2014] chose a combination of maximum significant wave height, $H_{s,max}$, peak wave period, T_p, peak water level, h and wave direction, θ_p.

In this project, it is selected to use:

- Maximum significant wave height, $H_{m0,M}$
- Peak wave period, $T_{p,M}$
- Wave direction, A_M
- Event duration, D

The time interval in between storms is inversely proportional to the erosion. The longer the time in betweens storms, the longer the time provided to the beach to recover from the event [Corbella and Stretch, 2012]. However, this variable will not be consider due to the characteristics of the numerical model. The chosen model does not take into consideration beach recovery, or even changes in the beach profile due to the effect of the storms. As a consequence, the coastal erosion is considered independent from the inter-arrival time of the storms.

In relation to the water level, the data is not appropriate to asses the joint behaviour of water level with any of the other variables. The water level variation is obtained from a different source and with different temporal characterization.

The selection of the variables serves to the purpose of describing a particular reality. For example, for offshore applications, two typical variables to correlate are wind speed and wave height [Morton and Bowers, 1996], which are two very important parameters in the determination of the structural response. In this project, the goal is to be able to generate a set of realizations of the aforementioned variables that are at all times representative of the typical climate of Nørlev Strand [Baptista et al., 2014], and that can describe the long term variations of the coast. The generated set of realization represents a year of time. With the current data would only be possible to simulate the effects of the climate from 1999 until 2012. However, with a statistical model of the climate it is possible to create a climate that can be adapted to different conditions in different periods of time, and that is independent from seasonal effects. This latter, would be the case if the simulations were carried out with the data from a specific year.

A standard procedure consist on treating each variable individually and fitting them to marginal distributions. Then, the variables with the same return period are combined by means of combination factors. However, these variables are not independent from each other, and not considering their degree of dependence increases the subjectivity in the quantification of their effects [Martín-Hidalgo et al., 2014]. If designing a structure, this approach would be sufficient, but the objective is to asses an existent erosive trend as accurately as possible. As a consequence, an alternative to this approach is to construct a formulation to describe the dependence structure of the variables [De Michele et al., 2007], [Li et al., 2014], [Corbella and Stretch, 2012], [Haver and Nyhus, 1986], [Martín-Hidalgo et al., 2014]. All in all, in this section not only the individual treatment of the variables is described, but also how the relation in between them is obtained.

3.4.2 Significant wave events

Not all the data is used, instead, a selection of relevant events is done, based on the steps to perform a extreme value analysis [Morton and Bowers, 1996].

In principle, despite of the separation of the wave data in the four groups exhibited in Table 2.1 of Subsection 2.1.3, only the summer/winter separation is maintained. The objective is to asses whether the separation of Table 2.1 is correct or not. The data in summer and winter is originally separated in 8 directions, and the following procedure applied independently for all of them.

Four direction sectors are neglected from the beginning, which are NE, E, SE and S.

Waves coming from those sectors have no direct influence over the coast of Nørlev Strand, as discussed in Subsection 2.1.3.

The definition of significant events is based on the wave heights. The significant event is defined as the set of wave heights that exceed a certain threshold, ξ, and that form an independent group of values respect to the rest of the data.

First it is defined an initial ξ. The wave heights that exceed ξ are extracted from the data. Those values over the threshold are separated in significant events by declustering the data. Declustering, in this context, means imposing that there is a certain temporal separation in between those events, in order to be consider independent phenomena [Morton and Bowers, 1996] [Liu and Frigaard, 1999].

In this project, ξ is different for the 8 directions and different for each season. It is chosen 24 h as cluster interval, or time in between significant events. If two values over the threshold are separated 24 h or less, they belong to the same event. Figure 3.3 illustrates this concept.

From each significant event, it is extracted the maximum significant wave height. These maximums are, as well, a group of independent values, that are potential extreme wave events [Morton and Bowers, 1996]. In order to reduce the statistical uncertainty, at least 25 to 30 values have to be extracted [Sørensen, 2011]. Once obtained the maximum of each significant event, those are fitted to different probability distributions and the fitting error is found.

In this manner, a partial data set of individual events are defined. This procedure is also called peak over threshold method (POT) [Liu and Frigaard, 1999].

It is important to note that the values used in the fitting depend directly on the selection of ξ, and so the parameters of the distribution and the results derived from this distribution [Baptista et al., 2014]. Due to this fact, this procedure is programmed as an iteration. The value of ξ and the chosen distribution are the ones that minimize the fitting error.

In this point is when it is done the selection of the representative sectors. Two problems were presented: either the thresholds that allowed the inclusion of all sectors were too low, and as a consequence, the fittings were poor; or there were not enough values per sector in order to reach the required 25 to 30 values, when a larger ξ was used. The only two sectors that had enough values to constitute a representative sample were $[250° - 295°]$ and $[340° - 25°]$, which are the same sectors chosen initially.

The candidate distributions used in this procedure are

- Generalized Pareto distribution
- Generalized extreme value distribution
- Weibull 2-parameter distribution
- Gumbel distribution

The fitting method used is the Maximum Likelihood Method, and the fitting error is obtained through the normalized mean squared error, NMSE. The NMSE is defined in the

interval $[1, -\infty)$. The closer to 1, the better the fitting [MathWorks, 2017b].

$$NMSE = 1 - \frac{(x_{data} - x_{distr})^2}{(x_{data} - mean(x_{data}))^2} \tag{3.18}$$

However, this error function quantifies how good is the overall fitting. It has to be remembered that the type of fitting depends also on reality represented by the stochastic variable. For example, for design loads it is recommended to pay extra attention to the upper tail fitting. In this case, the NMSE is sufficient, as it is pretended an overall agreement with the original climate.

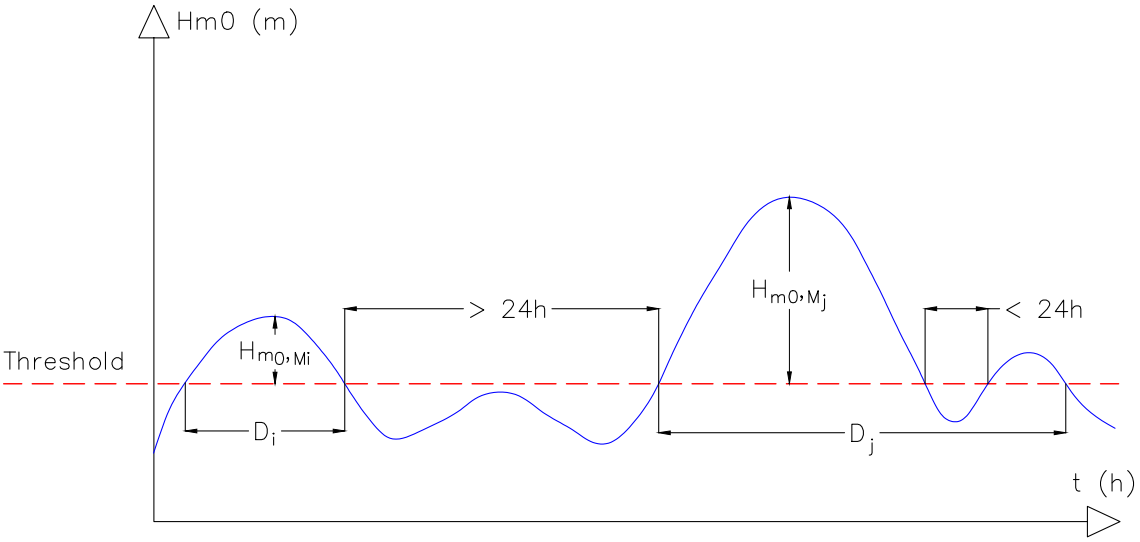

Figure 3.3. Graphic explanation of the significant event. On the image two significant events are presented, with their correspondent associated variables.

Having defined the concept of significant wave event, it is possible to narrow down the definition of the variables used:

- $H_{m0,M}$ is the maximum significant wave height within the temporal span of the significant event.
- $T_{p,M}$ is the peak wave period associated with $H_{m0,M}$
- A_M is the wave direction correspondent to $H_{m0,M}$
- D is the total time interval that spans the significant event, and where it is fulfilled that $H_{m0} > \xi$

A similar definition for the variables was used by Li et al. [2014].

3.4.3 Wave height

As explained in the previous subsection, the wave height is the principal parameter in the definition of the significant events. The results from the iterative process that lead to the definition of an appropriate threshold, exhibits the following results:

Table 3.4. Probability distributions used to fit the wave data, threshold and fitting error.

Group	ξ [m]	Distribution	Parameters (k,σ,μ)	NMSE
G1	1.7	Generalized Extreme Value	(0.32, 0.24, 1.96)	0.90
G2	2.7	Generalized Extreme Value	(0.35, 0.23, 2.94)	0.92
G3	2.7	Generalized Extreme Value	(0.52, 0.30, 3.00)	0.88
G4	3.9	Generalized Extreme Value	(0.31, 0.43, 4.34)	0.86

Wave input in Littoral processes FM

The wave heights are input together with duration, direction, period and spreading factor. The spreading factor is set as the default value (0.5). These four variables can be input as constant values or in the form of a time series. For most of the studies made it is considered that these parameters are variable in time, however, for the studies of profile length and resolution, constant values are sufficient.

Littoral Processes FM uses two different spectral descriptions for the individual wave heights. On one hand, it uses Rayleigh waves and on the other hand it uses Battjes and Janssen formulation [MIKE by DHI, 2016]. The main difference in between using Rayleigh and Battjes and Janssen formulations, is that the first one is more conservative, as it does not take into consideration wave breaking due to limited water depth [Liu and Frigaard, 1999]. As a consequence, the waves that propagate towards the coast are larger than when using Battjes and Janssen. In 4.2.8 it is quantified the difference in between one formulation and the other.

Both formulations use H_{rms}, which relation with the H_{m0} used in this project is through the mean wave height as [Liu and Frigaard, 1999]:

$$\begin{aligned} H_{rms} &= 1.13 \cdot \overline{H} \\ H_s &= 1.6 \cdot \overline{H} \\ H_{m0} &= 1.07 \cdot H_s \end{aligned} \tag{3.19}$$

The User Guide [MIKE by DHI, 2016], does not recommend to use Battjes and Janssen if the profiles are not sufficiently long. This is the case of this project, and therefore, Rayleigh formulation is used.

3.4.4 Mean wave direction

Instead of appealing to the source of weighting the contributions from the different directions depending on the proportions found in the wave roses, it is decided to use a statistical description of the variable.

From the definition of the significant event, it has been established that the wave direction correspondent to the maximum significant wave height of each event, A_M is taken. All of these values constitute a set of data that have to be fitted to the candidate distributions.

Westerly directions, [250°−295°], are fitted separately from norterly directions, [340°−25°]. De Michele et al. [2007] consider also two main directions, but both are fitted to a single beta distribution. However, in this case it was not possible to achieve a good fitting with a single distribution, and therefore, both sectors are treated separately.

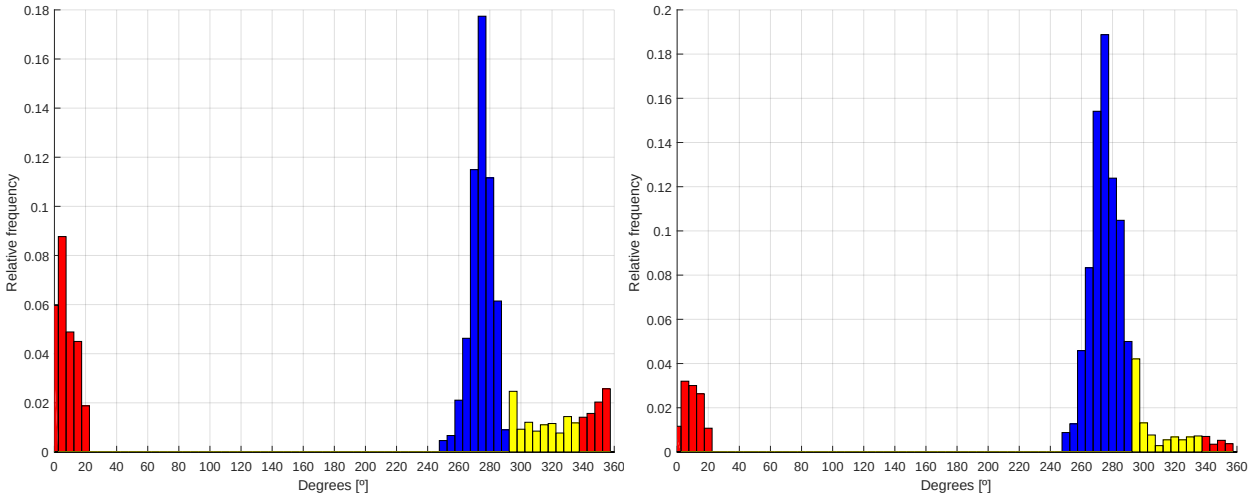

Figure 3.4. Histogram of A_M. Left: A_M in summer. Right: A_M in winter.

Figure 3.4, shows a histogram of frequencies with the A_M values, for both summer and winter. Red values are northern directions and blue values are western directions. The values in yellow does not correspond to the selected sectors. Even though, due to the fitting made, some of those values where used. The candidate distributions for the directions are:

- Lognormal
- Normal
- Weibull 2-param
- Generalized extreme value

The results from the fitting are displayed in the table below:

Table 3.5. Distributions used to fit the mean wave directions and fitting error.

Group	Distribution	Parameters	NMSE
G1	Generalized extreme value	(k: -0.44, σ: 9.39, μ: 366.01)	0.99
G2	Weibull	(a: 281.42, b: 44.42)	0.99
G3	Weibull	(a: 373.50 b: 53.80)	0.98
G4	Generalized extreme value	(k: -0.54, σ: 9.37, μ: 278.20)	0.99

Note: *In order to fit the northern sector to a distribution, it has been applied a linear translation to the directions from* $0°$ *to* $25°$ *to avoid the discontinuity shown in the figure. Observe that this is the reason why* μ *for G1 and a for G3 are larger than 360.*

3.4.5 Event duration

In order to define the duration of the storms, two methods were used:

The simplest one consist on extracting the duration values associated to the definition of significant event and fitting those to the candidate distributions. The other method is based on the definition of storm magnitude.

First method: significant event

The duration of the events is directly defined from the significant event. The duration of the event, D_e is defined as the time in hours since the first wave exceeds the threshold, until the time when the last wave exceeds the threshold, followed by a period of 24 h with no more crossings. The durations correspondent to each event compose a set of values that are fitted to the candidate distributions. The results are displayed in the following table:

Table 3.6. Probability distributions used to describe the event duration, and fitting error. First method.

Group	Distribution	Parameters	NMSE
G1	Weibull (2-param)	a: 20.96, b: 1.60	0.95
G2	Generalized extreme value	k: 0.31, σ: 7.63 μ: 9.39	0.97
G3	Generalized extreme value	k: 0.40, σ: 5.32 μ: 8.44	0.96
G4	Weibull (2-param)	a: 15.00, b: 1.24	0.97

Second method: storm magnitude

This approach is linked to the establishment of a correlation in between $H_{m0,M}$ and D. The sea storm magnitude, M is a variable that binds H and D, which are the two principal varibles used in the characterization of the energy of the storm [De Michele et al., 2007]. In the simplest case, described by Boccotti [2000], the storm presents a triangular shape, and thus, M is defined as:

$$M = \frac{1}{2}(H - \xi) \cdot D \tag{3.20}$$

where the factor $H - \xi$ is the wave height over the threshold.

Several shapes for the storm magnitude as well as methods to calculate them have been referred by numerous authors. The suitability of one shape or another depends on the type of waves considered - sea waves, swell waves or both -. According to Martín-Hidalgo et al. [2014], the shape that adapts best to both sea and swell is the trapezoid [Soldevilla et al., 2015].

The method selected to build the storm shape is the Equivalent Magnitude Storm (EMS), described by Martín-Hidalgo et al. [2014]. This approach is based on the fact that different pairs (H, D) lead to the same M [De Michele et al., 2007]. As the significant event is defined with the same principle as the storm of De Michele et al. [2007], Martín-Hidalgo et al. [2014], Boccotti [2000] and Soldevilla et al. [2015], in order to determine the magnitude of the storm $H = H_{m0,M}$ and D are used.

The following procedure is explained in Soldevilla et al. [2015].

After the data is declustered, ξ is subtracted from all H_{m0} of each significant event, obtaining the event in terms of equivalent wave heights, $H_{m0,eq}$. Next, the real magnitude of the storm is calculated as follows:

$$M = \int_0^D (H_{eq}(t))dt \tag{3.21}$$

In order to calculate the shape that is representative of the climate, all of the significant events have to be transformed. All $H_{m0,eq}$ are divided by the maximum wave height of the event, $H_{m0,M,eq}$. Then, the time axis is divided by the total duration, D of the event, obtaining a scale that goes from 0 to 1. The result is a new array of unit significant events, with maximum wave height of 1 m, total duration 1 h, and random shape.

Each unit significant event is approximated by a trapezoid shape by obtaining the two vertices that encompass better the total area. In this manner, each unit significant event becomes a unit trapezoid. Finally, it is calculated the mean position of the two vertices for each individual unit trapezoid. The result is the equivalent trapezoid, with area M_{eq}. For each wave group a M_{eq} is calculated. Figure 3.5 contains a graphic explanation of the construction process. In the Appendix B.3 the storm shaped for each wave group are plotted.

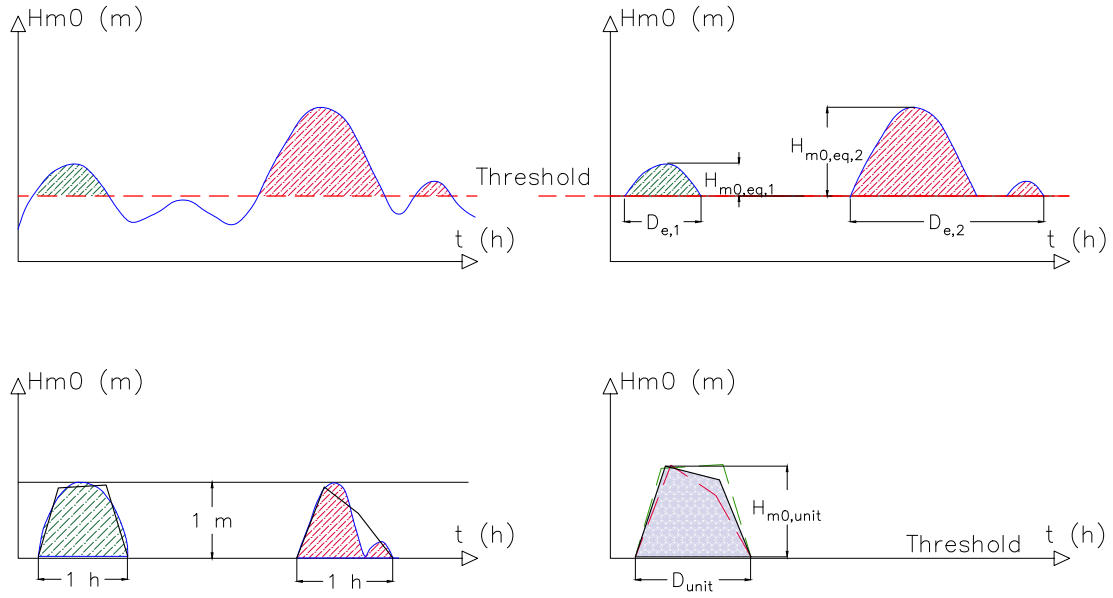

Figure 3.5. Calculation process of the EMS. Top left: definition of magnitude. Top right: calculation of individual event durations and significant equivalent wave heights (over threshold). Bottom left: scaling to unit dimensions and fitting to trapezoids. Bottom right: unit trapezoid by calculating the average of all events (enlarged for clarification).

Finally, the new duration for each significant event, D_t is determined from Equation (3.22), as it is the only unknown. This equation states that the area of M_{eq} scaled by $H_{m0,eq}$ and D_t results in the real area of the storm.

$$M_{real,i} = M_{eq} \cdot H_{m0,eq,i} \cdot D_{t,i} \tag{3.22}$$

Once again, this durations are fitted to a marginal distribution. Table 3.7 summarizes the

results.

Table 3.7. Probability distributions used to describe the event duration, and fitting error. Second method.

Group	Distribution	Parameters	NMSE
G1	Generalized extreme value	k: 0.33, σ: 8.87, μ: 11.82	0.97
G2	Generalized extreme value	k: 0.31, σ: 6.66, μ: 8.71	0.93
G3	Generalized extreme value	k: 0.48, σ: 4.99, μ: 8.00	0.95
G4	Weibull (2-param)	a: 14.52, b: 1.37	0.97

Duration input in Littoral Processes FM

There are three possible time formulations: real time, scenario formulation in time and individual scenario events [MIKE by DHI, 2016]. As explained before, what is simulated is a period of one year. The time series that groups together wave, period, direction, spreading factor and duration, is a result from a statistical representation. Each of the events represented are independent from each other, and therefore it is used the formulation of individual scenario events. By using this formulation, it is avoided the necessity of describing the time interval in between consecutive events. The duration of each event is defined as percentage of the year and it is obtained by dividing the duration of each event by the duration of a full year of 365 days.

3.4.6 Wave period

In order to calculate the wave period, it is assumed that the relation in between peak period and significant wave height can be described linearly through the following expression [Liu and Frigaard, 1999, p.60]:

$$T_p = \sqrt{\frac{\beta \cdot H_s}{g}} \tag{3.23}$$

where β is a parameter to be estimated through linear fitting.

Four β values are obtained, according to the criteria established in Table 2.1. The linear fitting is made only with the $H_{m0,M}$ values and their concomitant $T_{p,M}$. In the project, the wave height used is H_{m0}, but as the formulation requires H_s, the following relation is applied:

$$H_{m0} = 1.07 \cdot H_s \tag{3.24}$$

Both wave heights are approximately equal, and it is a common practice to assume $H_{m0} > H_s$.

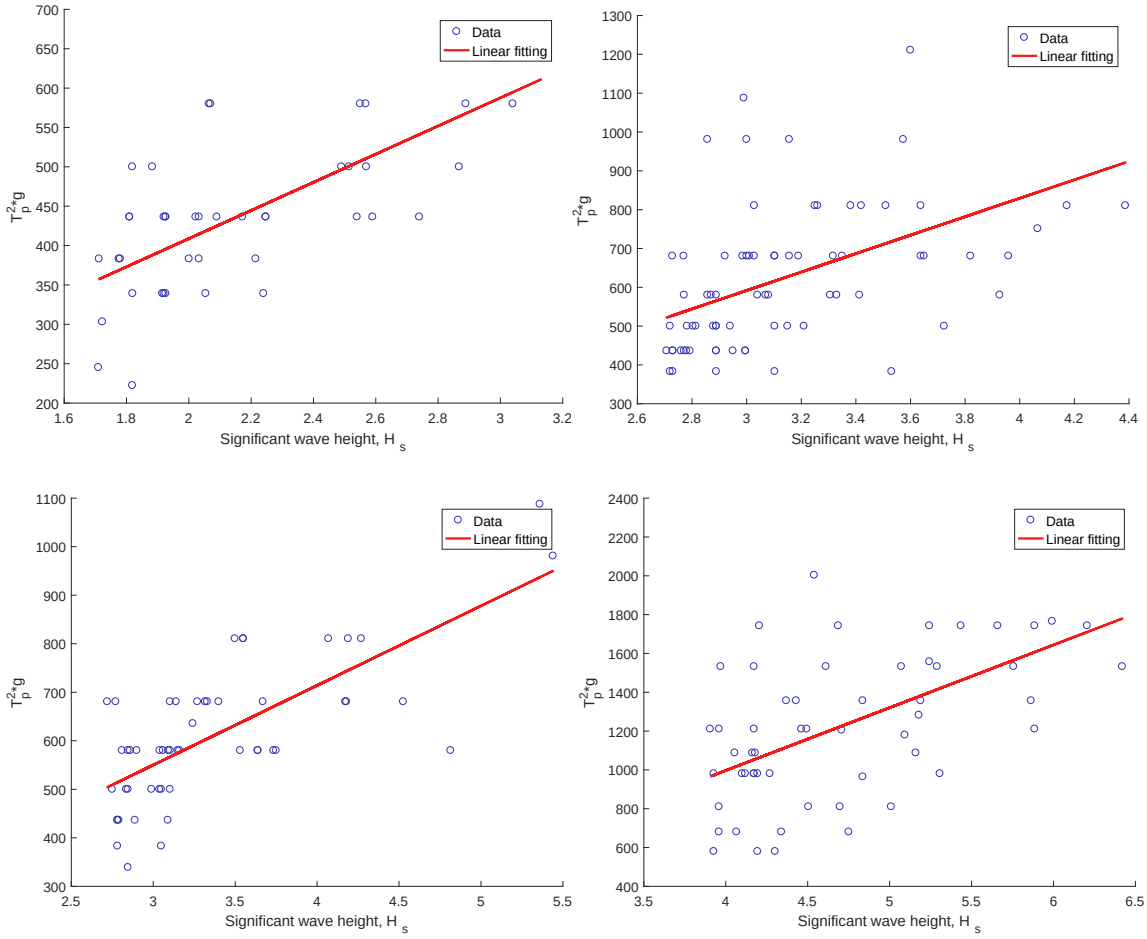

Figure 3.6. Linear fitting to H_s and T_p^2/g. β is defined as the slope of the curve. Left top: G1. Right Top: G2. Left bottom: G3. Right bottom: G4.

As seen from the Figures 3.6, the fitting is made separately for each wave group. As the waves are mostly fetch limited, the periods of the waves from the West tend to be larger than the periods from the waves from the North, as the distance they span is significantly different.

The numerical results of β are summarized in the table below:

Table 3.8. β values

Group	β
G1	179
G2	238
G3	164
G4	323

These results are in good agreement with the interval suggested by Liu and Frigaard [1999] (Equation (**??**), except for β in G4, which is larger than expected.

$$130 < \beta < 280 \tag{3.25}$$

It is also evaluated the linear correlation coefficient in between $H_{m0,M}$ and $T_p^2 \cdot g$ for the four wave groups. This is done through Pearson's ρ. The results can be seen in Table 3.9.

Table 3.9. Linear correlation coefficients for $T_p^2 \cdot g$ and $H_{m0,M}$, and R^2.

	Pearson's ρ	R^2
G1	0.668	0.51
G2	0.599	0.25
G3	0.755	0.53
G4	0.574	0.32

Finally, in order to check the goodness of the linear model, Table 3.9 also shows the coefficient of determination, R^2, which is used to asses the quality of the linear fitting:

$$R^2 = 1 - \frac{\sum_{i=1}^{n}(y_i - \hat{y}_i)^2}{\sum_{i=1}^{n}(y_i - \overline{y})^2} \tag{3.26}$$

The closer to one, the better predicted is the model [MathWorks, 2017a].

It is clear that not considering a correlation in between $T_p^2 \cdot g$ and $H_{m0,M}$ is a wrong assumption, however, it is also possible to see, not only from the plots in Figure 3.6 but also in the Table 3.9 that there is no full correlation in between them. As all Pearson's ρ are larger than 0.5, it is decided that is sufficient for the model and though, adopted being aware of its limitations.

Period input in Littoral Processes FM

The module uses different wave periods when using one spectral formulation or the other. If Rayleigh formulation is used, the zero-upcrossing period, T_z is used, while if Battjes and Janssen is used, the peak period, T_p, is utilized. According to Badulin [2014], T_a, the mean over spectrum period defined by Hwang et al. [1998] is equivalent to the T_z. Moreover, Badulin [2014] states that all periods are related by a certain coefficient. In the case of the T_p, used in this project, and T_z expected for Rayleigh formulation, the relation according to Hwang et al. [1998] is:

$$\frac{T_p}{T_z} = 1.29 \pm 0.14 \tag{3.27}$$

3.4.7 Currents

No currents are input to the module. However, Littoral Processes FM is able to calculate the currents generated locally in the area of interest, from the momentum balance equations and from the radiation stress.

3.4.8 Water level variation

One input of high relevance in the calculations is the water level variation. In this case, only the water level variation due to astronomical tides is treated. Littoral Processes FM

calculates the wave setup and storm surge from the point in which the known water level variation is input, which is the first grid point of the bathymetry (offshore). As the total water level variation is not known is the first grid point, only the astronomical tides are input, assuming that they are uniform in the whole area.

As forwarded in Subsection 2.1.1, there are two sources for the determination of the water level variation. It is assumed that the tides can be described as a stationary process, due to the fact that astronomical tides depend on the action of the Moon's and Sun's gravity over the Earth's surface [Madsen, 2003].

From the tidal tables of the DMI [Nielsen, 2015], as the data is referenced to the lowest astronomical tide, the total water level variation due to the tides is obtained directly. In average, the water level variation is 178 cm and the maximum water level variation is 0.4 m.

From the Sea level station monitoring facility of UNESCO/IOC and the Flanders Marine Institute [VLIZ] it was obtained a month of water level variation measurements. As the data covers not only astronomical tides, but also wave setup, storm surge, etc., it was necessary to bandpass the signal to separate the astronomical tides. Once separated, the astronomical tide component is fitted to a probability distribution. Nørlev Strand is located in between 57° and 58° latitude. According to Raichlen [2014], around these latitudes both high and low tide have almost the same magnitude. Added to the fact that we are in front of a stationary process, it is decided to use the normal distribution to describe tides. The quality of the fitting is assessed with the NMSE, which is 0.955 for the astronomical tides.

The high tide is obtained by calculating the 98% quantile of the astronomical tide distribution, while the low tide is obtained equally but using the 2% quantile, therefore they have the same absolute value. The total water level variation due to the astronomical tides from this calculation is 0.42 m.

It is decided to utilize the result of the astronomical tides obtained from the Sea level monitoring facility, as the result is more conservative, and comes from actual measurements. The other components of the water level variation are not used in this project. As the measurements are obtained from only one month, they are subdued to seasonal effects and cannot make a representative picture of the actual phenomena.

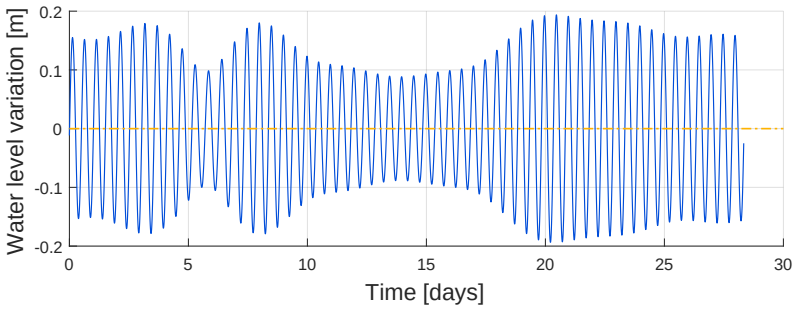

Figure 3.7. Astronomical tide in one month.

The period that can be read from the graph is a 12 h period, and it is clean from other frequencies. However, there are some distortions around day 6th, and the plot does not

reach 30 days. This latter is due to the fact that the data is not complete. The plot obtained for the tides, agrees quite well with what can be expected from this latitude [Madsen, 2003].

3.4.9 Analysis of correlation in between climate variables

As stated at the beginning of the section, the goal behind this analysis is to find a proper way of evaluating the joint behaviour of the climate variables. Nor the correlation with water level variation, nor the correlation with currents is object of this subsection. In case of the water level, as explained in subsection 3.4.1, it is not possible to make a relevant correlation with the available data, while in the case of the currents, there is no data available.

Here only the correlation in between $H_{m0,M}$, $T_{p,M}$, D_e or D_t and A_M is treated. In subsection 3.4.6 is shown how $T_{p,M}$ and $H_{m0,M}$ are correlated, therefore it is sufficient to explain the joint behaviour of $H_{m0,M}$, D_e or D_t and A_M. This latter is studied by means of *copulas*.

Quantification and qualification of the correlation

It is interesting to evaluate how necessary is to consider the correlation in between the variables. Table 3.10 shows the linear correlation coefficients for the pairs of variables (A_M,D_e), (A_M,D_t) ($H_{m0,M}$,A_M), ($H_{m0,M}$,D_e) and ($H_{m0,M}$,D_t), and for every wave group. Each of them have a different degree of correlation. The linear correlation is quantify to Pearson's ρ.

Table 3.10. Pearson's linear correlation coefficient

Group	A_M,D_e	A_M,D_t	$H_{m0,M}$,A_M	$H_{m0,M}$,D_e	$H_{m0,M}$,D_t
G1	0.05	0.04	0.04	0.86	0.82
G2	0.11	0.15	0.08	0.67	0.58
G3	0.20	0.23	-0.01	0.62	0.63
G4	0.16	0.26	0.32	0.69	0.74

From Table 3.10 the correlations (A_M,D) and (A_M,$H_{m0,M}$) in G1, are negligible, while the others are very small. This is due to the fact that the correlation coefficients used cannot describe properly the manner in which both variables correlate. However, is the linear correlation coefficient the one that is used further to describe the dependence structure in between variables.

In Figure 3.8, the climate variables are plotted against each other. The two top plots represent D_e and $H_{m0,M}$ against all possible directions. Similar as in Figure 3.4, the events accumulate around the two directions selected as significant for this project. In the top right plot can also be seen how the waves above most wave thresholds are predominantly coming from the west and the north.

The plots in the bottom of Figure 3.8, are only plotted for the significant directions selected, as the calculation of the storm magnitude was done only for the significant events coming

from North and West. Both D_e and D_t show the same behaviour respect to $H_{m0,M}$.

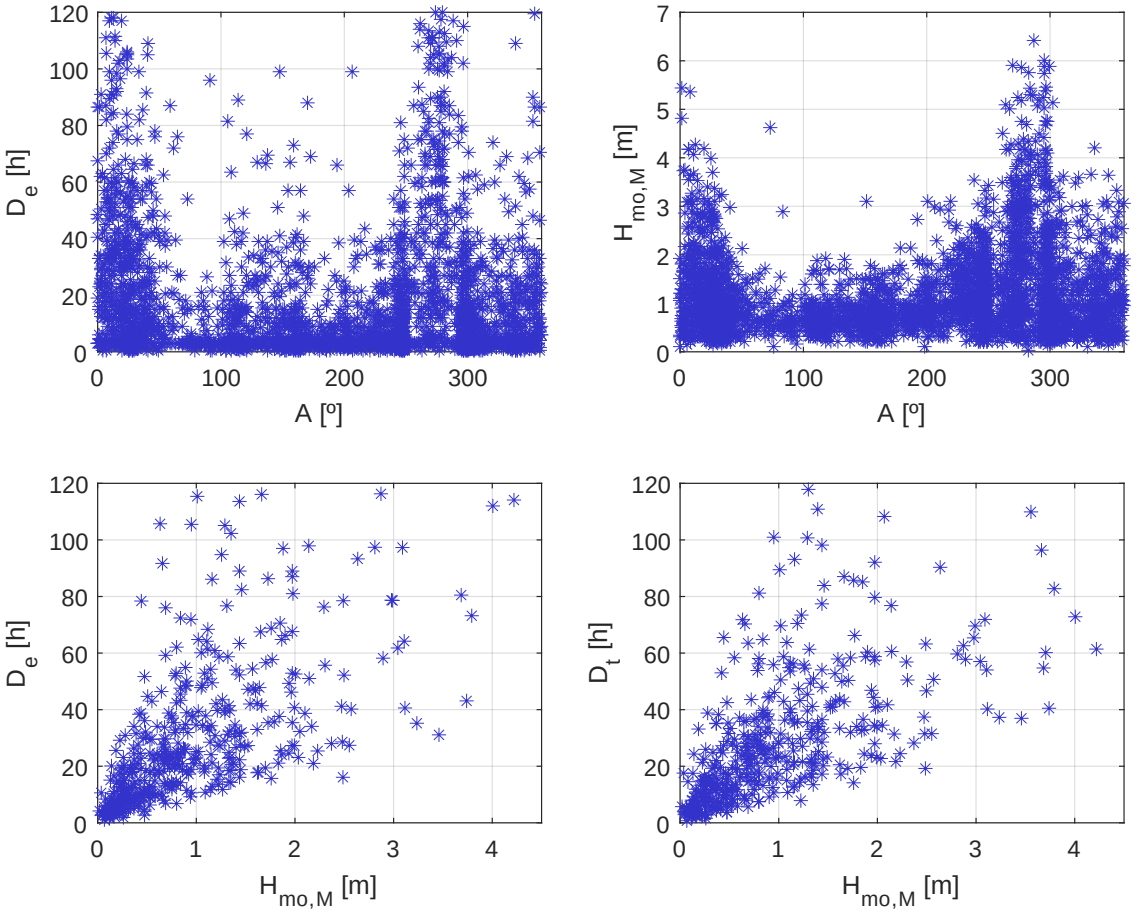

Figure 3.8. Relation in between climate variables. Top left: D_e against A (all directions). Top right: $H_{m0,M}$ against A (all directions). Botom left: D_e against $H_{m0,M}$ (significant directions plotted). Botom left: D_t against $H_{m0,M}$ (significant directions plotted)

Multivariate distributions: Copulas

As explained by De Michele et al. [2007] and Li et al. [2014], a copula is a n-dimensional function that describes the dependence between two stochastic variables, by means of their marginal probability distribution functions.

The description of the dependence structure is independent from the actual marginal distributions, and as a consequence, there are no restrictions when choosing them. On the other hand, using a joint distribution is out of the possibilities of this project, due to the fact that there is not available an empirical formulation that relates H, A and D.

Copulas in this project are used in order to generate a set of realizations from a group of correlated variables [Li et al., 2014]. In this manner, it is possible to increase the amount of data use for simulations as well as to obtain new realizations of the climate variables that have the same dependence structures as the observed ones. The new realizations are generated randomly.

In simple terms, a copula can be defined as a function that transforms a probability in an

n-dimensional space into a 1-dimensional space.

$$\mathbf{C} : [0,1]^n \rightarrow [0,1] \tag{3.28}$$

The n-dimensional cumulative distribution function can be written as:

$$F(x_1, ..., x_n) = \mathbf{C}(F_1(x_1), ..., F_d(x_d)) \tag{3.29}$$

where $F_1(x_1), ..., F_d(x_d)$ are the marginal cumulative distribution functions, F is joint cumulative distribution function of the marginals and $\mathbf{C}$ is the n-copula. Based on Sklar's theorem, if $F_1(x_1), ..., F_d(x_d)$ are continuous functions, which is the case for all marginal distributions in the project, then C is unique [Nelsen, 2007].

In this project the multivariate normal copula and the Gumbel copula are used. The multivariate normal copula belongs to the Gaussian or elliptical copula class, and its dependence structure is modelled in terms of the linear correlation matrix [Yan et al., 2007], constructed from Pearson's ρ. Equation (3.30), is used to determine the Guassian copulas.

$$C(u_1, ...u_n) = F\left(F_1^{-1}(u_1), ..., F_p^{-1}(u_n)\right) \tag{3.30}$$

Gumbel copula is a one-parameter family within Archimedian copulas. Archimedian copulas are constructed from a generator function, φ. φ is a n-monotonic function which formulation depends on the Archimedian family considered [Yan et al., 2007] [Nelsen, 2007].

$$C(u_1, ...u_n) = \varphi^{-1}\left(\varphi(u_1) + ... + \varphi(u_n)\right) \tag{3.31}$$

Equation 3.31 corresponds to the expression of Archimedian copulas in terms of the generator φ, while Equation (3.32) [Yan et al., 2007] [Nelsen, 2007] contains the generator and its inverse. θ is the copula parameter, which has to be estimated when fitting the copula to the data. θ for Gumbel family fulfils that $\theta \leq 1$.

$$\begin{aligned} \varphi(t) &= (-\ln(t))^\theta \\ \varphi^{-1} &= \exp\left(-t^{1/\theta}\right) \end{aligned} \tag{3.32}$$

where [Nelsen, 2007]:

$$\varphi(t) = \varphi(u_1) + ... + \varphi(u_n) \tag{3.33}$$

Gumbel family depends on rank correlation coefficients, either Spearman's or Kendall's.

According to De Michele et al. [2007], the statistics of M are directly related to bivariate distribution of the pair (H,D). Indeed, De Michele et al. [2007] shows that the difference in between the empirical distribution of M and the distribution generated with a bivariate function of (H,D) is negligible. In based of this, two approaches are used to correlate the variables:

- Construction of a bivariate copula (M,A) and link Tp to H linearly
- Construction of a three variate copula (H,D,A) and link Tp to H linearly

Bivariate copula *(M,A)*

The first attempt to correlate the variables is made through the bivariate copula $\mathbf{C}(M, A_M)$. First it is necessary to fit M to a distribution function. Following the steps as for the previous calculations, four distributions, one for each wave group are obtained:

Table 3.11. Probability distributions used to describe the event magnitude, and fitting error.

Group	Distribution	Parameters	NMSE
G1	Generalized Pareto (2-param)	k: 0.16, σ: 22.81	0.97
G2	Generalized Pareto (2-param)	k: 0.07, σ: 8.57	0.96
G3	Generalized Pareto (2-param)	k: -0.08, σ: 20.33	0.98
G4	Generalized Pareto (2-param)	k: -0.06, σ: 27.53	0.98

In this case only two variables are being correlated, therefore a bivariate copula is used. It is decided to use an Archimedian copula. From the catalogue of MATLAB, only three families are available: Clayton, Frank and Gumbel families. These three families are fitted to the realizations of both variables in order to estimate θ. The fitting cannot be done directly to the realizations, but it has to be done in the space $\mathbf{[0,1]}^2$. The marginal distributions are used with this purpose; using the inverse cumulative distribution functions of both M and A_M, the probability associated to each realization is obtain. Having these probabilities, it is possible to estimate the copula parameters. In Table 3.12 it is shown the value of the copula parameter θ as well as the 95% confidence interval of the estimation.

Table 3.12. Probability distributions used to describe the event magnitude, and fitting error.

Group	θ	95% confidence interval
G1	1.04	[0.91-1.18]
G2	1.00	[0.84-1.16]
G3	1.04	[0.91-1.18]
G4	1.07	[0.95-1.19]

θ for a Gumbel copula belongs to the interval $\mathbf{[1,\infty)}$ [Yan et al., 2007] [Nelsen, 2007].

Trivariate copula *(H,D,A)*

The construction of the trivariate copula, requires again the transformation of the realizations of the three variables into probability, i.e., the $\mathbf{[0,1]}^3$ space. The marginal distributions used are the ones obtained as results in the previous subsections. Two trivariate copulas are calculated: one by using D_e and the other one by using D_t. MATLAB is again used to obtain the copula. The only copula class that can be easily generalized to higher dimensions than two is a Gaussian copula. It is selected arbitrarily to work with the normal multivariate distribution function. The only requisite to generate random samples using this kind of copulas is to use the linear correlation matrix as input. The correlation coefficients used were already shown in Table 3.10.

Implementation and results 4

4.1 Generation of climate realizations: climate model

In this first section of Chapter 4, it is shown the application of the climatic model to the project. After considering all data gathered in the preliminary studies of Chapter 2, and having explained the tools to generate realizations having correlated variables, the application comes straight forward.

The generation is programmed by using MATLAB. The product is a climatic model that has to be tested and calibrated before applying its results to Littoral Processes FM. With this model, not only random samples can be generated, but also the output can be modified depending on the required design conditions, or the period of time when the simulation takes place, i.e., climate change can be taken into account.

4.1.1 Inputs for the generation model and calibration

The generation creates realizations for a particular year. Knowing this, the following list of inputs apply:

- *Parameters to describe the marginal distributions of each variable.* Necessary to construct the copula.
- *Amount of events to generate per year.* It is a calibration parameter. Influences the stability of the results.
- *Year of generation.* Corresponds to the year in which the simulation takes place. Influences the wave height.
- *Proportion in which wave groups are combined.* It is a calibration parameter. Mainly influences the predominant mean wave direction.
- *Effective event duration.* It is a calibration parameter. Actual time that significant events represent respect to the totality of the year.
- *Selection of a event duration: D_e or D_t.* It becomes another parameter to test. The duration that leads to more stable results and closer to the reality is kept.

Amount of events per year

A priori, it seems that this parameter controls the fraction of the year in which significant events take place. However, the individual duration of each event can be scaled, such as the total duration (effective duration) is kept constant.

The amount of events per year is studied by doing a convergence study. Figure 4.1 is build by simulating 25 different climates of a certain number of elements. First, suppose that 25 climates of 50 events are generated. It is calculated the mean H, D, and A, of those 50 events for the 25 generations, and thus, 25 mean values for H, D, and A are obtained. The difference in between the maximum and the minimum of these means, is compared with the average of the means, to check the maximum expected variability of the result having different generations.

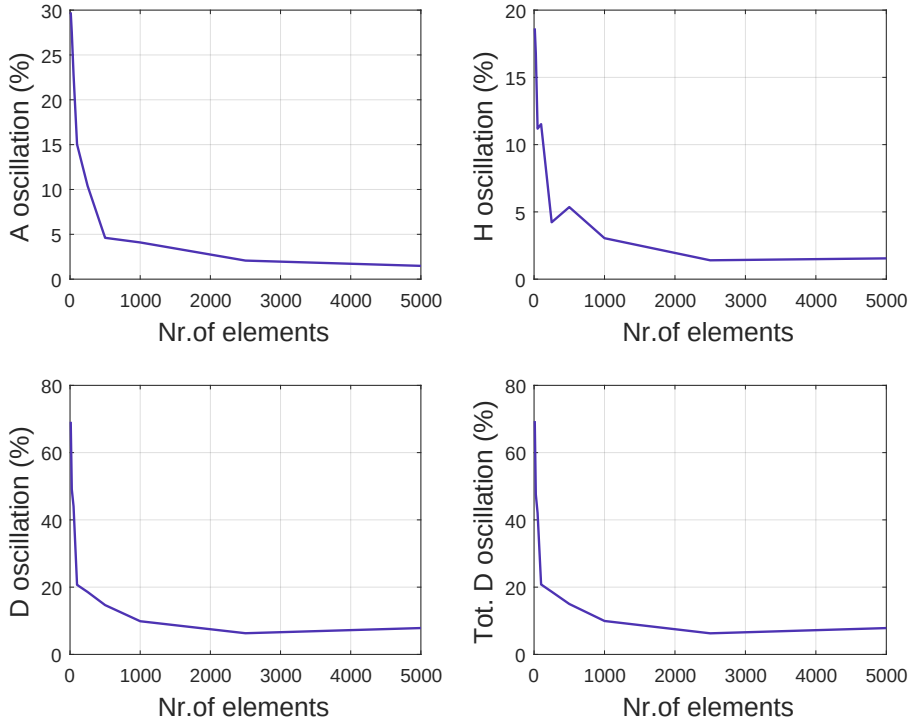

Figure 4.1. Oscillation of the results around the mean value (in percentage), respect to the number of elements used. Each plot represents a different variable under study

The results of the climatic model tend to oscillate around the actual solution, due to the randomness of the generation. The results from the generation are input in the numerical model. The oscillation observed in MATLAB is translated into an even larger deviation from the actual solution of the net sediment transport. Though the ideal would be to secure that the variability of the results is negligible, this cannot be achieve by keeping an optimal performance of the model, in terms of computational time. Nor it is possible to eliminate this uncertainty, as the deviation never oscillates around zero.

The most events generated, the less the solution varies. This is due to the fact that more values within each distribution are taken, and the most extreme events are balanced with the milder events. After 2500 events the solution stabilizes completely. Depending on the type of use given to the climatic model, the result with 2500 events might be the optimal. However, a large set of inputs has two consequences:

- Computational time increases drastically. In rough numbers, 10 events are computed in 2 s, but 50 events in 1 min. Here the difference is large, but moving towards larger amount of elements is found that 500 elements consume 15 min, 1000 elements

30 min and 2500 elements 1.1 h. The computational time is almost proportional to the amount of elements.

- The larger the amount of events, the more extreme events are generated. The mean of the wave heights is stabilized with 2500 events, but in the numerical model it has as a consequence the accumulation of the effects of more events. The extreme events have a particular large affection to the sediment transport, leading to unrealistic results.

Having considered these points, it is decided to adopt 100 events, as it is a comfortable amount of elements from the computational point of view and it is possible to obtain a relatively small confidence interval for the mean of the net sediment transport (see Subsection 4.2.9).

Selection of D_e or D_t

Using D_e or D_t depends on which probability distribution function for the event duration gives a more stable result when generating climates. For each definition of duration, 25 climates are generated and tested in Littoral Processes FM. It is calculated the confidence interval of the mean net sediment transport for both, and as a result D_t is chosen, as it provides the smallest confidence interval. The determination of which duration definition to use can be done immediately after deciding the number of wave events.

Proportions in which the wave groups are combined

Another calibration parameter is the combination factor of wave groups. It affects the main direction of the wave events. In principle, the tendency is for the waves to come from the NW, and the proportions are calibrated to fit with the mean of A_M. It is calculated the average amount of events per year that corresponds to each wave group. 155 events are found in 13 years of data. Table 4.1 shows the initial combination factors, and the combination factors used finally.

Table 4.1. Proportions in which the wave groups are combined

Group	Number of events in 13 years	Initial proportion [%]	Used proportion [%]
G1	50	32	12.5
G2	30	20	40
G3	34	22	12.5
G4	41	26	35

After the first iteration, the proportions are modified until it is obtain a reasonable value for the mean of the net sediment transport. The mean of the net sediment transport must be understood as the result obtained after simulating with 15 different climates. It has been assessed that for 100 events, 15 simulations give a good approximation of the mean net sediment transport, and no new information is added if more simulations are done. Note that the initial proportions are very different from the used proportions. The used proportions, on the other hand, are closer to what is seen in the wave roses of Subsection 2.1.3. The first set of proportionality factors are dependent on the definition of

the significant event which, in turn, depends mainly on how the threshold of the extreme value analysis of the waves is defined. As a consequence, the result of number of significant events is useful in the determination of the probability distribution functions, but not in the description of the real phenomena. The larger the threshold, the less amount of elements are gathered from one wave group.

Effective event duration

An optimal percentage of significant events per year is a 9%. This is found by iteration. The effective duration, the wave proportions and the bed roughness defined in the numerical model are manipulated together to achieve a close result to the one expected in reality.

4.1.2 Selection of copula model and use in the generation model

If considering the 2 dimensional copula for M and A_M, 100 realizations of M and A_M are calculated. In order to be able to apply Equation (3.22), a second equation has to be established. There are infinite combinations of H and D that can give the same magnitude. This is solved by using a linear relation in between H and D as it was made for $H_{m0,M}$ and $T_{p,M}$. However, and as it can be seen in Subsection 4.2.5, this solution is not appropriate.

When considering the 3-dimensional copula for $H_{m0,M}$,A_M and D_e or D_t, also 100 significant events are generated. In this case, the only variable left to consider in the generation is $T_{p,M}$. The copula generates randomly a set contained in the space $\mathbf{[0,1]}^3$. This gives a 100×3 matrix, which columns contain the probabilities for each stochastic variable. These probabilities, are introduced in the marginal inverse cumulative distributions and the set of new realizations is obtained. Given the new set of $H_{m0,M}$, $T_{p,M}$ is calculated by means of Equation (3.23) and the corresponding β from Table 3.8.

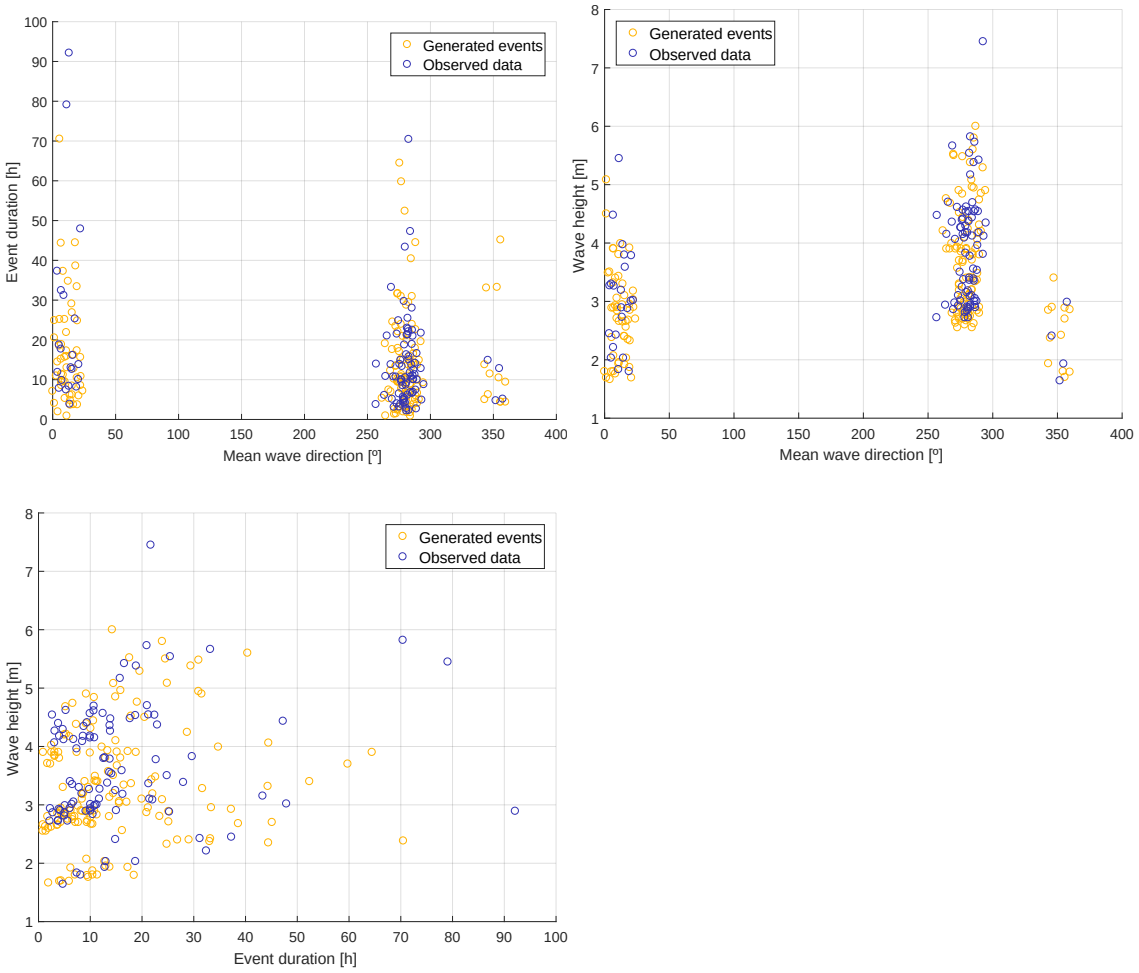

Figure 4.2. Generated values using copulas (blue) respect to observed values (yellow). The plots display the relation in between the variables that are related through copulas.

Finally, it is important to remember that for Rayleigh formulation it is needed H_{rms}, and T_z, so by employing Equations (3.19) and (3.27), $H_{m0,M}$ and $T_{p,M}$ are transformed. D has to be transformed into percentage of the year before input to Littoral Processes FM.

4.1.3 Adaptability of the climate model

Subsection 2.1.4 contains the main result regarding climate evolution. Figure 2.3 shows that there exist a clear growing trend for the mean significant wave height, from which a change rate can be estimated. This rate is used to adjust the generated wave heights to the different periods of time simulated. This is simply done by subtracting or adding to the set of generated $H_{m0,M}$ the decrement or increment or that corresponds.

In the case of the mean wave direction, it was not possible to stablish a clear tendency, and therefore it is not temporarily modified in a systematic manner. However, if required to asses a case in which the mean wave direction changes, or if it desired to evaluated the worse case scenario, by varying the wave proportions it is possible to achieve a shift in the predominant directions.

In Section 2.2 and Section 2.3 it has been shown that the bathymetry and the shoreline are both dynamic entities. The data obtained from these studies is used for calibration of the numerical model. Due to the characteristics of the numerical model, which are detailed in Section 3.1, the output of the model does not provide a modified bathymetry. Therefore, studies of past situations and current situation have to be carried out with their correspondent bathymetry. If predictions where need to be made, either the most recent bathymetry data have to be used, or another numerical model which provides cross-shore variations has to be used.

In Subsection 3.4.8 the water level variation was calculated. This calculation is made over the assumption that the astronomical tides are a stationary process. As a consequence, the selected value for the water level variation is kept constant for all types of simulations.

If the time that spans the prediction simulation is short enough, no modifications regarding water depth are made. However, if the time is large, i.e. 25 years, is made necessary to consider a sea level rise.

According to Statens Energistyrelsens [2008], and for a middle high scenario of climate change, 0.45 m to 1.05 m of sea level rise can be expected in the Danish West coast for 2100. This gives an annual grow rate comprised in the range [0.005 m/year, 0.011 m/year] (counted from the year of publication). If checked from the Danish Coastal Authority web site, in the page about sea level [Kystdirektoratet, 2009], it can be found that for 2100 in the West coast, the sea level rise is comprised in the interval [0.3 m,1.5 m], depending on the chosen scenario.

4.2 Model sensitivity

This section is devoted to test the sensitivity of the model. This study improves the knowledge over the numerical model, the area, the climate and, along with the calibration of the model, allows to check the theories applied to achieve a complete climate description.

The description of the parameters and initial values for some of them were given in the Chapter 3.

In order to asses the importance of each parameter respect to the sediment transport, it is calculated how much the net sediment transport varies with a certain variation of a specific parameter. This in done with percent increases.

4.2.1 Mean grain size and fall velocity

The mean grain size is a parameter that, in principle, is not subdued to variation. However, it is interesting to evaluate the relevance of this parameter in the sediment transport. The fall velocity is dependent on the mean grain size, therefore they are considered in conjunction. The percent variation is considered respect to 0.233 mm, which is the mean grain size used in the project.

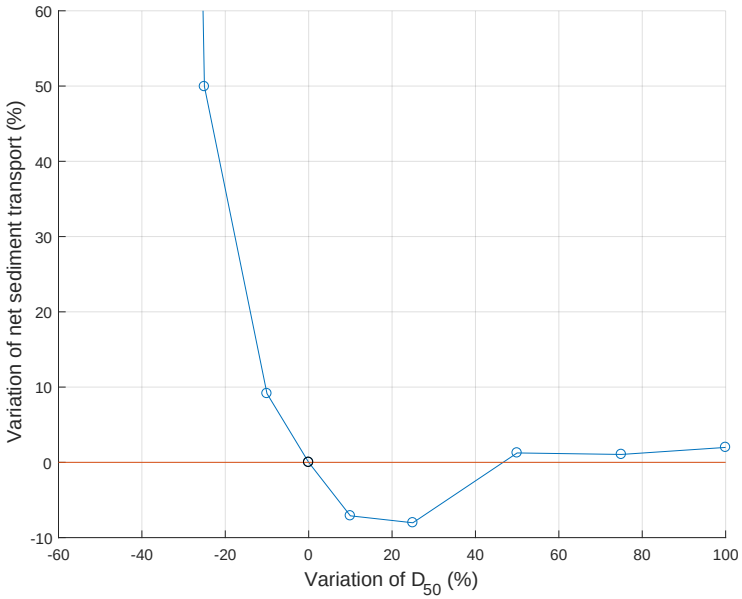

Figure 4.3. Sensitivity of the net sediment transport respect to the mean grain size. The red line marks the zero variation. From the line above, it represents an increase in sediment transport. From the line below, it represents a decrease.

With very small grain sizes, the waves energy wash all the sediments, which is what can be seen in the left part of the graph. There is a critical part in which with increasing grain size, the sediment transport decreases until a minimum. This minimum corresponds to a mean grain size 25% smaller than the project mean grain size. After this point it increases again and becomes quite stable, showing a very small growth rate. This could be caused by the increment in bed friction due to a larger grain size, which leads to more wave breaking.

However, the mean grain size has a major influence in the configuration of the beach, that cannot be computed or even estimated with the numerical simulations.

First, the beach profile shape is very sensitive to the main grain size as, in fact, a larger sediment grain size results in a steeper profile (see Equation (4.1) [Dean, 2003]. This is well known in the beach nourishment practice, where is typical to use a slightly larger mean grain size to achieve smaller refill volumes (intersecting profiles).

$$\begin{aligned} h(y) &= A \cdot y^{\frac{2}{3}} \\ A &= 0.067\omega^{0.44} \end{aligned} \tag{4.1}$$

where $h(y)$ is the water depth at a y distance from the shoreline, in m, A is the profile scale parameter in $m^{\frac{1}{3}}$, and ω is the fall velocity, input in cm/s. Equation (4.1) is the beach equilibrium profile, which depends on the mean grain size through the fall velocity. According to this equation, the larger the mean grain size, the larger the water depth in the profile equilibrium. Subsequently, the effect of water depth change, has to be added to the effect of the grain size variation.

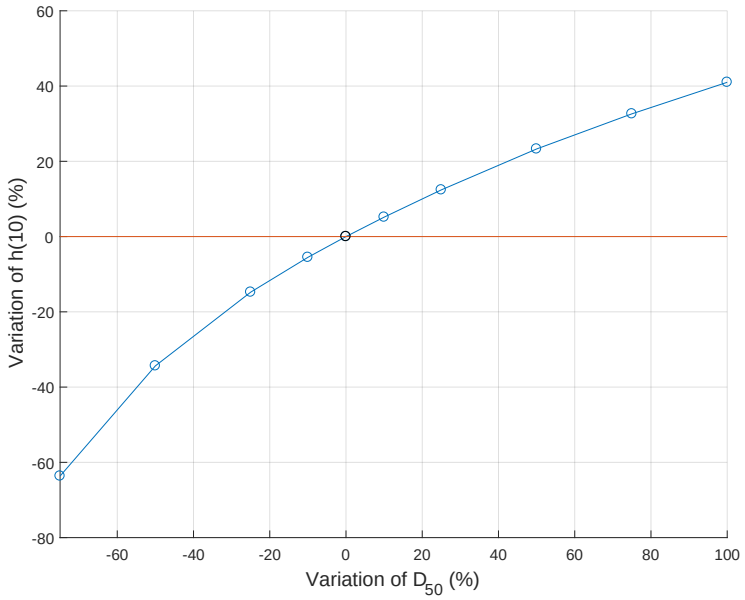

Figure 4.4. Relation in between the water depth at 10 m distance from the shoreline, with the grain sediment size. Example of the effect of D_{50} over the beach profile.

Furthermore, the type of wave breaking depends on the beach slope (see Equation (4.2)), which becomes steeper with larger mean grain size and milder with smaller grain mean size.

$$\xi_0 = tan\beta \left(\frac{H_0}{L_0} \right)^{-\frac{1}{2}} \tag{4.2}$$

where β is the beach slope, H_0 and L_0 are the the wave height and wave length in deep water, and ξ_0 is known as the Iribarren number, or surf similarity parameter. It predicts the manner in which waves break. The steeper the beach, the larger ξ_0, and the more turbulent the breaking becomes [Engineers, 2002]. Turbulent breaking implies more stirring, and more sediment in suspension, which increases the potential transport.

In this project it was also assumed that the distribution of the particle is uniform in the cross shore profile. This is not necessarily true. In fact, there is a tendency for the particles to be sorted by sized across the profile, both spatially and temporarily [Medina et al., 1994]. Typically, the coarser grain particles located in the breaker zone, while towards both offshore and onshore, finest particles can be found, depending on the energy dissipated [Wang et al., 1998]. This is a limitation encounter in this project, as there is not data available to characterize neither the spatial, nor the temporal variation of the grain size.

In conclusion, the effects of the main grain size variation on the sediment transport cannot be properly evaluated, as they also depend on the morphology of the beach, and the variability of the grain size distribution.

4.2.2 Water level variation

The relation between the water level variation and the net sediment transport is not linear, but they are proportional. The smaller the water level variation considered, the smaller

the sediment transport obtained. The reference value is the project water level variation, 0.42 m.

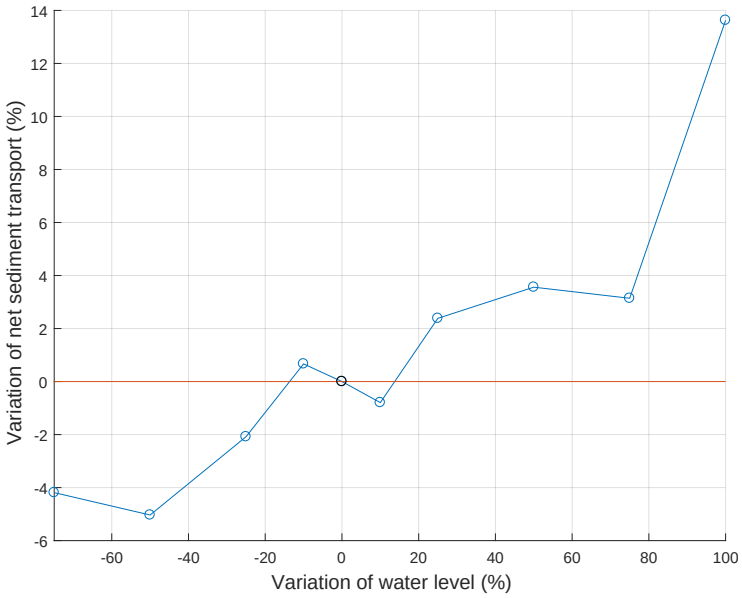

Figure 4.5. Sensitivity of the net sediment transport respect to the water level variation. The red line marks the zero variation. From the line above, it represents an increase in sediment transport. From the line below, it represents a decrease.

The curve displayed in Figure 4.5 looks odd. It is expected that larger water levels leads to larger sediment transport without the presence of breaks in the curve. The plot is expected to have a parabolic shape, with the same gradient it shows currently.

A higher water level allows larger wave heights to approach the coast. The water depth increases and waves that would usually break offshore, move forward onshore. On the other hand, the shoreline moves landwards, as the water reaches a higher point, which increments the chances of large waves producing damage to the beach dunes, and posteriorly, the property behind.

Global climate change produces, among other effects, an increase in the mean water level and strengthens the storms, and as a consequence, the storm surge. This is the reason why it can be expected that the sea level rise will worsen the situation in Nørlev Strand and other coastal localities.

4.2.3 Wave height

The net sediment transport is very sensitive to the wave height. For example, as it can be seen from the CERC formula, the term correspondent to the breaking wave height is to the power of 2.5

$$Q = \frac{5}{8} \cdot \frac{H_b^{\frac{5}{2}} \sqrt{\frac{g}{k}}}{(1-p)(s-1)} \frac{\sin(2 \cdot (\beta - \alpha_b))}{2} \tag{4.3}$$

In Figure 4.6, the relation in between H and the net sediment transport has an exponential tendency. The highest transport is obtained by doubling the wave height. Doubling the

wave height has implied quadruplicating the net sediment transport.

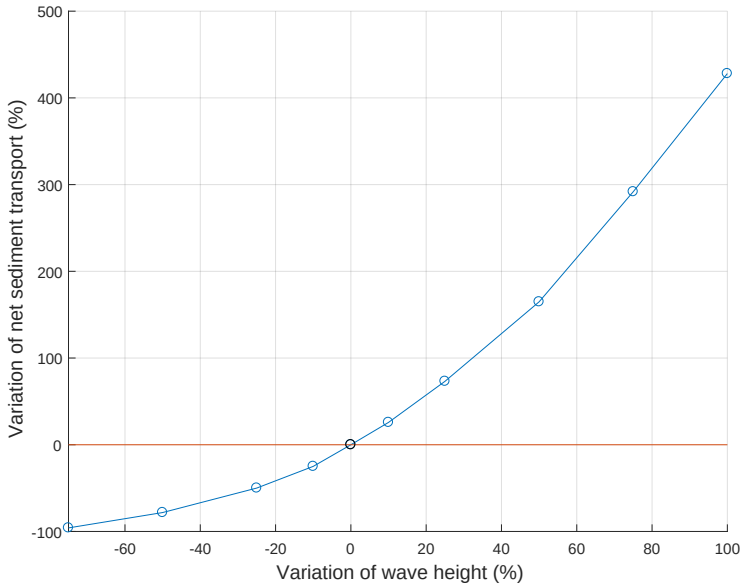

Figure 4.6. Sensitivity of the net sediment transport respect to the significant wave height. The red line marks the zero variation. From the line above, it represents an increase in sediment transport. From the line below, it represents a decrease.

The wave height is the main variable when referring to the energy content of the waves, and at the same time, in the simulations the main input source are the waves. The total energy density per unit area of the water waves is defined as [Andersen et al., 2014]:

$$E = \frac{1}{8} \cdot \rho g H^2 \tag{4.4}$$

where, again, the wave height term appears to the power of 2.

4.2.4 Wave period

According to the results of the sensitivity analysis, in principle the net sediment transport increases with increasing wave period. Van Gent et al. [2008] has also shown this effect. This relations is not completely clear, and in fact, Figure 4.7 shows some odd behaviour for small periods. With very large periods, the waves will become more stable and their Iribarren number will also decrease. As a consequence, the breaking is produced later and less turbulent, reducing the erosive tendency.

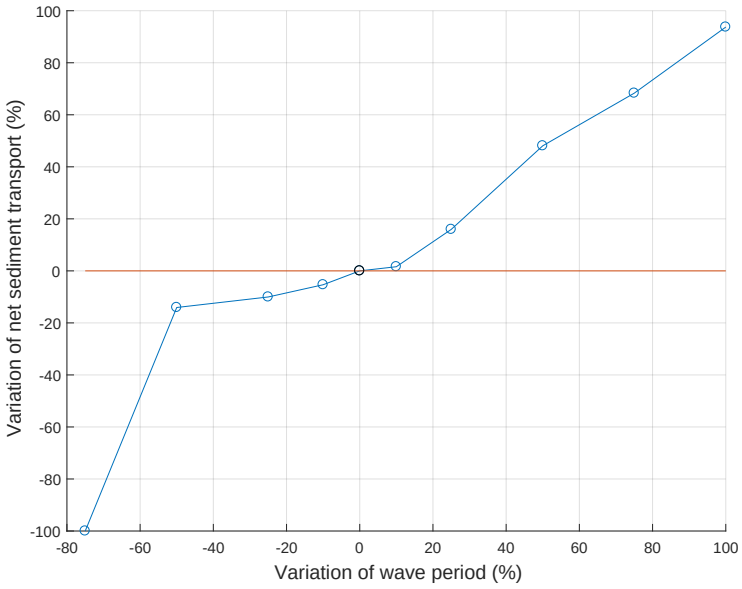

Figure 4.7. Sensitivity of the net sediment transport respect to the wave peak period. The red line marks the zero variation. From the line above, it represents an increase in sediment transport. From the line below, it represents a decrease.

4.2.5 Event duration

The event duration is linearly proportional with the net sediment transport. The larger the event, the larger the energy associated to it, and therefore the transport.

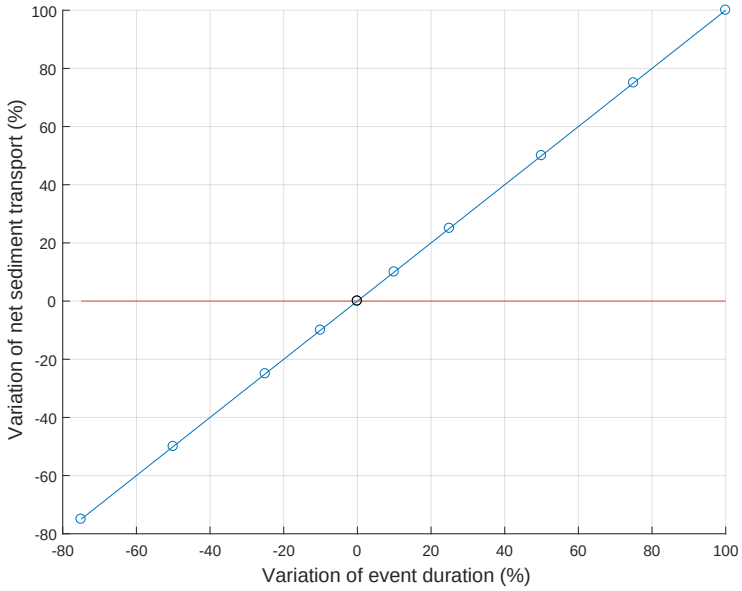

Figure 4.8. Sensitivity of the net sediment transport respect to the event duration. The red line marks the zero variation. From the line above, it represents an increase in sediment transport. From the line below, it represents a decrease.

As seen in Subsection 4.2.3, the net sediment transport is very sensitive to the wave height, approximately proportional to $H^{2.5}$. In Subsubsection 3.4.9, it was contemplated the possibility of doing a bivariate copula $\mathbf{C}(M, A_M)$. It is necessary to find a second

equation to be able to calculate $H_{m0,M}$ and D_e from Equation (3.22). The proposition of using a linear relation in between $H_{m0,M}$ and D_e is based on the fact that infinity pairs (H, D) lead to the same M. Given the different influence that each variables has on the transport, this assumption leads to wrong results. Added to the fact that the error in the determination of H results in a quadratic error in the net transport, this approach is discarded.

4.2.6 Bed roughness

The values of the bed roughness are previously calculated using theoretical formulations. From this calculation, a range of possible values are obtained, going from 0.0087 until 0.0869. The bed roughness is a value used in the calibrations, and it is expected that the project value would be located within the range.

From the calibration it is obtained that the optimum value for the bed roughness is 0.08.

As it can be seen in Figure 4.9, bed roughness and sediment transport are inversely proportional. The larger the bed roughness, the larger the fiction with the bottom and the more wave energy is dissipated.

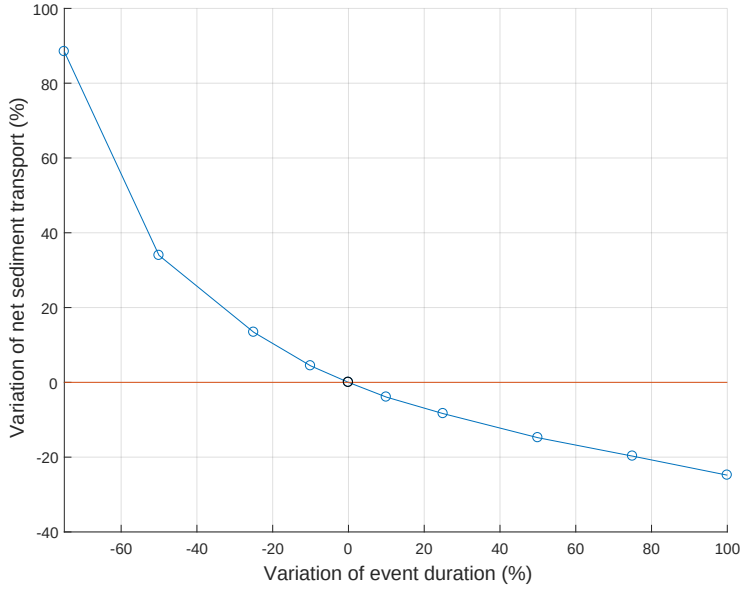

Figure 4.9. Sensitivity of the net sediment transport respect to the wave roughness. The red line marks the zero variation. From the line above, it represents an increase in sediment transport. From the line below, it represents a decrease.

4.2.7 Coastline alignment

In Littoral Processes FM, the coastline orientation is defined by the cross shore profiles orientation respect to the true north. To evaluate the sensitivity of the transport to the coastline orientation, or, what is the same, the mean wave direction, profiles with different orientations covering 360° each 15° are tested. The same climate is used for all orientations.

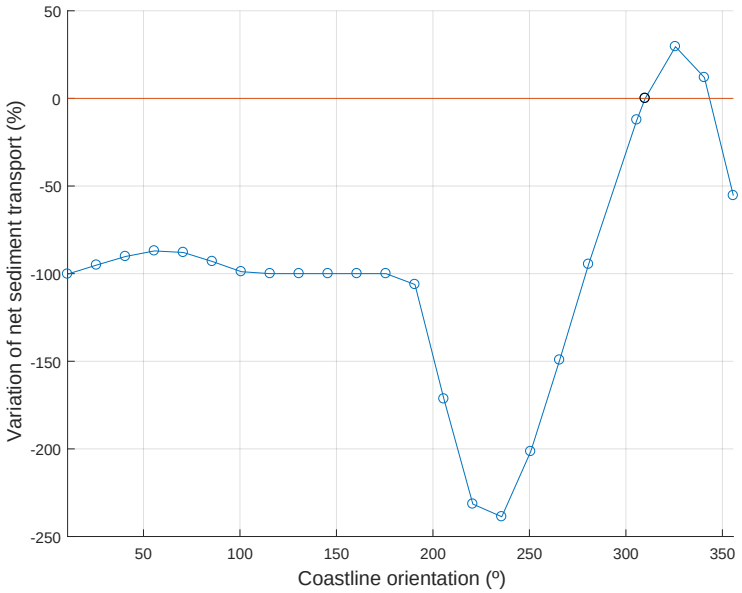

Figure 4.10. Variation of the sediment transport in relation to the coastline alignment. The signs criteria are defined in 3.1

The maximum of the net transport is found when the normal vector to the coastline forms an angle of 235° with the true north (See sign criteria in Figure 3.1). In such a case, the coastline alignment forms approximately (45°) with the mean wave direction of the western waves (275°). When the transport in the graph crosses −100%, it refers to negative values. If an observer stands in the coastline facing the water, the positive net sediment transport goes from left to right, and the negative from right to left. When the coastline forms 235°, this means going from North to South.

South from Thyborøn, the normal to the coastline forms angles smaller than 270°, and the net transport goes, indeed, from north to south, and with a larger magnitude than north from Thyborøn. When the waves from both north and west have their effect on the coast, as it happens with Nørlev Strand coastline orientation, there is gross transport flowing both towards the north and towards the south. As a consequence, the net sediment transport is reduced. However, when only one direction is predominant, as it is the case for smaller angles than 270°, there is no balance between positive and negative sediment transport. It has to be reminded that only waves from two sectors where considered. As a consequence, the magnitude of this maxima found at 235° cannot be predicted accurately.

When the normal to the coastline alignment forms in between 190° and 85°, the waves input in the model come "from land". Therefore, the sediment transport is zero. When the angle is smaller than 85°, and until it reaches 0°, only fractions of the waves coming from the North have effect on the coastline, and therefore, there is a small transport, which starts to reduce in magnitude when the coastline starts to become perpendicular to northerly waves.

With the real coastline orientation (310°), the net sediment transport becomes larger when the normal to the coastline alignment forms (325°), which implies that westerly waves form and angle of approximately 45° degrees with the predominant wave direction.

The conclusions drawn from this study, in relation to Figure 2.4, is that shifts in the mean wave direction, particularly towards south, enhance the magnitude of the net sediment transport and the erosive potential.

4.2.8 Quatification of difference in between Rayleigh and Battjes and Janssen formulation

The goal is to estimate the difference in between the transport that can be expected when using Rayleigh respect to what could suppose using Battjes and Janssen. Different climates are simulated with both Rayleigh and Battjes and Jenssen formulation. Table 4.2 shows the normalized net sediment transport generated with 10 randomly generated climates, for both formulations. The normalization is done respect to the mean significant wave height. The third column of the table contains the difference in percentage that suppose using Rayleigh respecto to using Battjes and Janssen.

Some results obtained when using Battjes and Janssen result odd. They were discarded from the calculation, but the result showed the sediment transport going from north to south, instead of the expected south to north. Battjes and Janssen require larger profiles to fulfil the conditions explicated in Subsection 3.2.1, and when the profiles are insufficiently long, the model does not behave properly.

Table 4.2. Annual net transport generated with Rayleigh and Battjes and Janssen formulation. The last column contains the difference in percentage

Climate	Rayleigh $[m^3/year]$	Battjes and Janssen $[m^3/year]$	Difference [%]
1	216,551	163,202	32.7
2	28,317	41,936	-32.5
3	60,124	67,624	-11.1
4	202,790	161,596	25.5
5	154,230	118,518	30.1
6	182,820	144,573	26.4
7	106,877	92,391	15.7
8	107,943	84,257	28.11
9	31,397	35,330	-11.1
10	121,574	100,455	21.0
		Average	**12.5**

The percent differences follows Equation (4.5):

$$\% = \frac{Transp.Rayleigh - Transp.Battjes}{Transp.Battjes} \tag{4.5}$$

In average, with Rayleigh formulation the net sediment transport is overestimated by a 12%. This result must be taken with care, because as mention, Battjes and Jenssen can motivate wrong behaviours of the model.

4.2.9 Confidence interval of the transport results

Once the model is calibrated, it is necessary to check how does the climate generation model behaves. A confidence interval is defined for the mean of the net and gross transports.

It is defined through a Student's T distribution, because the standard deviation of the stochastic variable is unknown. The standard deviation of the population and the mean of the population are used instead. The check is done for 25 different climates and for the 6 profiles, giving a total of 90 values of net sediment transport.

In order to calculate the confidence interval, the following equation is used:

$$C_i = \overline{x} \pm Z_{p\%} \cdot s \tag{4.6}$$

where $Z_{p\%}$ is the number of standard deviations that define the interval. This number is tabulated for the Student't T, and depends on the size of the population and the level of confidence required.

Table 4.3. $Z_{p\%}$ and confidence interval of the mean for a population of 90 realizations

Level of confidence	$Z_{p\%}$	C_i net transport	Variation respect to the mean [%]
99 %	2.682	± 21,990	± 7.5
95 %	2.011	± 16,601	± 5.6
90 %	1.677	± 13,886	± 4.7

The 95% confidence interval shows a variation respect to the mean of a ± 5.6 %, which is accepted as a good result. It is possible to state that the oscillations seen respect to the mean of the variables in Subsection 4.1.1, results in an relatively small confidence interval for the mean of the net sediment transport.

The mean value of the net transport, as well as the value obtained in the bathymetry study and the deviation in between both is shown in Table 4.4. Unfortunately, it is not possible to make the same check with the results of the gross sediment transport due to the lack of calibration data.

Table 4.4. Mean net transport and deviation from reality

Net transport (model) $[m^3/year]$	Net transport (bathymetry) $[m^3/year]$	Deviation [%]
-274,796	-271,269	1.3%

As seen in Table 4.4, the difference is negligible. The result can be approximated easily as much as wanted, and with minimum computational time spared on it. Knowing the flaws of the model makes it easier to achieve a result with a good quality, with less iterations.

Conclusion 5

The first conclusion drawn from this project is that the effects of the maritime climate are going to be intensified in successive years. It has been observed an increase of 20% of the mean significant wave height from 1999 until 2012. In terms of sediment transport, it implies a 50% increase of the net sediment transport. After 2006, the mean wave direction has experienced a shift of approximately 5° towards south for summer events and 4° towards north for winter events. Winter events are 1 m to 1.5 m larger than summer events, and therefore winter events are more relevant in the quantification of sediment transport. A shift towards north implies a larger relative angle in between coastline and mean wave direction, and therefore a smaller transport. This shift in direction, thus, attenuates the sediment transport. Even though, the transport is not only affected by these two factors, but it has been shown that are two factors of great importance.

As the morphology of the coast is experiencing irreversible changes, intensification of climatic events is translated into greater risk of damage of the properties in the coast. Increasing depths in the offshore contours of the beach allows larger wave heights to approximate the coastline. These type of events added to an increasing trend in the sea level, leads to more pronounced and more frequent attacks of the waves to the beach dunes, and the houses protected by those. This implies that despite the actions taken in the coast, such as the removal of the groins, the erosion of Nrlev Strand is structural, and can only be moderated or delayed. The construction of the revetment can protect the houses from the effects of the storms, but it does not avoid the relapse of the coastline, which means that without a constant campaign of beach nourishments, the revetment toe will eventually be reach by the water and eroded from there.

Regarding the nourishment, from the data, seems that the type of nourishment used is either backshore or beach nourishment. Though it is a necessity to continue these actions to maintain the functionality of the beach and the integrity of the revetment, the results of the thesis suggest that shoreface nourishment would improve the efficiency in terms of reduction of the energetic content of the waves that reach the beach. This will help in the mitigation of storm effects.

Respecting the developed climatic model, it has been shown that it adapts quite well to the description of the climate. Results from the model sensitivity section and their comparison with reality allows to conclude that it is possible to use this approach as a tool for risk assessment. However, the confidence intervals obtained for the solution are still quite large, so further work is still needed to be done. Feeding the model with new information can potentially improved these confidence intervals.

An extra study that could be perform is the analysis of how the revetment of Skallerup

Klit and the groins affect the sediment supply of Nørlev Strand. Is logical to think that both type of structures act by reducing the amount of sediment that reaches the beach, aggravating the erosion. Some of the results of this thesis, point as well towards this.

The next step should be to test the model in risk assessment. This can be derived easily by exploiting the concept of copulas, from which it can be defined the return period of the significant events, and thus, their relation to the possible erosion magnitude. Adding this, to the fact that the climatic model can be adapted to future scenarios, it can be used in short to mid term simulations.

Bibliography

Ahrens, **2000**. John P Ahrens. *A fall-velocity equation.* Journal of waterway, port, coastal, and ocean engineering, 126(2), 99–102, 2000.

Andersen, **2016**. Thomas Lykke Andersen. *Wind generated waves I.* Department of Civil Engineering, Aalborg Universitet, 2016.

Andersen et al., **2014**. Thomas Lykke Andersen, Peter Frigaard and Hans F Burcharth. *Lecture notes for the course in water wave mechanics*, Department of Civil Engineering, Aalborg University, 2014.

Aouiche et al., **2016**. Ismail Aouiche, Lahcen Daoudi, Edward J Anthony, Mouncef Sedrati, Elhassane Ziane, Abderrazak Harti and Philippe Dussouillez. *Anthropogenic effects on shoreface and shoreline changes: Input from a multi-method analysis, Agadir Bay, Morocco.* Geomorphology, 254, 16–31, 2016.

Badulin, **2014**. SI Badulin. *A physical model of sea wave period from altimeter data.* Journal of Geophysical Research: Oceans, 119(2), 856–869, 2014.

Baptista et al., **2014**. Paulo Baptista, Carlos Coelho, C Pereira, C Bernardes and F Veloso-Gomes. *Beach morphology and shoreline evolution: monitoring and modelling medium-term responses (Portuguese NW coast study site).* Coastal Engineering, 84, 23–37, 2014.

Bird, **1985**. Eric Charles Frederick Bird. *Coastline changes. A global review.* John Wiley and Sons Inc., New York, NY, 1985.

Birkemeier, **1985**. William A Birkemeier. *Field data on seaward limit of profile change.* Journal of Waterway, Port, Coastal, and Ocean Engineering, 111(3), 598–602, 1985.

Bøje and Nørgaard, **2016**. Charlotte Bøje and Bo Nørgaard. *Aftale om kystsikring på plads*, 2016. URL `https://nordjyske.dk/nyheder/aftale-om-kystsikring-paa-plads/49760026-0553-4b85-b77d-3b122a83e3d3`.

Boak and Turner, **2005**. Elizabeth H Boak and Ian L Turner. *Shoreline definition and detection: a review.* Journal of coastal research, pages 688–703, 2005.

Boccotti, **2000**. Paolo Boccotti. *Wave mechanics for ocean engineering*, volume 64. Elsevier, 2000.

Corbella and Stretch, **2012**. S Corbella and DD Stretch. *Multivariate return periods of sea storms for coastal erosion risk assessment.* Natural Hazards and Earth System Sciences, 12(8), 2699–2708, 2012.

Davidson-Arnott and Pollard, **1980**. Robin GD Davidson-Arnott and Wayne H Pollard. *Wave climate and potential longshore sediment transport patterns, Nottawasaga Bay, Ontario.* Journal of Great Lakes Research, 6(1), 54–67, 1980.

De Michele et al., **2007**. C De Michele, G Salvadori, G Passoni and R Vezzoli. *A multivariate model of sea storms using copulas.* Coastal Engineering, 54(10), 734–751, 2007.

Dean, **2003**. Robert G Dean. *Beach nourishment: theory and practice*, volume 18. World Scientific Publishing Co Inc, 2003.

Engineers, **2002**. US Army Corps Of Engineers. *Coastal engineering manual.* Engineer Manual, 1110, 2–1100, 2002.

European Marine Observation and Data Network. European Marine Observation and Data Network. *Portal for Bathymetry. Bathymetry Viewing and Download service.* URL `http://portal.emodnet-bathymetry.eu/mean-depth-full-coverage`.

Gammelgaard, **2016**. Jakob Gammelgaard. *Afgørende møde om kystsikring.* 2016.

Grundejerforeningen Nørlev Strand, **2016**. Grundejerforeningen Nørlev Strand. *Status på kystsikring, juni 2016.* 2016.

Haver and Nyhus, **1986**. S Haver and KA Nyhus. *A wave climate description for long term response calculations.* 4, 27–34, 1986.

Hjørring kommune. Økonomisk Forvaltning, **2016**. Hjørring kommune. Økonomisk Forvaltning. *Byopgørelser pr. 1. januar for årene 2000 og 2013-2016*, 2016. URL `https://hjoerring.dk/om-kommunen/fakta-om-hjoerring-kommune`.

Hjørring kommune. Økonomisk Forvaltning, **2017**. Hjørring kommune. Økonomisk Forvaltning. *Folketal efter herkomst i Hjørring kommune og hele landet*, 2017. URL `https://hjoerring.dk/om-kommunen/fakta-om-hjoerring-kommune`.

Hwang et al., **1998**. Paul A Hwang, William J Teague, Gregg A Jacobs and David W Wang. *A statistical comparison of wind speed, wave height, and wave period derived from satellite altimeters and ocean buoys in the Gulf of Mexico region.* Journal of Geophysical Research, 103(C5), 10451–10468, 1998.

Korevaar, **2012**. CG Korevaar. *North Sea Climate: based on observations from ships and lightvessels.* Springer Science & Business Media, 2012.

Kystdirektoratet, **2017**. Kystdirektoratet. *Anlæg på søterritoriet.* 2017.

Kystdirektoratet, **2015**. Kystdirektoratet. *Møde om kysterosionen ved Nørlev Strand and høfderne ved Skallerup Klit.* 2015.

Kystdirektoratet, **2009**. Kystdirektoratet. *Vandstande*, 2009. Online; accessed 2017-06-02.

Li et al., **2014**. F Li, PHAJM van Gelder, JK Vrijling, DP Callaghan, RB Jongejan and R Ranasinghe. *Probabilistic estimation of coastal dune erosion and recession by statistical simulation of storm events.* Applied Ocean Research, 47, 53–62, 2014.

Liu, **1999**. Zhou Liu. *Sediment transport.* Aalborg Universitet, 1999.

Liu and Frigaard, **1999**. Zhou Liu and Peter Frigaard. *Generation and analysis of random waves.* Aalborg Universitet, 1999.

Lorenz, **1980**. Claude Lorenz. *Géologie des pays européens: France, Belgique, Luxembourg*, volume 1. Dunod, 1980.

Madsen, **2003**. Per A. Madsen. *Tides: their origin and their prediction.* 2003.

Martín-Hidalgo et al., **2014**. Melva Martín-Hidalgo, Mª Jesús Martín-Soldevilla, Vicente Negro, Paloma Aberturas and JS López-Gutiérrez. *Storm evolution characterization for analysing stone armour damage progression.* Coastal Engineering, 85, 1–11, 2014.

MathWorks, **2017a**. MathWorks. *Linear Regression*, 2017. URL `https://se.mathworks.com/help/matlab/data_analysis/linear-regression.html`.

MathWorks, **2017b**. MathWorks. *goodnessOfFit*, 2017. URL `https://se.mathworks.com/help/ident/ref/goodnessoffit.html`.

Medina et al., **1994**. R Medina, MA Losada, IJ Losada and C Vidal. *Temporal and spatial relationship between sediment grain size and beach profile.* Marine Geology, 118 (3-4), 195–206, 1994.

MIKE by DHI, **2016**. MIKE by DHI. *Littoral Processes FM*, 2016.

Miljø- og Fødevareministeriet and COWI. Miljø- og Fødevareministeriet and COWI. *Danmarks Miljøportal.* URL `http://arealinformation.miljoeportal.dk/distribution/`.

Moore et al., **1999**. Laura J Moore, Benjamin T Benumof and Gary B Griggs. *Coastal erosion hazards in Santa Cruz and San Diego Counties, California.* Journal of Coastal Research, pages 121–139, 1999.

Morton and Bowers, **1996**. ID Morton and J Bowers. *Extreme value analysis in a multivariate offshore environment.* Applied Ocean Research, 18(6), 303–317, 1996.

Morton and McKenna, **1999**. Robert A Morton and Kimberly K McKenna. *Analysis and projection of erosion hazard areas in Brazoria and Galveston Counties, Texas.* Journal of Coastal Research, pages 106–120, 1999.

Nelsen, **2007**. Roger B Nelsen. *An introduction to copulas.* Springer Science & Business Media, 2007.

Nielsen, **2015**. Palle Bo Nielsen. *Tidal tables*, 2015. URL `https://www.dmi.dk/en/hav/maalinger/tidal-tables/`.

Pranzini and Williams, **2013**. Enzo Pranzini and Allan Thomas. Per Sørensen Williams. *Coastal erosion and protection in Europe.* Routledge, 2013.

Raichlen, **2014**. Fredric Raichlen. *MIT Press Essential Knowledge: Waves.* MIT Press, 2014.

Robinson and Kenneth H. Brink, **1998**. Allan R. Robinson and John W. Loder Kenneth H. Brink. *The Sea. The Global Coastal Ocean: Regional Studies and Synthesis*. John Wiley & Sons, Inc, 1998.

Saye and Pye, **2006**. Samantha E Saye and Kenneth Pye. *Variations in chemical composition and particle size of dune sediments along the west coast of Jutland, Denmark*. Sedimentary Geology, 183(3), 217–242, 2006.

Silva et al., **2016**. Filipe Galiforni Silva, Paulo Henrique Gomes Oliveira Sousa and Eduardo Siegle. *Longshore transport gradients and erosion processes along the Ilha Comprida (Brazil) beach system*. Ocean dynamics, 66(6-7), 853–865, 2016.

Soldevilla et al., **2015**. Mª Jesús Martín Soldevilla, Melva Martín-Hidalgo, Vicente Negro, JS López-Gutiérrez and Paloma Aberturas. *Improvement of theoretical storm characterization for different climate conditions*. Coastal Engineering, 96, 71–80, 2015.

Sørensen, **2011**. John Dalsgaard Sørensen. *Statistical analysis using the Maximum-Likelihood method*. 2011.

Statens Energistyrelsens, **2008**. Statens Energistyrelsens. *Strategi for tilpasning til klimaændriger i Danmark*. 2008.

Styrelsen for Dataforsyning og Effektivisering. Styrelsen for Dataforsyning og Effektivisering. *Kortforsyningen*. URL `https://kortforsyningen.dk/`.

Thomas Lykke Andersen and Burcharth, **2014**. Peter Bak Frigaard Thomas Lykke Andersen and Hans Falk Burcharth. *Lecture Notes for the Course in Water Wave Mechanics*. Department of Civil Engineering, Aalborg Universityt, 2014.

Thorngaard, **2015**. Nikolaj Tangaa Thorngaard. *Sommerhus ved Nørlev Strand bliver stående lidt endnu*, 2015.

UNESCO/IOC and the Flanders Marine Institute (VLIZ). UNESCO/IOC and the Flanders Marine Institute (VLIZ). *Sea level station monitoring facility*. URL `http://www.ioc-sealevelmonitoring.org/station.php?code=hirt`.

Van de Noort, **2011**. Robert Van de Noort. *North Sea archaeologies: a maritime biography, 10,000 BC-AD 1500*. Oxford University Press, 2011.

Van Gent et al., **2008**. MRA Van Gent, JSM van Thiel de Vries, EM Coeveld, JH De Vroeg and J Van de Graaff. *Large-scale dune erosion tests to study the influence of wave periods*. Coastal Engineering, 55(12), 1041–1051, 2008.

Wang et al., **1998**. Ping Wang, Richard A Davis Jr and Nicholas C Kraus. *Cross-shore distribution of sediment texture under breaking waves along low-wave-energy coasts*. Journal of Sedimentary Research, 68(3), 1998.

Williams. Ian Williams. *Sorting*. Online; accessed 2017-06-02.

Yan et al., **2007**. Jun Yan et al. *Enjoy the joy of copulas: with a package copula*. Journal of Statistical Software, 21(4), 1–21, 2007.

Zarillo et al., 2008. Gary A Zarillo, Justin Kelley and Vickie Larson. *A GIS based tool for extracting shoreline positions from aerial imagery (BeachTools) revised.* 2008.

List of Corrections

Appendix to preliminary studies A

A.1 Wave climate evolution

In this appendix are presented all the annual wave roses discussed in Subsection 2.1.4.

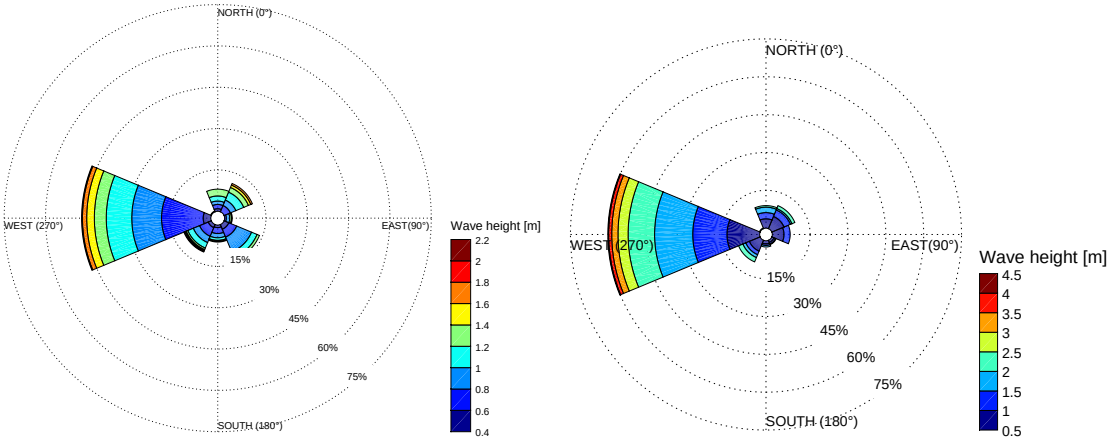

Figure A.1. Annual wave roses. Left: summer 1999. Right: winter 1999

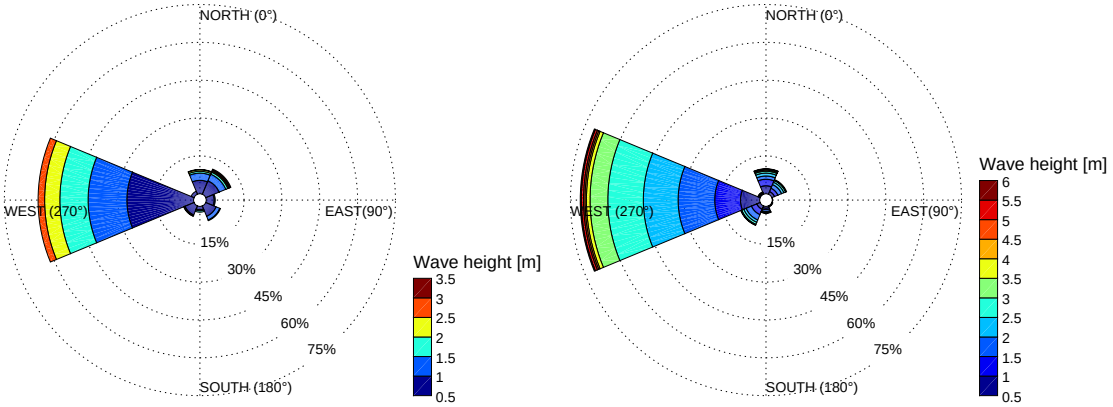

Figure A.2. Annual wave roses. Left: summer 2000. Right: winter 2000

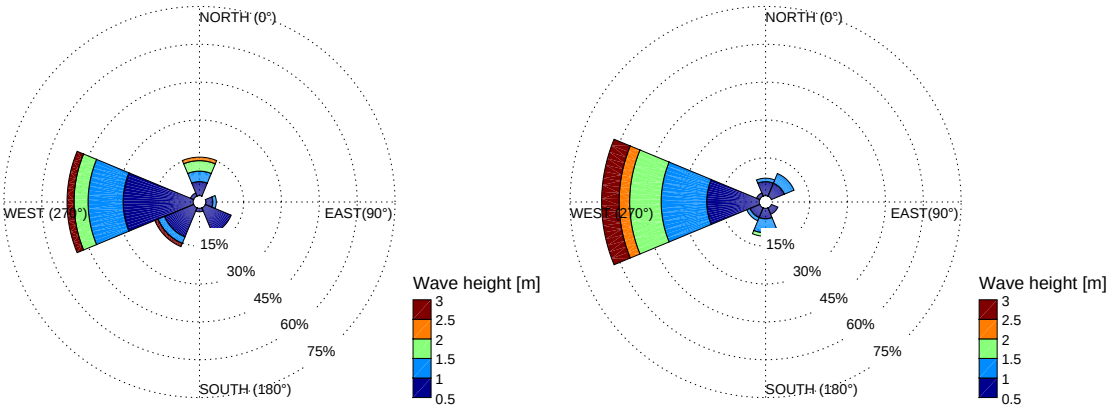

Figure A.3. Annual wave roses. Left: summer 2001. Right: winter 2001

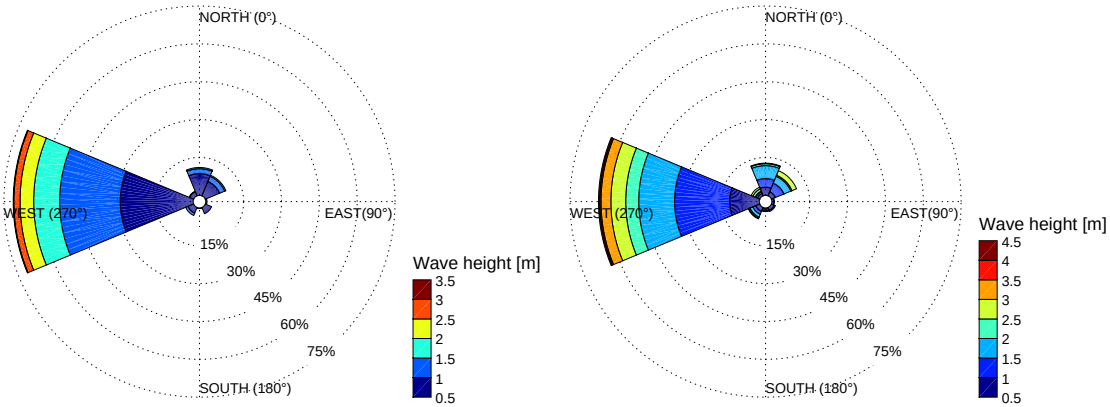

Figure A.4. Annual wave roses. Left: summer 2002. Right: winter 2002

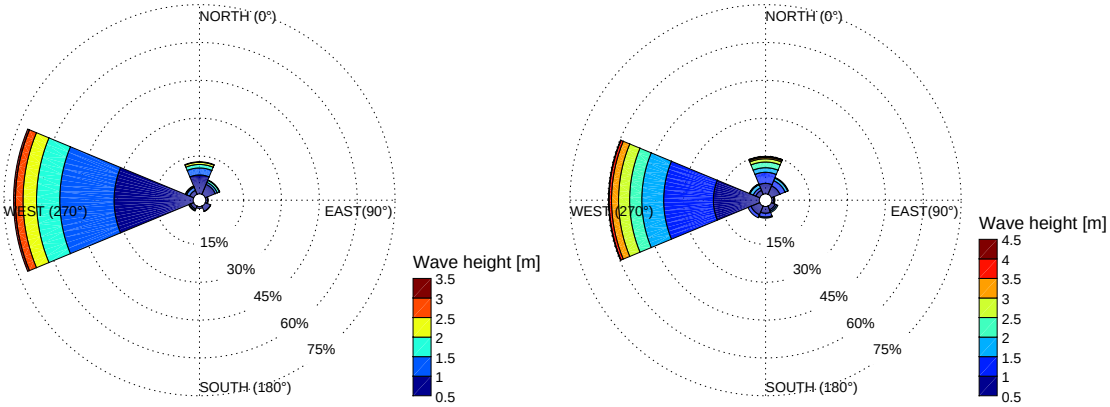

Figure A.5. Annual wave roses. Left: summer 2003. Right: winter 2003

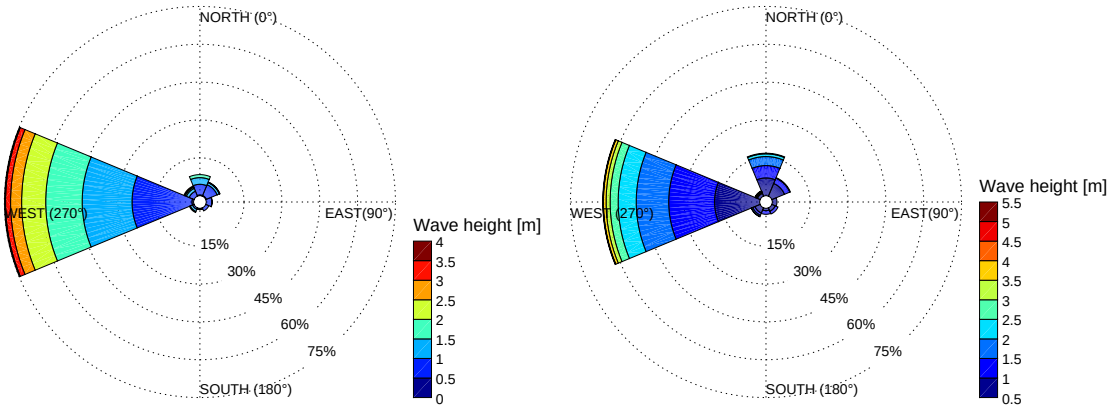

Figure A.6. Annual wave roses. Left: summer 2004. Right: winter 2004

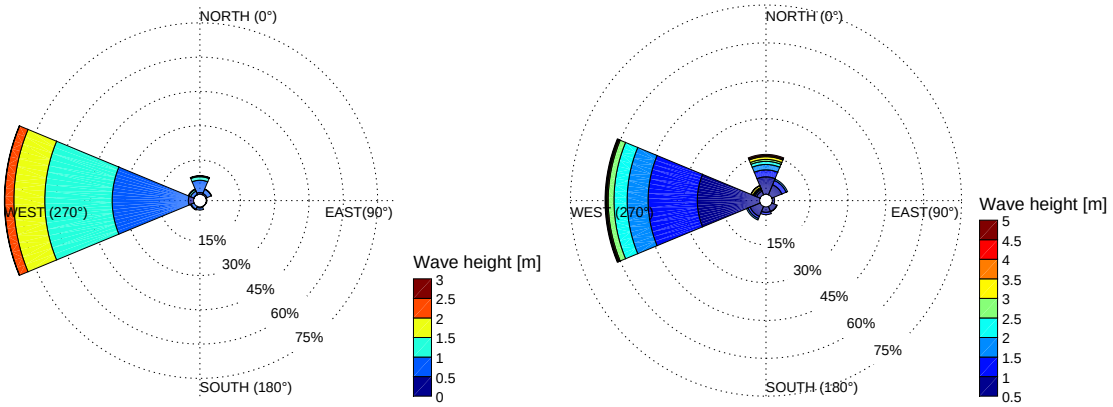

Figure A.7. Annual wave roses. Left: summer 2005. Right: winter 2005

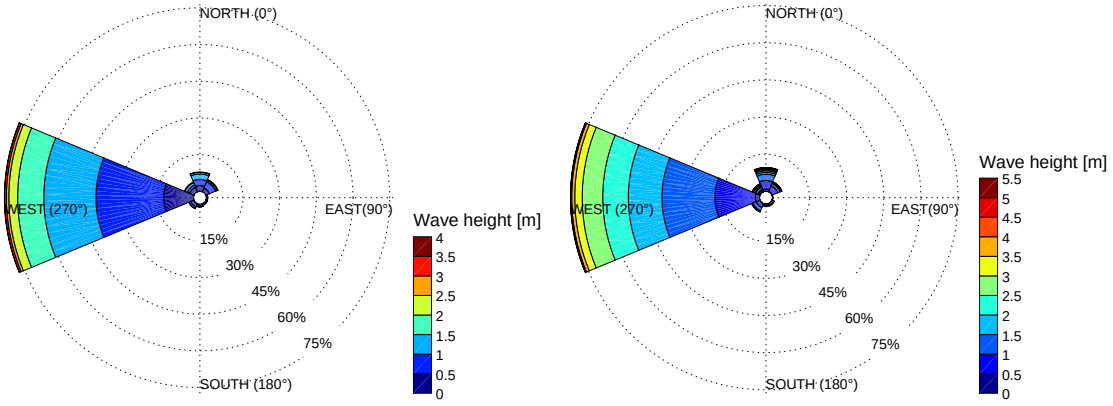

Figure A.8. Annual wave roses. Left: summer 2006. Right: winter 2006

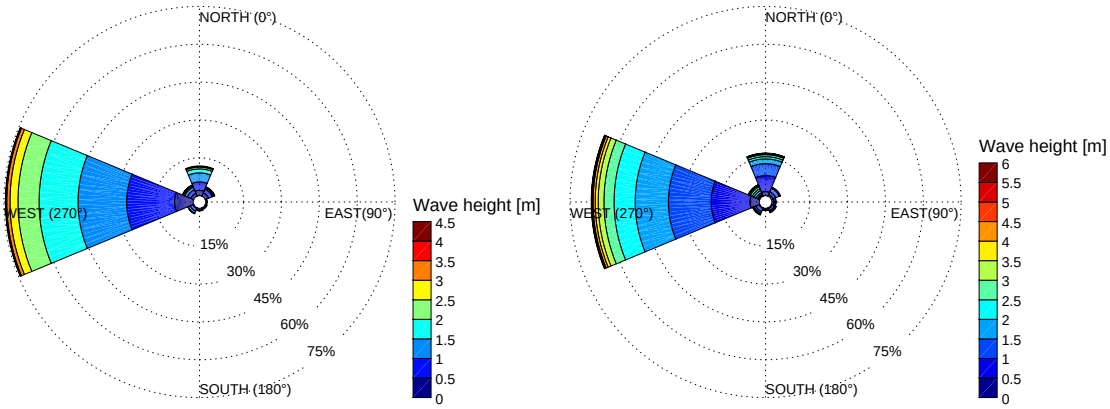

Figure A.9. Annual wave roses. Left: summer 2007. Right: winter 2007

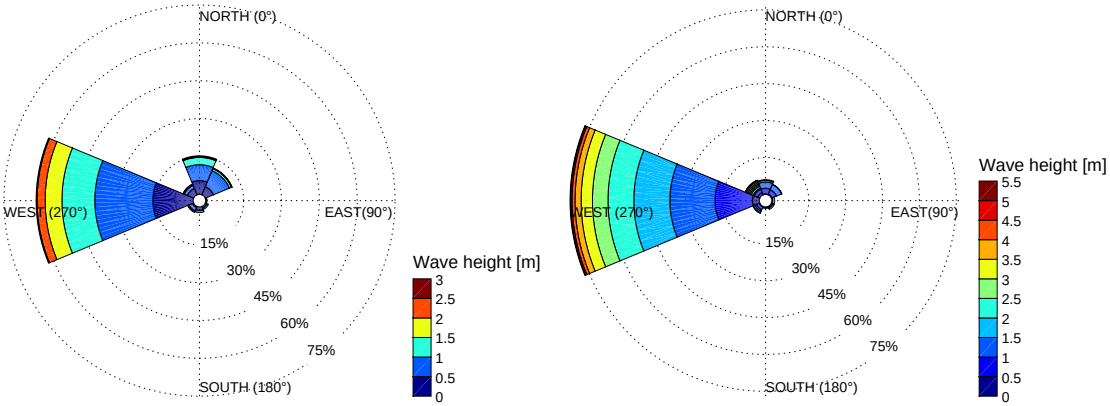

Figure A.10. Annual wave roses. Left: summer 2008. Right: winter 2008

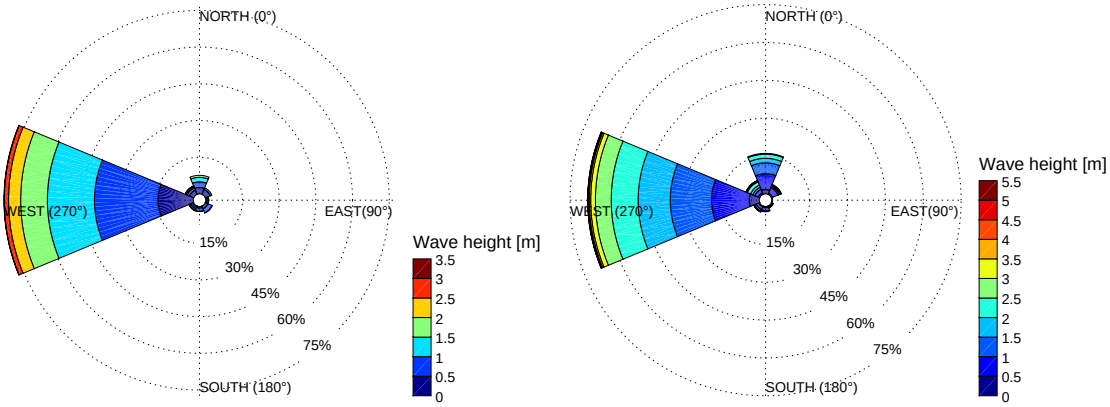

Figure A.11. Annual wave roses. Left: summer 2009. Right: winter 2009

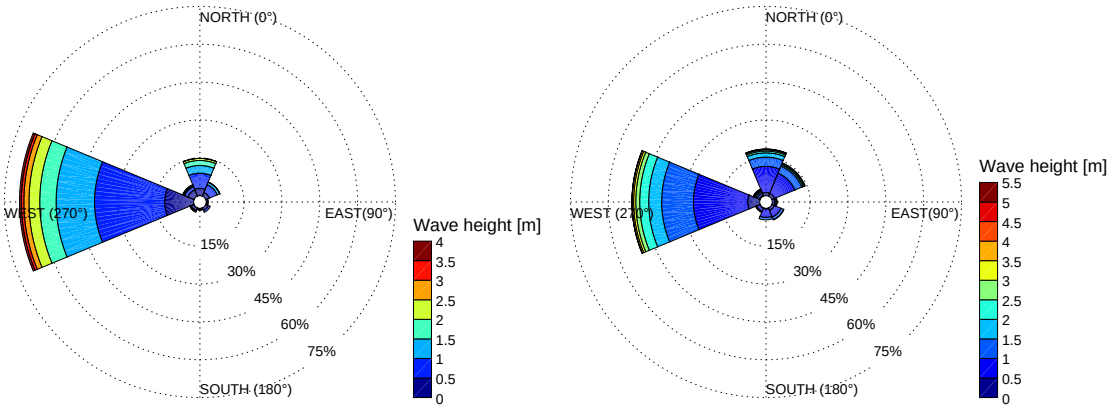

Figure A.12. Annual wave roses. Left: summer 2010. Right: winter 2010

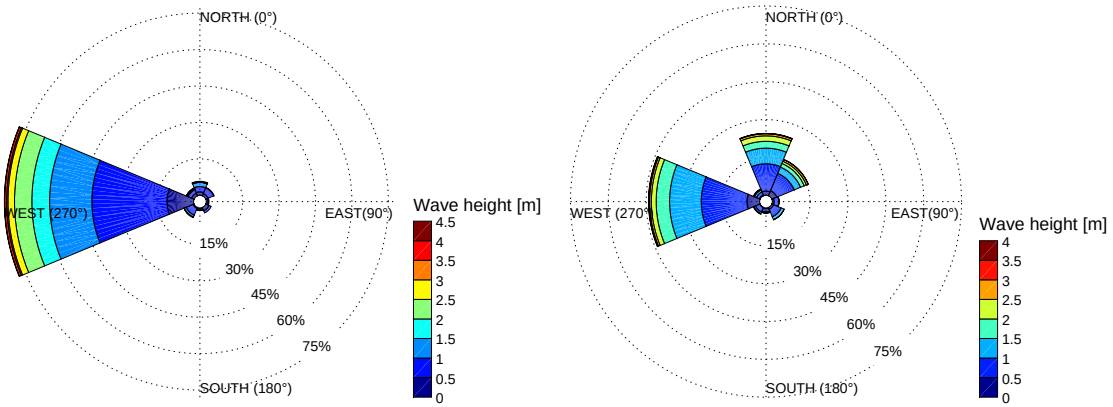

Figure A.13. Annual wave roses. Left: summer 2011. Right: winter 2011

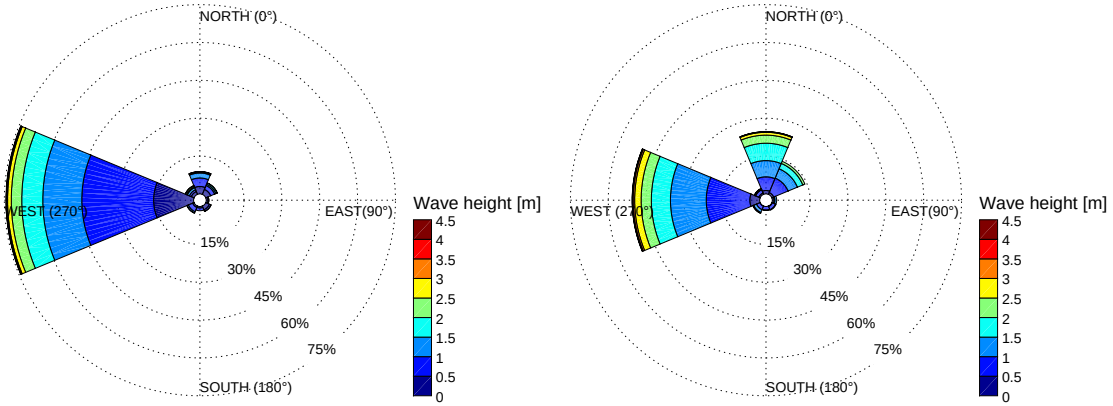

Figure A.14. Annual wave roses. Left: summer 2012. Right: winter 2012

A.2 Evolution of beach profiles

In this section are presented the evolution of profiles 1610, 1620, 1640 and 1660, which weren't included in the main report.

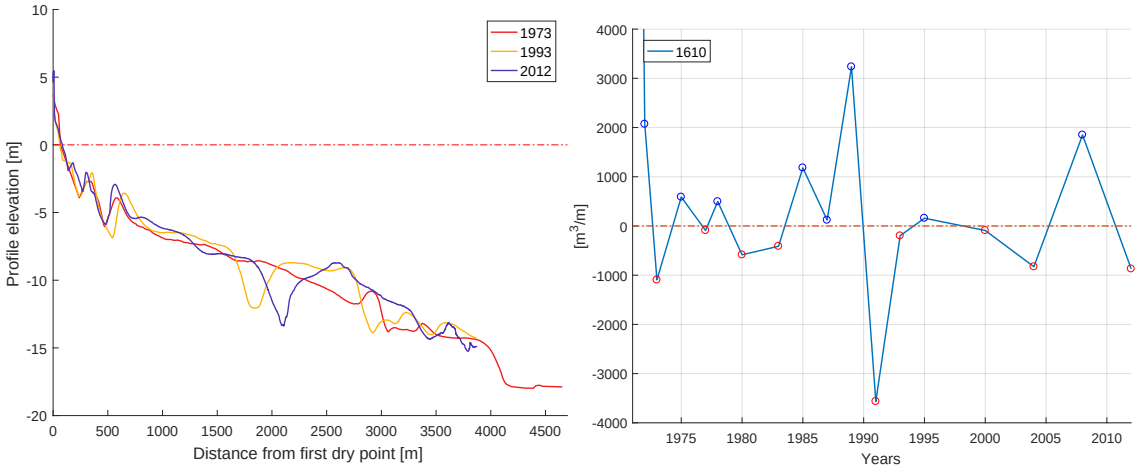

Figure A.15. Profile 1610. Left: Morphological evolution. Right: Volumetric evolution $[m^3/m]$.

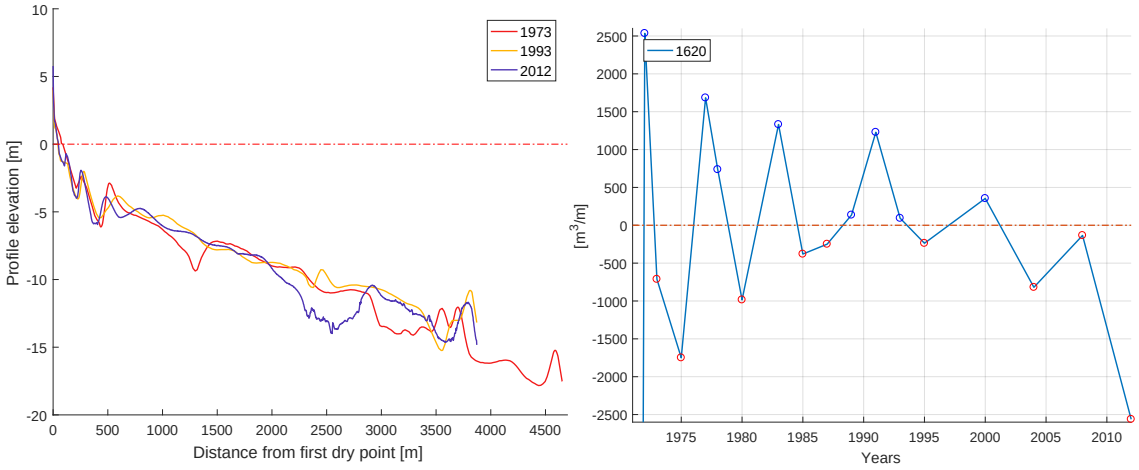

Figure A.16. Profile 1620. Left: Morphological evolution. Right: Volumetric evolution $[m^3/m]$.

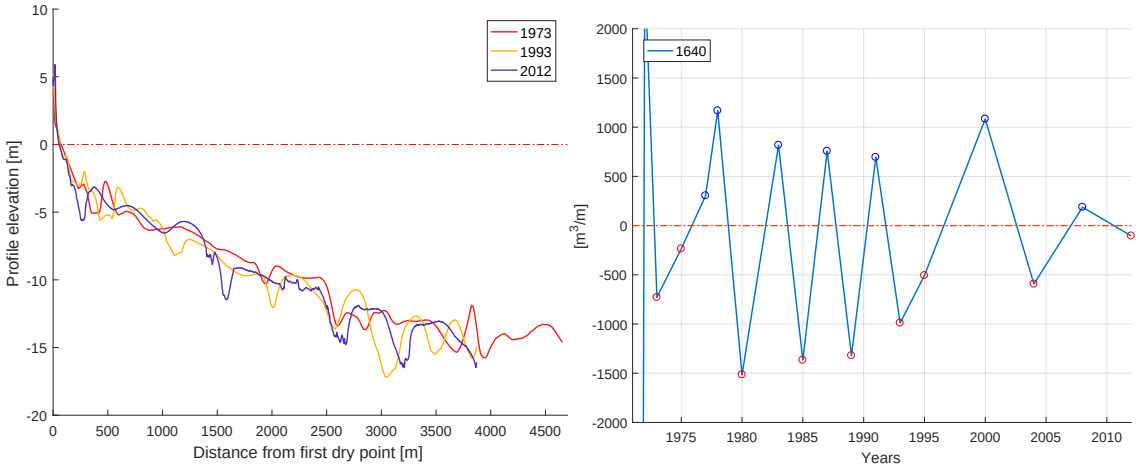

Figure A.17. Profile 1640. Left: Morphological evolution. Right: Volumetric evolution $[m^3/m]$.

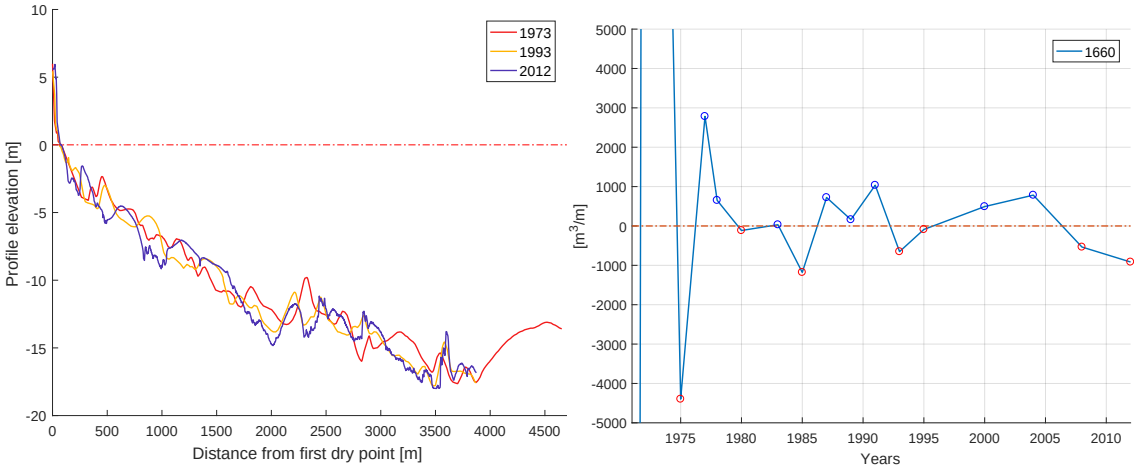

Figure A.18. Profile 1660. Left: Morphological evolution. Right: Volumetric evolution $[m^3/m]$.

A.3 Complete results of the shoreline change quantification

Table A.1 contains the results of the study when using the instant water line as shoreline indicator:

Table A.1. Relative distance in between profiles of different years. A negative number represents erosion and a positive number accretion

Year	P1600	P1610	P1620	P1630	P1640	P1650	P1660	P1670
1945-1954	-49.1	13.7	67.2	21.7	34.1	32.2	6.4	-13.24
1954-1960/64	29.5	57.2	-5.6	-29.0	-34.9	-49.1	-6.8	-80.0
1960/64-1979	-22.3	-12.6	4.8	23.6	-23.5	-9.8	-15.5	25.4
1979-1985	-9.3	-4.6	-2.5	-38.2	-25.6	-11.6	-21.6	-11.3
1985-1992/95	22.6	4.8	-9.5	6.5	-17.0	-47.1	-17.5	-27.2
1992/95-2004	-8.6	8.5	-19.7	-24.6	-10.3	-51.6	-9.7	10.8
2004-2012	-7.7	-14.6	18.3	2.6	-1.9	-20.5	-19.3	-7.2
2012-2016	16.31	-17.0	-11.5	-18.6	-18.8	-13.5	-29.3	-13.0
Rate 1 [m/year]	-0.40	0.50	0.58	-0.79	-1.38	-2.27	-1.60	-1.63

The last row of the table, with the name *Rate*, represents the annual rate of accretion (+) or recession (-) of the shoreline in that specific profile. *Rate* can be calculated either by finding the difference in between first year with data and the last one, and then dividing by the number of years with data, or by adding the numbers in the table and dividing by the number of years. Despite the fact that the numbers displayed in the row *Rate* can adjust to the common sense, some of the individual results are unrealistic. Profiles 1650 and 1660 are located downstream from the groins, in the neighbouring area. Therefore, these two profiles are specially affected by the groins, and show large movements after 1985.

It is worth noticing that the largest movements take place before 1964. More than a climatic condition, it seems a problem in the superposition and georeferenciation of the

images pre 1964, probably due to the development of the equipment used to take and reference the photographies.

Table A.2 shows the results correspondent to the first digitalization using the wet-dry line as indicator only, while Table A.3 using also the landward edge of the shore protection structure as indicator.

Table A.2. Relative distance in between profiles of different years. A negative number represents erosion and a positive number accretion.

Year	P1600	P1610	P1620	P1630	P1640	P1650	P1660	P1670
1954-1999	-3.9	4.1	-10.9	-53.4	-53.3	-102.2	-55.2	-56.8
1999-2016	18.3	-13.6	-41.8	-19.8	-64.6	-68.6	-20.6	0.0
Rate 2 [m/year]	0.23	-0.15	-0.85	-1.18	-1.90	-2.75	-1.22	-0.92

Table A.3. Relative distance in between profiles of different years. A negative number represents erosion and a positive number accretion.

Year	P1600	P1610	P1620	P1630	P1640	P1650	P1660	P1670
1954-1999	-15.8	25.2	-23.4	-57.2	-58.6	-101.1	-54.3	-89.2
1999-2008	-4.60	4.53	-24.6	6.8	-7.4	-31.5	-23.7	0.0
2008-2016	51.7	-20.8	-5.1	-2.9	-37.6	-36.2	-6.9	0.0
Rate 3 [m/year]	0.51	0.14	-0.86	-0.86	-1.67	-2.72	-1.37	-1.44

These last two tables have also less years into consideration. The reason behind it is reducing the amount of errors that are accumulated after digitalizing many more lines. It is also motivated due to the fact that the individual results in between successive years are not the objective of the study, but the final rate of change of the shoreline.

Appendix to description of numerical model and inputs

B

B.1 Profile plots from morphological characteristics

In this section of the Appendix, the rest of the plots from the resolution and length check of the cross shore profiles are displayed.

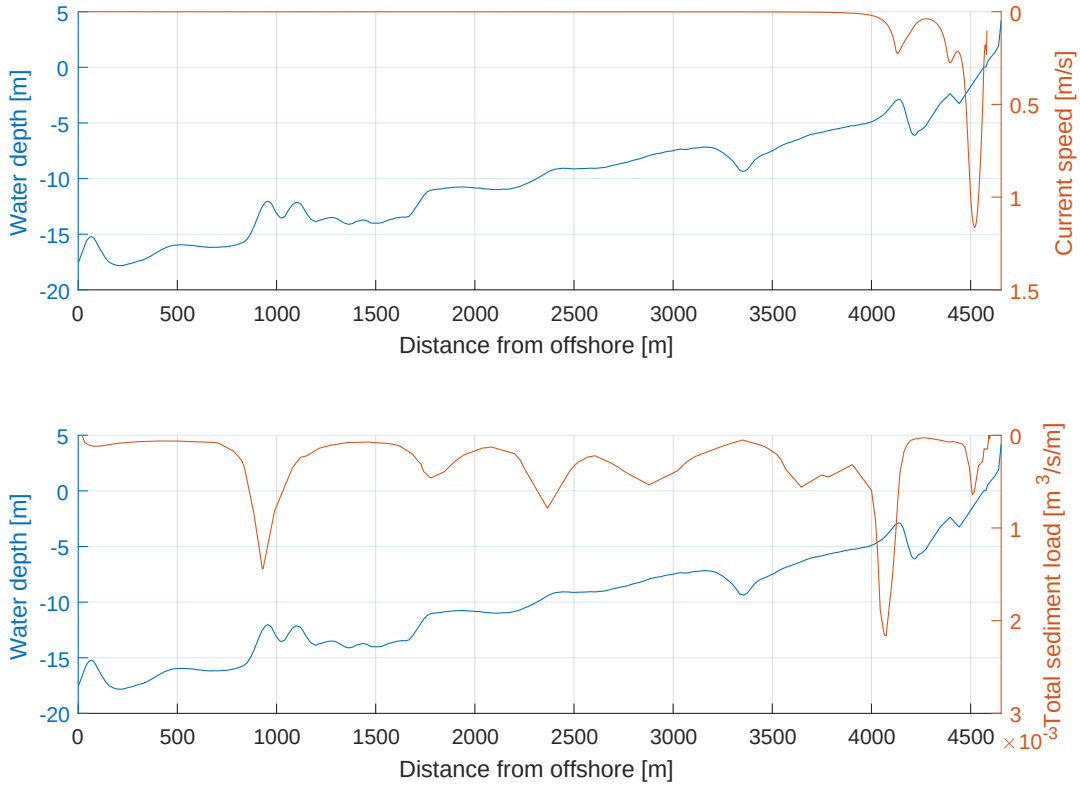

Figure B.1. Top: mean event simulation. Resolution check. Bottom: extreme event simulation. Length check.

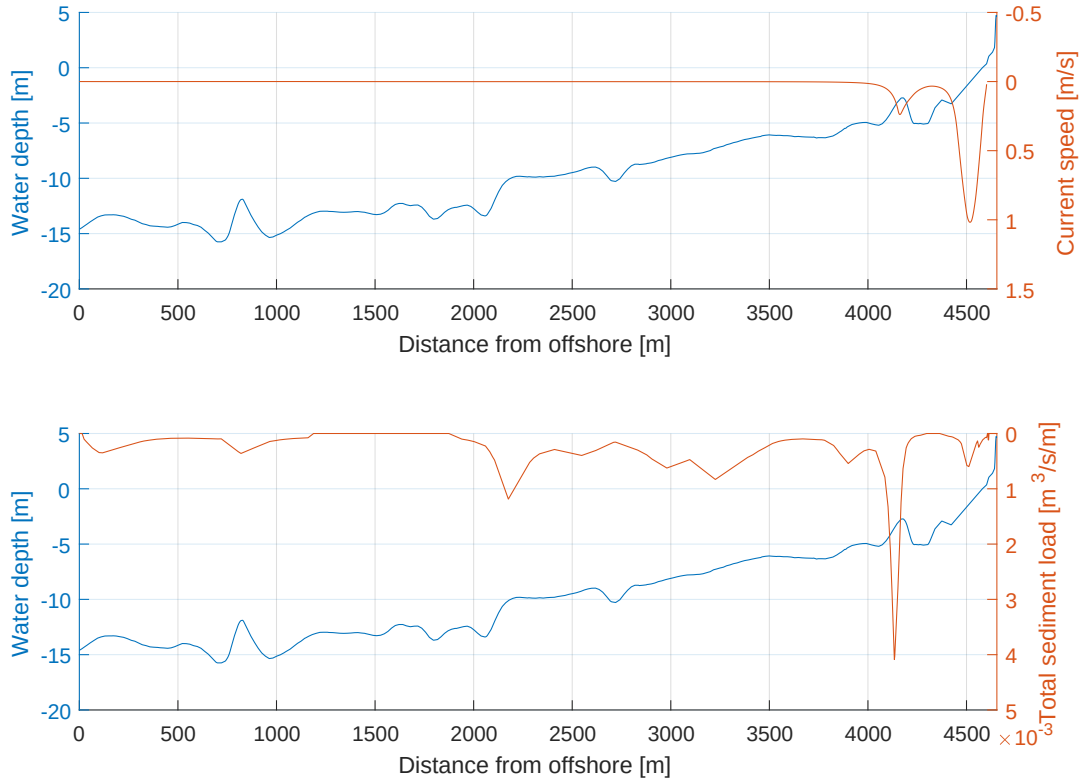

Figure B.2. Top: mean event simulation. Resolution check. Bottom: extreme event simulation. Length check.

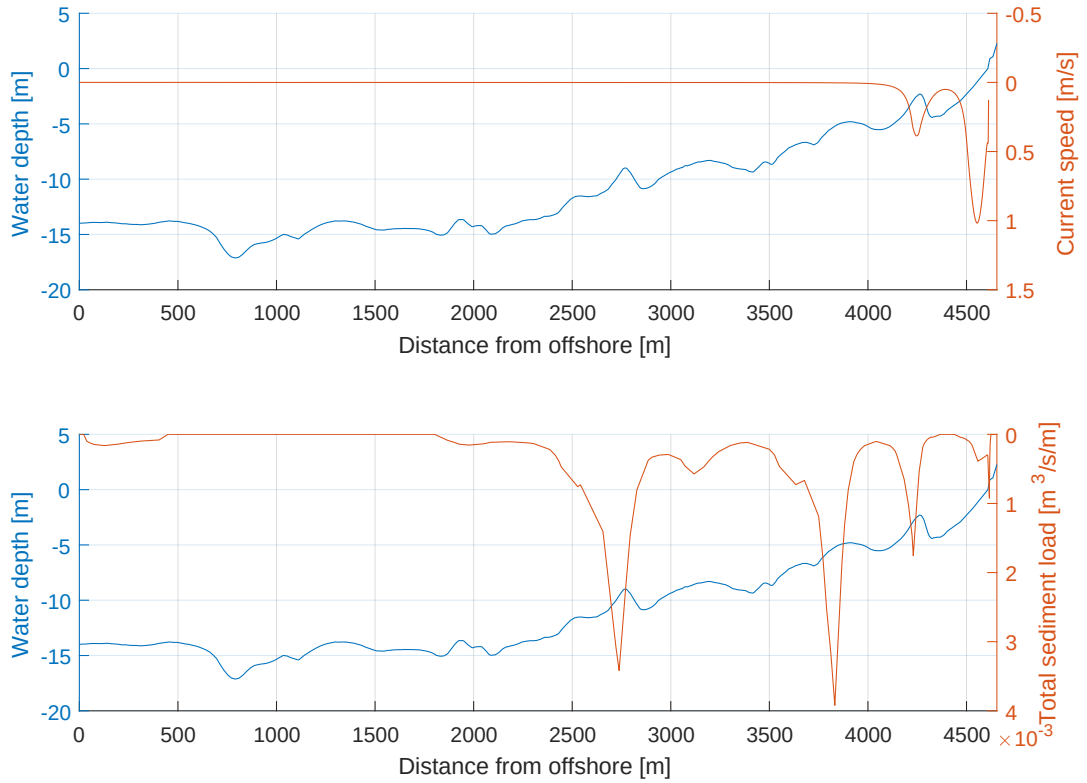

Figure B.3. Top: mean event simulation. Resolution check. Bottom: extreme event simulation. Length check.

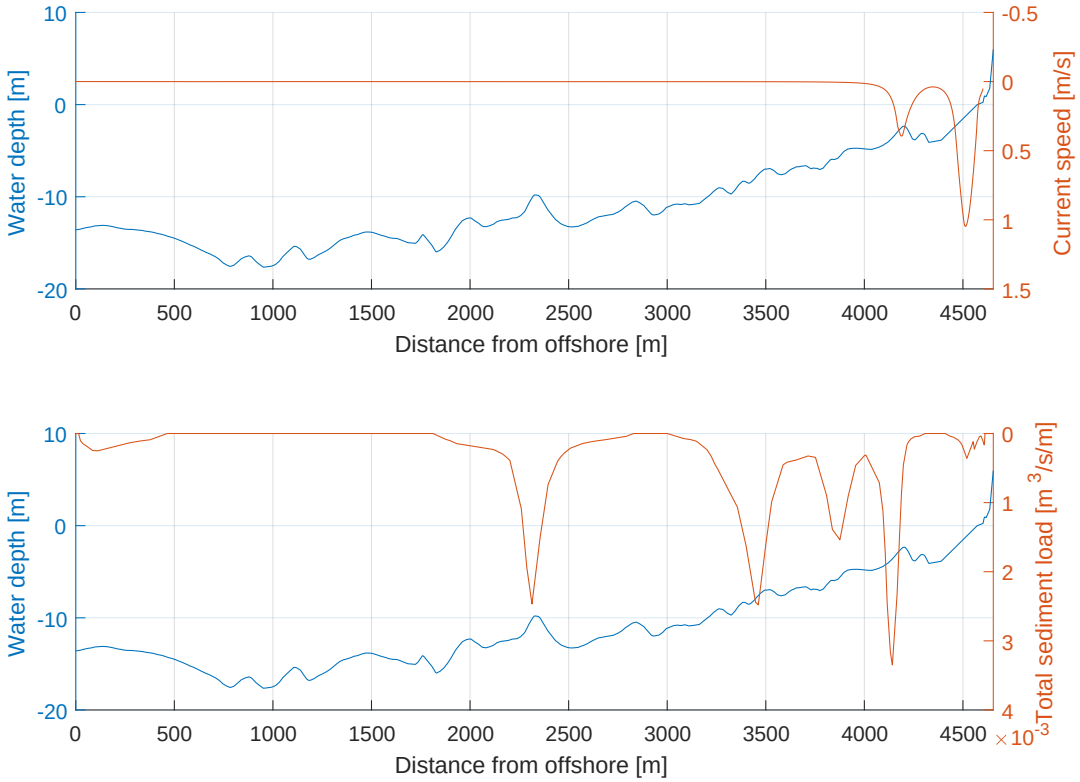

Figure B.4. Top: mean event simulation. Resolution check. Bottom: extreme event simulation. Length check.

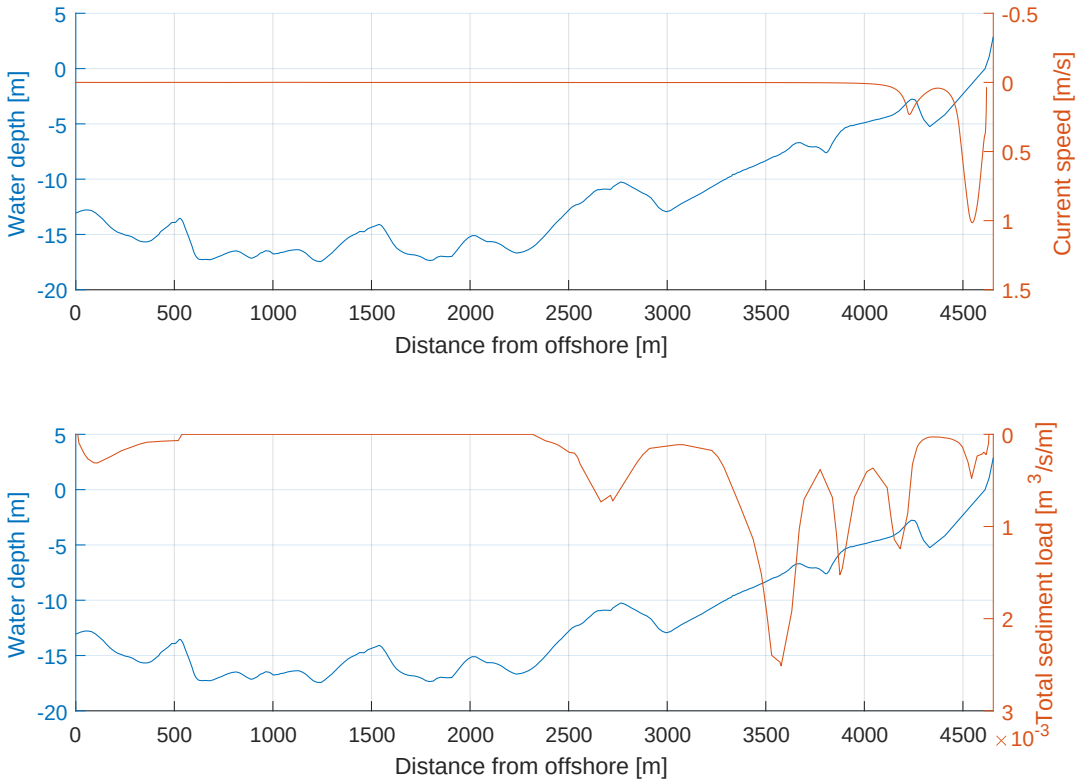

Figure B.5. Top: mean event simulation. Resolution check. Bottom: extreme event simulation. Length check.

B.2 Numerical values of parameters from Section 3.3

Table B.1. Other parameters involved in the calculation of the sediment characteristics that are inputs in the numerical model

Constant	Summer	Winter
H_e [m]	4.6414	5.9896
$\overline{H}$ [m]	1.0428	1.3762
σ_H	0.6426	0.8238
T_e [s]	8.2496	9.2602
S_ω	3.5116	3.5116
$\tau_{\omega,max}$ $[N/m^2]$	0.0161	0.0540
f_ω	0.0251	0.0162
U_m [m/s]	0.0353	0.0807
κ_s [m]	$5.825 \cdot 10^{-4}$	$5.825 \cdot 10^{-4}$
A [m] (amplitude oscillat.)	0.0240	0.0602
H_r [m]	0.0087	0.0219
L_r [m]	0.0479	0.1203
A (Archimedes buoy. ind.)	196.728	196.728
C_l	0.0251	0.0251
C_t	0.1286	0.1286

B.3 Appendix to storm magnitude

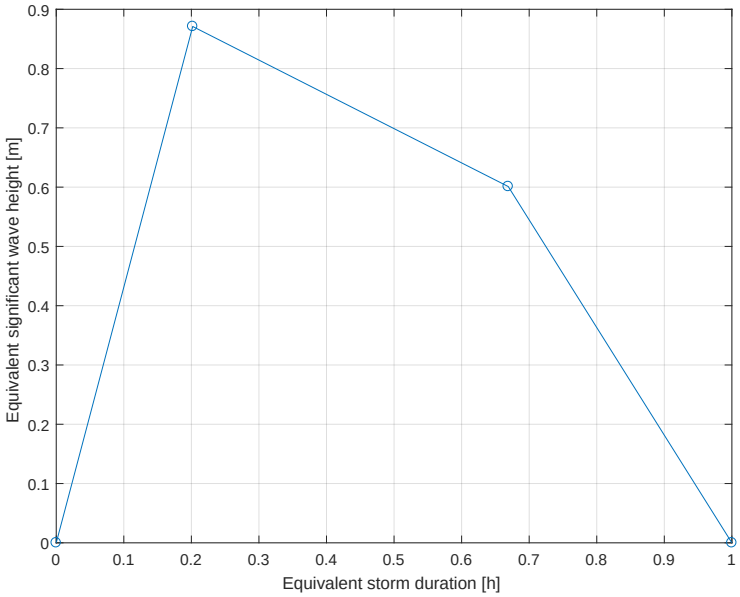

Figure B.6. Equivalent trapezoid for wave group G1, obtained using the EMS approach. It represents a general shape for this wave group in Nørlev Strand.

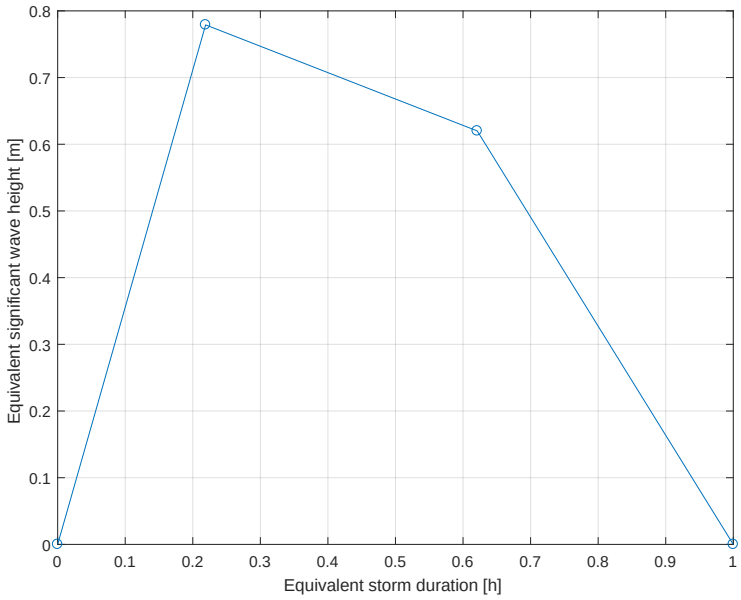

Figure B.7. Equivalent trapezoid for wave group G2, obtained using the EMS approach. It represents a general shape for this wave group in Nørlev Strand.

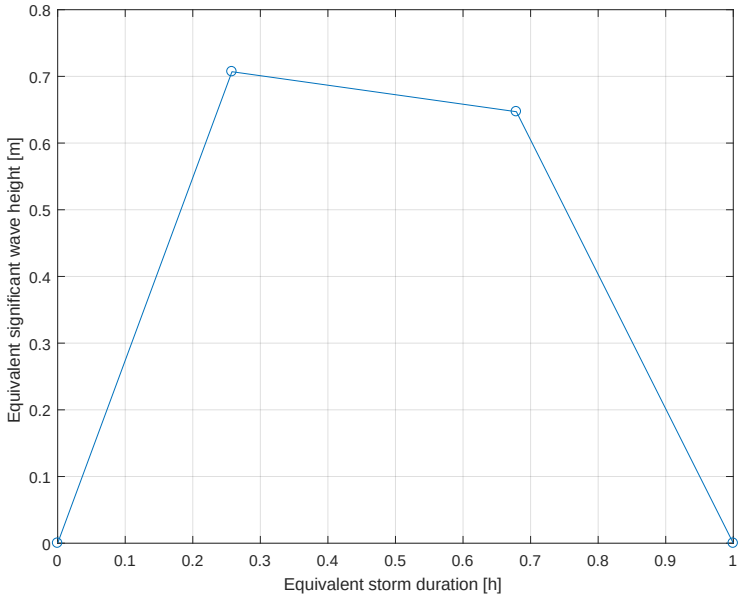

Figure B.8. Equivalent trapezoid for wave group G3, obtained using the EMS approach. It represents a general shape for this wave group in Nørlev Strand.

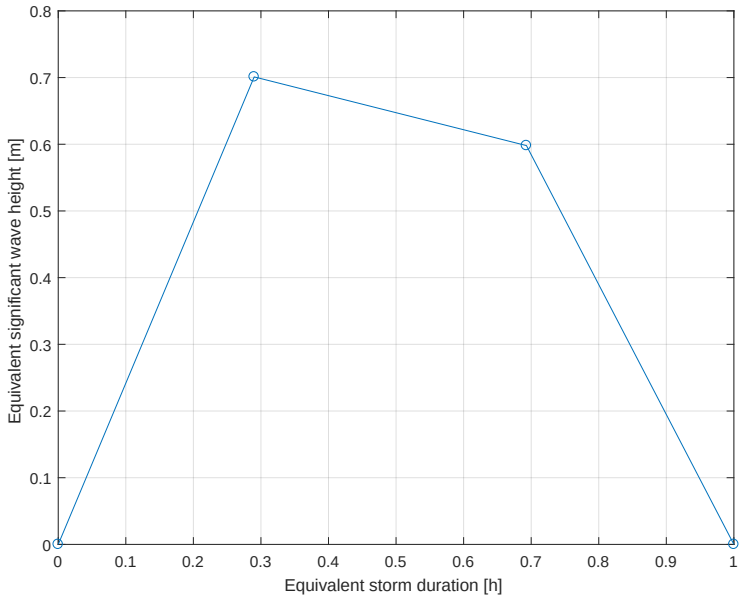

Figure B.9. Equivalent trapezoid for wave group G4, obtained using the EMS approach. It represents a general shape for this wave group in Nørlev Strand.